Electronic Supplementary Material (ESI) for Chemical Communications.

<Supporting Information>

Light-switched selective catalysis with NADH mimic functionalized metal–organic capsules

Jianwei Wei, Liang Zhao,* Yu Zhang, Peng Zhou, Guangzhou Liu and Chunying Duan

State Key Laboratory of Fine Chemicals, Zhang Dayu School of Chemistry, Dalian University of Technology, Dalian 116024, P. R. China.

Corresponding Author

*E-mail: zhaol@dlut.edu.cn

Contents

1. Experimental Section.

All the chemicals and solvents were of reagent grade quality obtained from commercial sources and used without further purification. The elemental analyses of C, H and N were performed on a Vario EL III elemental analyzer. ^{1}H NMR spectra were measured on a BRUKER 400M spectrometer. ESI mass spectra were carried out on an HPLC-Q-Tof MS spectrometer using acetonitrile as the mobile phase. UV-Vis spectra were measured on an HP 8453 spectrometer. The fluorescent spectra were measured on Edinburgh FLS1000. Isothermal Titration Calorimetry (ITC) was performed on a Nano ITC (TA Instruments Inc. — Waters LLC). The solution of $Ru(bpy)_3^{2+}$ (1.0 mM) was prepared in CH_3CN/H_2O (1:1 in volume), whereas the solution of the Zn−**TPB** (1.0 mM) and Ni−**TPB** (1.0 mM) was prepared in CH_3CN.

Electrochemical test

Electrochemical measurements were performed on ZAHNER ENNIUM Electrochemical Workstation with a conventional three-electrode system with a custom-designed Ag/AgCl electrode as a reference electrode, platinum silk with 0.5 mm diameter as a counter electrode, and glassy carbon electrode as a working electrode. The measurements were performed at room temperature after the system had been degassed with argon.

Light switchable selective photoinduced hydrogenation reaction

Photoinduced hydrogenation reaction was carried out in a 20 mL flask. As the standard method, the catalysts (0.05 mM), substrates (10.0 mM) and $HCOOH/H_2A$ (0.05 M/0.1 M) in CH_3CN/H_2O (1:1 in volume, pH 5.0) were added to obtain a total volume of 5.0 mL. The flask was sealed with a septum, and degassed by bubbling argon for 15 min under atmospheric pressure at room temperature. The pH of this solution was adjusted to a specific pH by adding H_2SO_4 or NaOH and measured with a pH meter. After that, the samples were irradiated by a 100 W LED Lamp at 420 nm or 455 nm, the reaction temperature was 298.15K by using a water filter to absorb heat. Following the completion of the reaction, the mixture was extracted with CH_2Cl_2.

The combined organic extracts were concentrated under vacuum. The conversions were determined by GC analysis (NMR was used for substrates 2, 3, 11, and 12) of the crude products with 1,3,5-trimethoxybenzene added as the internal standard.

Nonlinear fitting of host-guest complex system[S1]

For a 1:1 encapsulation process:

$$y = k\frac{\left([H]_0 + [G]_0 + \frac{1}{K_a}\right) - \sqrt{\left([H]_0 + [G]_0 + \frac{1}{K_a}\right)^2 - 4[H]_0[G]_0}}{2} + y_0$$

Here, the nonlinear fitting of y and $[G]_0$ is followed by this equation.

For a 1:2 encapsulation process:

$$y = k_1\frac{[H]_0K_{a1}[G]}{1 + K_{a1}[G] + K_{a1}K_{a2}[G]^2} + k_2\frac{[H]_0K_{a1}K_{a2}[G]^2}{1 + K_{a1}[G] + K_{a1}K_{a2}[G]^2} + y_0$$

$$[G] = [G_0] - [HG] - 2[HG_2] = [G_0] - \frac{[H]_0(K_{a1}[G] + 2K_{a1}K_{a2}[G]^2)}{1 + K_{a1}[G] + K_{a1}K_{a2}[G]^2}$$

Here, the nonlinear fitting of y and $[G]_0$ is followed by this equation.

2. Preparation and Characterizations.

Scheme 1. The synthetic routes of the H_2**TPB**.

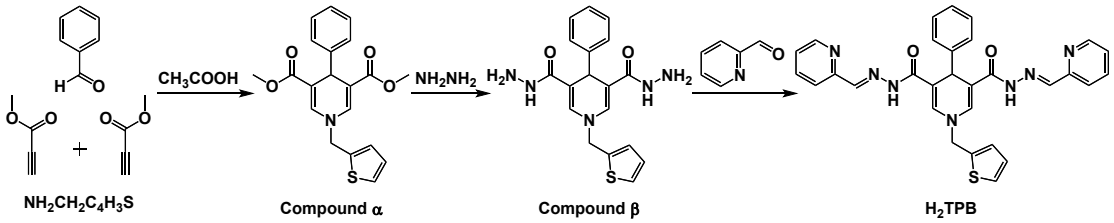

Synthesis of compound α

Methyl propiolate (1.68 g, 20 mmol), benzaldehyde (1.06 g, 10 mmol), and 2-thiophenemethanamine (1.13 g, 10 mmol) in glacial acetic acid (2.0 mL) were heated at 80 ℃ for 30 min.[S2] After cooling, the mixture was poured into water (20 mL) and stirred for 1 h. The solid product was filtered and washed with Et_2O (3×30 mL) to give pure compound 1, which was recrystallized by ethanol. Yield: 2.02 g, 54.8%. **^{1}H NMR** (400 MHz, $CDCl_3$, ppm): δ 7.34 (dd, *J* = 5.0, 1.4 Hz, 1H), 7.28 (d, *J* = 9.6 Hz, 4H), 7.22 (t, *J* = 7.5 Hz, 2H), 7.14 (t, *J* = 7.2 Hz, 1H), 7.07−6.99 (m, 2H), 4.89 (s, 1H), 4.73 (s, 2H), 3.61 (s, 6H). **^{13}C NMR** (101 MHz, $CDCl_3$, ppm) δ 167.22, 146.29, 138.75, 137.18, 128.27, 128.19, 127.46, 126.92, 126.62, 109.37, 53.35, 51.44, 37.45. **ESI-MS** calcd for $C_{20}H_{19}NO_4S$ 369.1035; Found 370.1137 $[M+H]^+$, 392.0970 $[M+Na]^+$.

Synthesis of compound β

A mixture solution of 80% hydrazine hydrate (50 ml) and compound 1 (3.69 g, 10 mmol) was stirred at 85℃ over 12 h. The white precipitate was formed, which was collected by filtration, washed with ethanol and dried in vacuum. Yield: 1.85 g, 50.1%. **^{1}H NMR** (400 MHz, DMSO-d_6, ppm): δ 8.66 (s, 2H), 7.53 (dd, *J* = 5.0, 1.3 Hz, 1H), 7.23−7.15 (m, 6H), 7.13 (dt, *J* = 4.7, 1.4 Hz, 1H), 7.11−7.03 (m, 2H), 5.00 (s, 1H), 4.80 (s, 2H), 4.15 (s, 4H). **^{13}C NMR** (101 MHz, DMSO-d_6, ppm) δ 166.44, 146.31, 140.27, 133.32, 127.87, 127.57, 127.12, 126.81, 126.36, 126.06, 109.01, 51.60, 35.40. **ESI-MS** calcd for $C_{18}H_{19}N_5O_2S$ 369.1259; Found 370.1353 $[M+H]^+$, 392.1178 $[M+Na]^+$.

Synthesis of H_2TPB

Compound 2 (3.69 g, 10 mmol) was added to an ethanol solution (50 mL) containing 2-pyridylaldehyde (2.35 g, 22 mmol). After 5 drops of acetic acid were added, the mixture was heated at 85℃ under magnetic stirring for 12 h according to the reference.[S3] The yellow solid was collected by filtration, washed with methanol and dried in vacuum. Yield: 3.36 g, 61.4%. **^{1}H NMR** (400 MHz, DMSO-d_6, ppm): δ 11.37 (s, 2H), 8.58 (dt, J = 4.9, 1.4 Hz, 2H), 8.24 (s, 2H), 7.89−7.77 (m, 4H), 7.59 (dd, J = 5.0, 1.3 Hz, 1H), 7.51 (s, 2H), 7.37 (q, J = 4.5 Hz, 2H), 7.32−7.26 (m, 2H), 7.25−7.20 (m, 3H), 7.15−7.07 (m, 2H), 5.35 (s, 1H), 4.96 (s, 2H). **^{13}C NMR** (101 MHz, DMSO-d_6, ppm) δ 163.81, 153.47, 149.42, 146.38, 145.27, 140.28, 136.72, 128.09, 127.70, 127.31, 126.68, 126.53, 126.28, 125.62, 124.01, 119.56, 109.39, 52.19, 36.12. **Elemental analysis** calcd for $C_{30}H_{25}N_7O_2S$: H, 4.60; C, 65.80; N, 17.90%; Found: H, 4.81; C, 65.61; N, 17.79%. **ESI-MS** calcd for $C_{30}H_{25}N_7O_2S$ 547.1790; Found 548.1887 $[M+H]^+$, 570.1662 $[M+Na]^+$.

Preparation of Zn−**TPB**

$Zn(CF_3SO_3)_2$ (36.1 mg, 0.10 mmol) and H_2**TPB** (54.8 mg, 0.10 mmol) were dissolved in CH_3CN/CH_3OH (20:1 in volume) to give a yellow solution. The solution was diffused with ether for several days at room temperature to give X-ray-quality yellow block crystals. Yield: 46%. **^{1}H NMR** (400 MHz, DMSO-d_6, ppm): δ 11.77 (s, 2H), 8.54 (s, 2H), 8.32 (s, 2H), 7.97 (m, 4H), 7.60 (m, 3H), 7.49 (s, 2H), 7.27 (m, 2H), 7.22 (m, 3H), 7.11 (m, 2H), 5.32 (s, 1H), 5.03 (s, 2H). **Elemental analysis** calcd for $Zn_4(C_{120}H_{99}N_{28}O_8S_4)\cdot 7CF_3SO_3\cdot 3CH_3CN$: H, 3.01; C, 44.16; N, 12.00%; Found: H, 3.05; C, 44.09; N, 11.89%. **ESI-MS**: m/z: 815.7940 $[H_3Zn_4(\mathbf{TPB})_4]^{3+}$, 1223.1879 $[H_2Zn_4(\mathbf{TPB})_4]^{2+}$.

Preparation of Ni−**TPB**

$Ni(BF_4)_2\cdot 6H_2O$ (34.0 mg, 0.10 mmol) and H_2**TPB** (54.8 mg, 0.10 mmol) were dissolved in 30 mL CH_3CN to give a yellow solution. The solution was diffused with ether for several days at room temperature to give X-ray-quality yellow block crystals. Yield: 35%. **Elemental analysis** calcd for $Ni_4(C_{120}H_{99}N_{28}O_8S_4)\cdot 7BF_4\cdot 2H_2O$: H, 3.38;

C, 46.98; N, 12.78%; Found: H, 3.61; C, 46.83; N, 12.59%. **ESI-MS**: *m*/*z*: 806.4614 $[H_3Ni_4(\mathbf{TPB})_4]^{3+}$, 1209.1890 $[H_2Ni_4(\mathbf{TPB})_4]^{2+}$.

3. Single Crystal X-ray Crystallography.

Intensities of the Zn−**TPB** and Ni−**TPB** were collected on a Bruker SMART APEX CCD diffractometer with graphite monochromated Mo-Kα (λ = 0.71073 Å) using the SMART and SAINT programs.[S4, S5] The structures were solved by direct methods and refined on F^2 by full-matrix least-squares methods with SHELXTL *version* 5.1.[S6]

Compound	Zn−**TPB**	Ni−**TPB**
Formula	$Zn_4(C_{120}H_{99}N_{28}O_8S_4)\cdot 7CF_3SO_3\cdot 4CH_3CN$	$Ni_4(C_{120}H_{99}N_{28}O_8S_4)\cdot 7BF_4\cdot 2.5H_2O$
M (g·mol^{-1})	3658.69	3077.06
Crystal system	Orthorhombic	Orthorhombic
Space group	P2(1)2(1)2	Pnma
a (Å)	19.2588(12)	29.073(3)
b (Å)	21.0194(13)	22.669(2)
c (Å)	23.1335(14)	28.741(3)
V (Å^3)	9364.6(10)	18942 (3)
Z	2	4
D_{calcd} (g·cm^{-3})	1.298	1.079
F (000)	3724	6268
μ (mm^{-1})	0.717	0.512
T (K)	170(2)	150(2)
Refl. collected/unique	59858/16456 [R_{int} = 0.0417]	95780 / 17112 [R_{int} = 0.1091]
R_1 [$I > 2\sigma(I)$]	0.0484	0.0894
wR_2 (all data)	0.1438	0.2427
Goodness of fit	1.023	1.050
Max/min Δρ(e Å^{-3})	0.47 and -0.56	0.46 and -0.40
CCDC Number	1961723	1961724

In the structural refinement of Zn−**TPB**, the non-hydrogen atoms were refined anisotropically. Hydrogen atoms within the ligand backbones and the solvent CH_3CN molecules were fixed geometrically at calculated distances and allowed to ride on the parent non-hydrogen atoms. To assist the stability of refinements, one benzene ring in the ligands and two $CF_3SO_3^-$ anions were restrained as idealized regular polygons. Thermal parameters on adjacent atoms in $CF_3SO_3^-$ anions were restrained to be

similar. All of the carbon, oxygen and fluoride atoms on two $CF_3SO_3^-$ anions were disordered into two parts with the *s.o.f* of each part being refined with free values, respectively. The SQUEEZE subroutine in PLATON was used.[S7]

In the structural refinement of Ni−**TPB**, all of the non-hydrogen atoms were refined anisotropically. Hydrogen atoms within the ligand backbones were fixed geometrically at calculated distances and allowed to ride on the parent non-hydrogen atoms. To assist the stability of refinements, all of the thiophene rings and three benzene rings in the ligands and two BF_4^- anions were restrained as idealized regular polygons. Thermal parameters on adjacent atoms in all of the thiophene rings and three benzene ring in the ligands and all of BF_4^- anions were restrained to be similar. two thiophene rings were disordered into two parts with the *s.o.f* of each part being fixed as 0.5. All of BF_4^- anions were disordered into two parts with the *s.o.f* of each part being refined with free values, respectively. The SQUEEZE subroutine in PLATON was used.[S7]

Figure S1. An ORTEP plot of the molecular tetrahedron Zn−**TPB**, showing 30% probability displacement ellipsoids of non-hydrogen atoms. Hydrogen atoms are omitted for clarity. Symmetry code A: -*x*, -*y*+1, *z*.

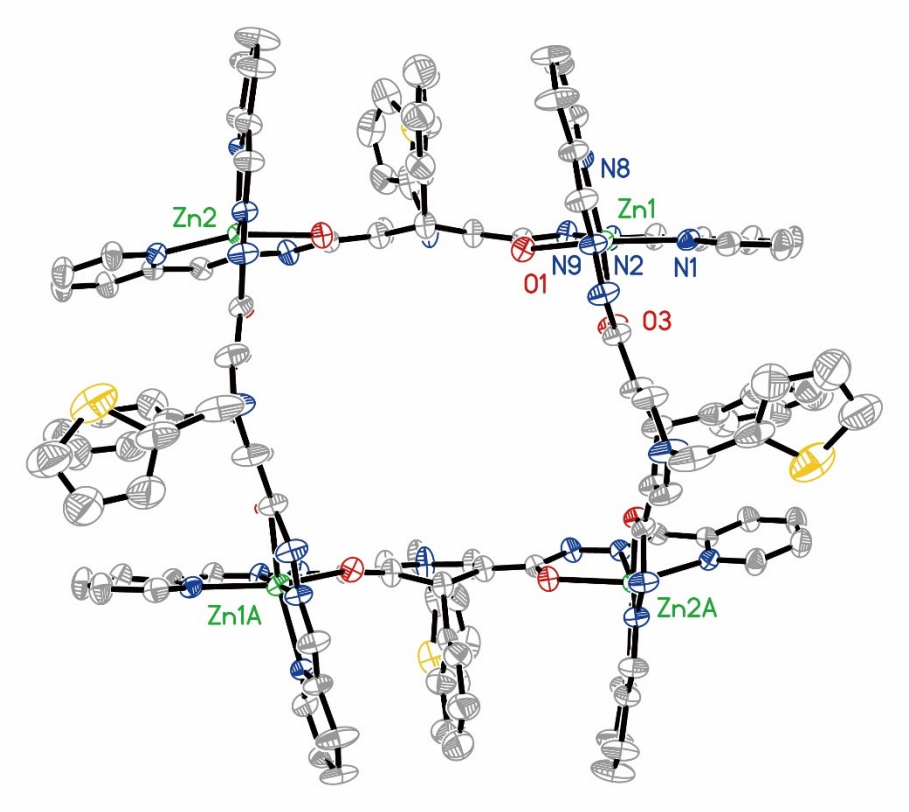

Table S1. Selective bond distance (Å) in Zn−**TPB**.

	bond distance (Å)		bond distance (Å)
Zn(1)-N(2)	2.072(5)	Zn(1)-O(1)	2.166(4)
Zn(1)-N(9)	2.077(5)	Zn(1)-N(1)	2.170(5)
Zn(1)-O(3)	2.157(4)	Zn(1)-N(8)	2.174(5)
S(1)-C(30)	1.659(12)	N(6)-C(13)	1.328(7)
S(1)-C(27)	1.711(10)	N(7)-C(24)	1.365(8)
S(2)-C(60)	1.663(16)	N(7)-C(25)	1.377(8)
S(2)-C(57)	1.680(12)	N(7)-C(26)	1.484(8)
O(1)-C(7)	1.254(7)	N(8)-C(31)	1.320(8)
O(2)-C(11)	1.233(7)	N(8)-C(35)	1.349(8)
O(3)-C(37)	1.243(7)	N(9)-C(36)	1.254(8)
O(4)-C(41)	1.240(6)	N(9)-N(10)	1.345(6)
N(1)-C(1)	1.330(8)	N(10)-C(37)	1.373(8)
N(1)-C(5)	1.350(8)	N(11)-N(12)	1.343(7)
N(2)-C(6)	1.258(8)	N(11)-C(41)	1.380(7)
N(2)-N(3)	1.354(6)	N(12)-C(42)	1.257(8)
N(3)-C(7)	1.365(8)	N(13)-C(47)	1.326(8)
N(4)-N(5)	1.363(7)	N(13)-C(43)	1.336(7)
N(4)-C(11)	1.371(7)	N(14)-C(55)	1.364(8)
N(5)-C(12)	1.259(7)	N(14)-C(54)	1.383(8)
N(6)-C(17)	1.311(8)	N(14)-C(56)	1.483(8)

Table S2. Selective bond angle (°) in Zn−**TPB**.

	bond angle (°)		bond angle (°)
N(2)-Zn(1)-N(9)	179.6(2)	N(5)-Zn(2)-N(12A)	173.13(19)
N(2)-Zn(1)-O(3)	106.81(18)	N(5)-Zn(2)-O(4A)	106.52(16)
N(9)-Zn(1)-O(3)	73.48(16)	N(12A)-Zn(2)-O(4A)	73.52(16)
N(2)-Zn(1)-O(1)	73.82(16)	N(5)-Zn(2)-N(13A)	104.57(18)
N(9)-Zn(1)-O(1)	106.51(17)	N(12A)-Zn(2)-N(13A)	74.94(18)
O(3)-Zn(1)-O(1)	97.49(16)	O(4A)-Zn(2)-N(13A)	148.40(16)
N(2)-Zn(1)-N(1)	75.16(18)	N(5)-Zn(2)-N(6)	74.26(18)
N(9)-Zn(1)-N(1)	104.5(2)	N(12A)-Zn(2)-N(6)	112.56(19)
O(3)-Zn(1)-N(1)	86.18(18)	O(4A)-Zn(2)-N(6)	88.98(17)
O(1)-Zn(1)-N(1)	148.48(16)	N(13A)-Zn(2)-N(6)	104.87(18)
N(2)-Zn(1)-N(8)	104.34(19)	N(5)-Zn(2)-O(2)	73.30(16)
N(9)-Zn(1)-N(8)	75.40(17)	N(12A)-Zn(2)-O(2)	99.84(17)
O(3)-Zn(1)-N(8)	148.74(16)	O(4A)-Zn(2)-O(2)	94.85(15)
O(1)-Zn(1)-N(8)	88.54(17)	N(13A)-Zn(2)-O(2)	88.65(17)
N(1)-Zn(1)-N(8)	104.46(18)	N(6)-Zn(2)-O(2)	147.07(16)

Symmetry code A: -*x*, -*y*+1, *z*

Figure S2. An ORTEP plot of the molecular tetrahedron Ni−**TPB**, showing 30% probability displacement ellipsoids of non-hydrogen atoms. Hydrogen atoms are omitted for clarity. Symmetry code A: *x*, -*y*+3/2, -*z*.

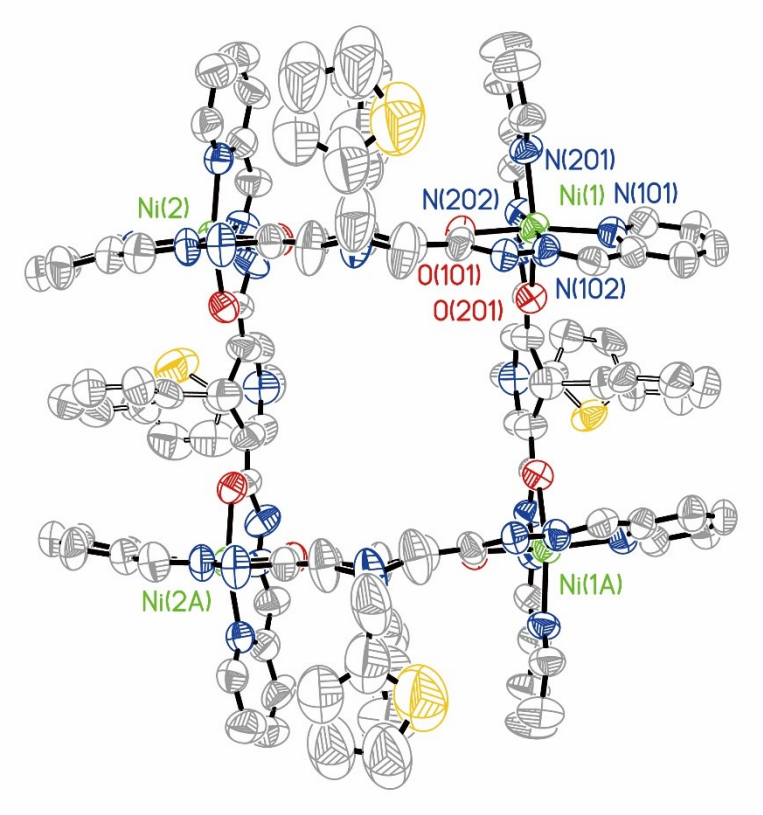

Table S3. Selective bond distance (Å) in Ni−**TPB**.

	bond distance (Å)		bond distance (Å)
Ni(1)-N(102)	1.962(6)	Ni(1)-N(201)	2.081(5)
Ni(1)-N(202)	2.023(5)	Ni(1)-O(201)	2.088(4)
Ni(1)-N(101)	2.061(6)	Ni(1)-O(101)	2.094(5)
O(101)-C(107)	1.215(8)	N(201)-C(201)	1.358(8)
O(102)-C(113)	1.253(8)	N(202)-C(206)	1.292(7)
O(201)-C(207)	1.249(7)	N(202)-N(203)	1.348(6)
O(301)-C(307)	1.238(8)	N(203)-C(207)	1.394(7)
N(101)-C(101)	1.326(8)	N(204)-C(210)	1.401(6)
N(101)-C(105)	1.377(8)	N(204)-C(210A)	1.401(6)
N(102)-C(106)	1.283(7)	N(204)-C(226)	1.507(10)
N(102)-N(103)	1.361(7)	N(301)-C(301)	1.320(10)
N(103)-C(107)	1.406(8)	N(301)-C(305)	1.353(10)
N(104)-C(113)	1.349(8)	N(302)-C(306)	1.248(8)
N(104)-N(105)	1.355(7)	N(302)-N(303)	1.315(8)
N(105)-C(114)	1.270(8)	N(303)-C(307)	1.339(8)
N(106)-C(115)	1.302(8)	N(304)-C(310A)	1.342(8)
N(106)-C(119)	1.342(8)	N(304)-C(310)	1.342(8)
N(201)-C(205)	1.357(8)	N(304)-C(326)	1.457(13)

Symmetry code A: *x*, -*y*+3/2, -*z*

Table S4. Selective bond angle (°) in Ni−**TPB**.

	bond angle (°)		bond angle (°)
N(102)-Ni(1)-N(202)	174.3(2)	N(105)-Ni(2)-N(302)	175.0(3)
N(102)-Ni(1)-N(101)	79.2(3)	N(105)-Ni(2)-N(301)	99.9(3)
N(202)-Ni(1)-N(101)	103.3(3)	N(302)-Ni(2)-N(301)	78.2(3)
N(102)-Ni(1)-N(201)	106.4(3)	N(105)-Ni(2)-O(301)	105.0(2)
N(202)-Ni(1)-N(201)	78.3(3)	N(302)-Ni(2)-O(301)	76.6(3)
N(101)-Ni(1)-N(201)	99.4(2)	N(301)-Ni(2)-O(301)	154.7(3)
N(102)-Ni(1)-O(201)	98.19(19)	N(105)-Ni(2)-O(102)	75.9(2)
N(202)-Ni(1)-O(201)	76.8(2)	N(302)-Ni(2)-O(102)	99.3(2)
N(101)-Ni(1)-O(201)	89.53(17)	N(301)-Ni(2)-O(102)	88.70(19)
N(201)-Ni(1)-O(201)	154.9(2)	O(301)-Ni(2)-O(102)	93.02(17)
N(102)-Ni(1)-O(101)	76.9(2)	N(105)-Ni(2)-N(106)	78.0(3)
N(202)-Ni(1)-O(101)	100.5(2)	N(302)-Ni(2)-N(106)	106.9(3)
N(101)-Ni(1)-O(101)	156.1(3)	N(301)-Ni(2)-N(106)	101.5(2)
N(201)-Ni(1)-O(101)	88.0(2)	O(301)-Ni(2)-N(106)	88.2(2)
O(201)-Ni(1)-O(101)	93.23(17)	O(102)-Ni(2)-N(106)	153.3(3)

4. ESI-MS Spectra

Figure S3. ESI-MS of Zn−**TPB** (0.1 mM) in CH_3CN solution. The inserts show the measured and simulated isotopic patterns at *m*/*z* = 815.7940 and 1223.1879, respectively.

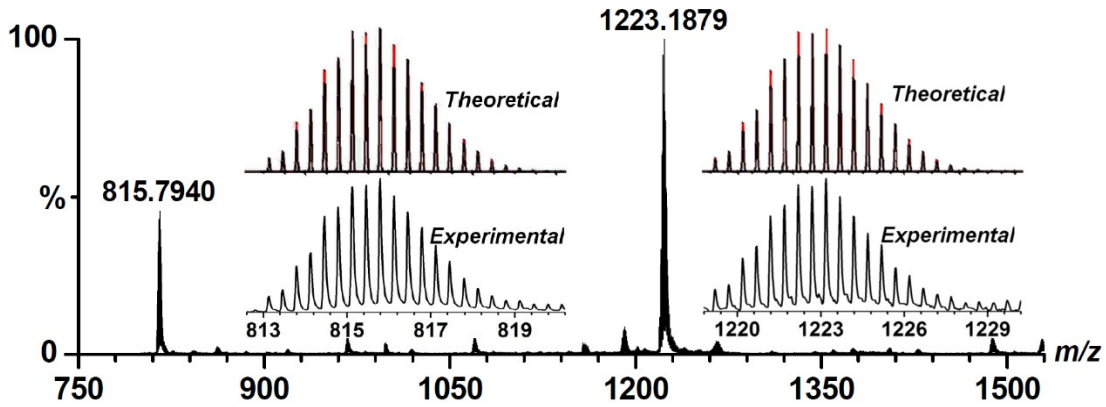

Peak	Value of *m*/*z*	Specie assigned
1	815.7940	$[H_3Zn_4(\mathbf{TPB})_4]^{3+}$
2	1223.1879	$[H_2Zn_4(\mathbf{TPB})_4]^{2+}$

Figure S4. ESI-MS of Zn−**TPB** (0.1 mM) upon addition of 5 equiv of nitrobenzene (**1**) in CH_3CN solution. The inserts show the measured and simulated isotopic patterns at *m*/*z* = 1346.1938.

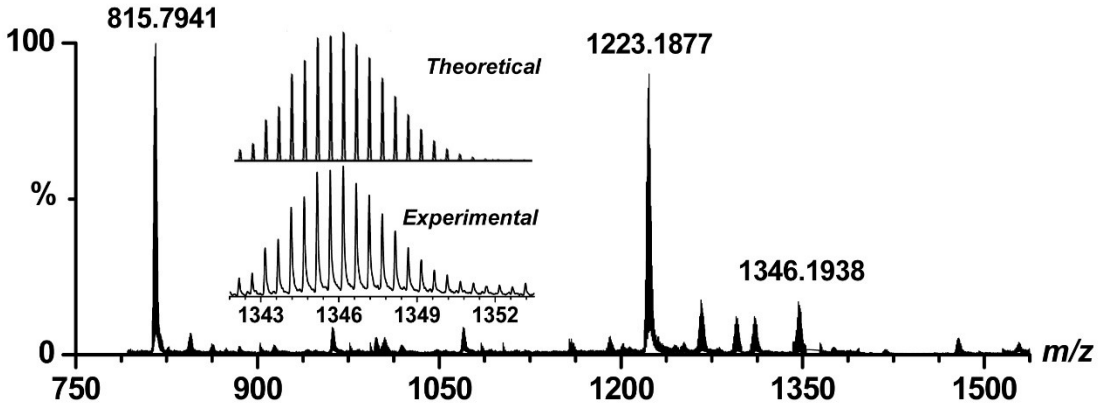

Peak	Value of *m*/*z*	Specie assigned
1	815.7941	$[H_3Zn_4(\mathbf{TPB})_4]^{3+}$
2	1223.1877	$[H_2Zn_4(\mathbf{TPB})_4]^{2+}$
3	1346.1938	$[H_2Zn_4(\mathbf{TPB})_4 \supset (\mathbf{1})_2]^{2+}$

Figure S5. ESI-MS of Zn−**TPB** (0.1 mM) upon addition of 5 equiv of *N*-phenylhydroxylamine (**1b**) in CH_3CN solution. The inserts show the measured and simulated isotopic patterns at *m*/*z* = 1332.1789.

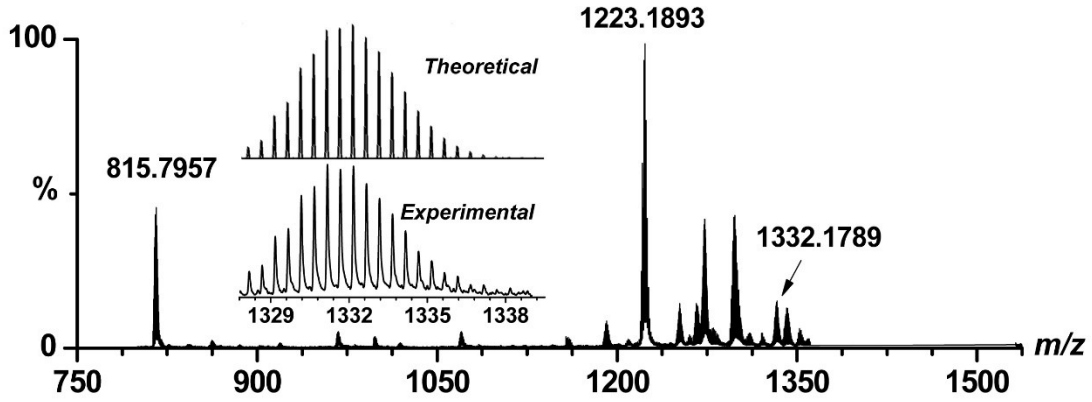

Peak	Value of *m*/*z*	Specie assigned
1	815.7957	$[H_3Zn_4(\mathbf{TPB})_4]^{3+}$
2	1223.1893	$[H_2Zn_4(\mathbf{TPB})_4]^{2+}$
3	1332.1789	$[H_2Zn_4(\mathbf{TPB})_4 \supset (\mathbf{1b})_2]^{2+}$

Figure S6. ESI-MS of Zn−**TPB** (0.1 mM) upon addition of 5 equiv of **ATP** in CH_3CN/H_2O solution. The inserts show the measured and simulated isotopic patterns at m/z = 1476.6865.

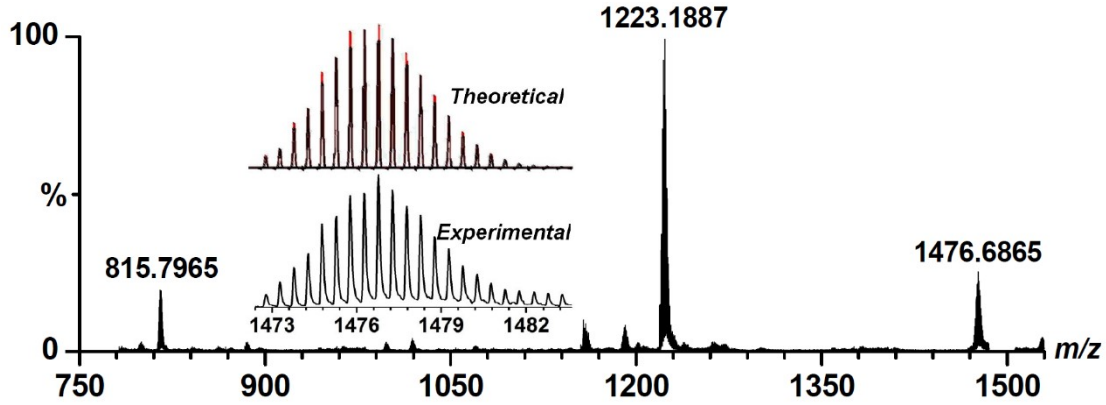

Peak	Value of m/z	Specie assigned
1	815.7911	$[H_3Zn_4(\mathbf{TPB})_4]^{3+}$
2	1223.1821	$[H_2Zn_4(\mathbf{TPB})_4]^{2+}$
3	1476.6865	$[H_2Zn_4(\mathbf{TPB})_4 \supset \mathbf{ATP}]^{2+}$

Figure S7. ESI-MS of Ni−**TPB** (0.1 mM) in CH_3CN solution. The inserts show the measured and simulated isotopic patterns at *m*/*z* = 806.4615 and 1209.1890, respectively.

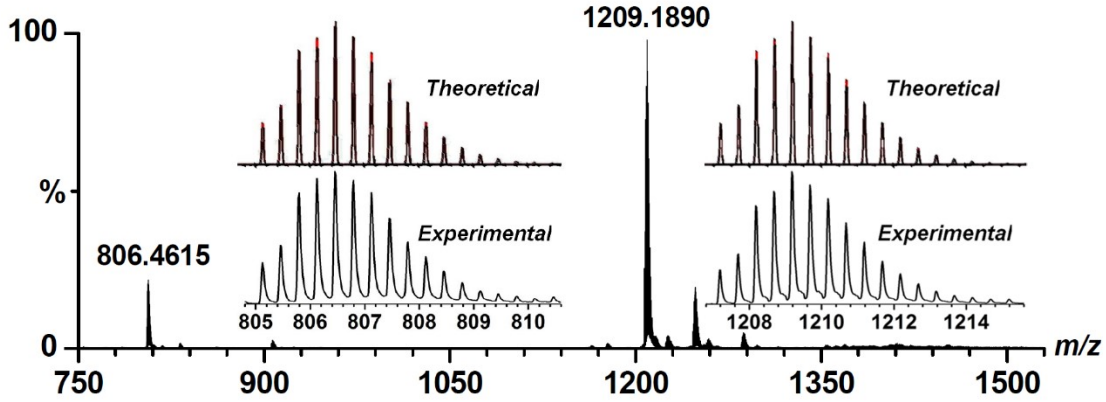

Peak	Value of *m*/*z*	Specie assigned
1	806.4615	$[H_3Ni_4(\mathbf{TPB})_4]^{3+}$
2	1209.1890	$[H_2Ni_4(\mathbf{TPB})_4]^{2+}$

Figure S8. ESI-MS of Ni−**TPB** (0.1 mM) upon addition of 5 equiv of nitrobenzene (**1**) in CH_3CN solution. The inserts show the measured and simulated isotopic patterns at *m*/*z* = 1332.2252.

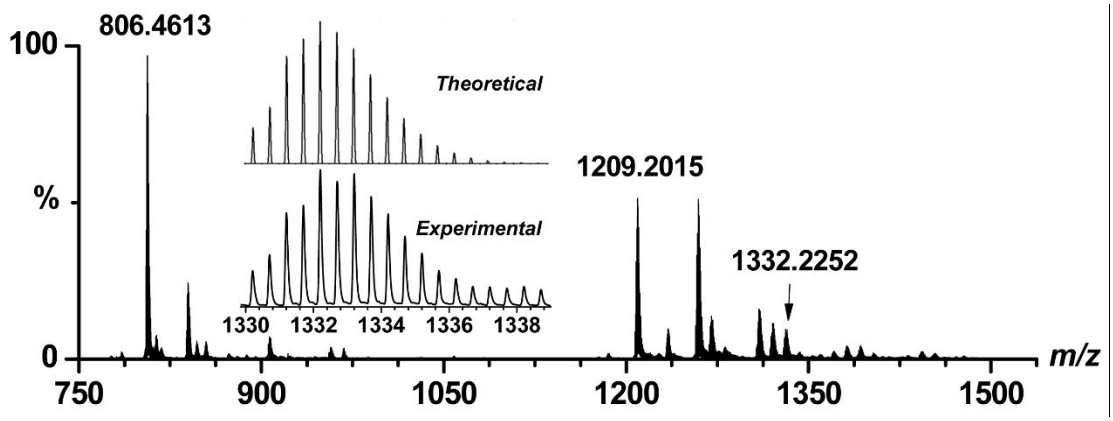

Peak	Value of *m*/*z*	Specie assigned
1	806.4613	$[H_3Ni_4(\mathbf{TPB})_4]^{3+}$
2	1209.2015	$[H_2Ni_4(\mathbf{TPB})_4]^{2+}$
3	1332.2252	$[H_2Ni_4(\mathbf{TPB})_4 \supset (\mathbf{1})_2]^{2+}$

Figure S9. ESI-MS of Ni−**TPB** (0.1 mM) upon addition of 5 equiv of *N*-phenylhydroxylamine (**1b**) in CH_3CN solution. The inserts show the measured and simulated isotopic patterns at *m*/*z* = 1318.2352.

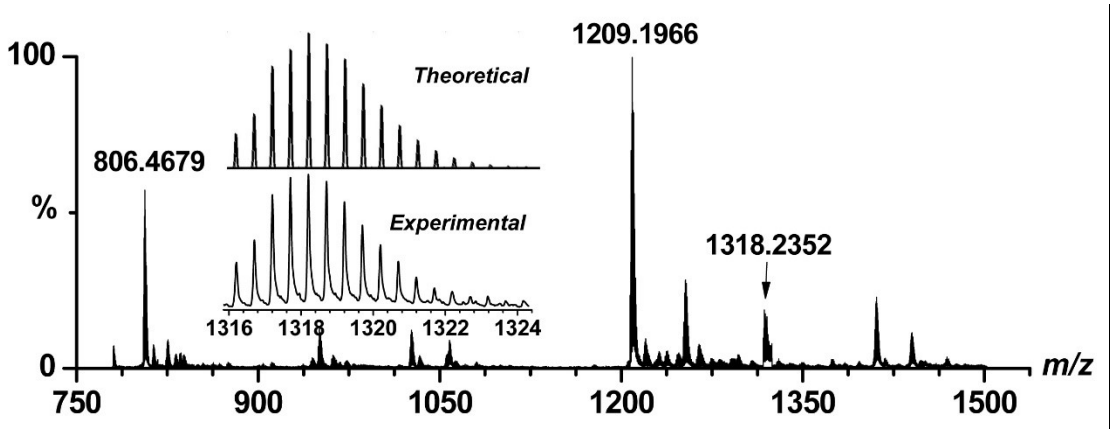

Peak	Value of *m*/*z*	Specie assigned
1	806.4679	$[H_3Ni_4(\mathbf{TPB})_4]^{3+}$
2	1209.1966	$[H_2Ni_4(\mathbf{TPB})_4]^{2+}$
3	1318.2352	$[H_2Ni_4(\mathbf{TPB})_4 \supset (\mathbf{1b})_2]^{2+}$

Figure S10. ESI-MS of Ni−**TPB** (0.1 mM) upon addition of 5 equiv of **ATP** in CH_3CN/H_2O solution. The inserts show the measured and simulated isotopic patterns at m/z = 1462.6998.

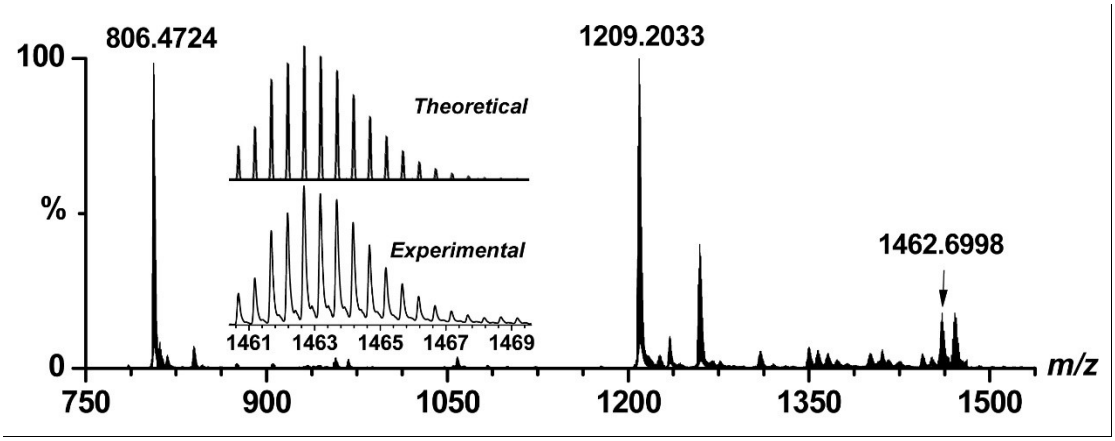

Peak	Value of m/z	Specie assigned
1	806.4724	$[H_3Ni_4(\mathbf{TPB})_4]^{3+}$
2	1209.2033	$[H_2Ni_4(\mathbf{TPB})_4]^{2+}$
3	1462.6998	$[H_2Ni_4(\mathbf{TPB})_4 \supset \mathbf{ATP}]^{2+}$

5. Data for Spectral Titrations.

5.1 UV-Vis Spectral Titrations

Figure S11. Family of UV-Vis of Zn−**TPB** (10 μM, red), Ni−**TPB** (10 μM, green) and $Ru(bpy)_3^{2+}$ (0.1 mM) in CH_3CN/H_2O (1:1, pH 5.0).

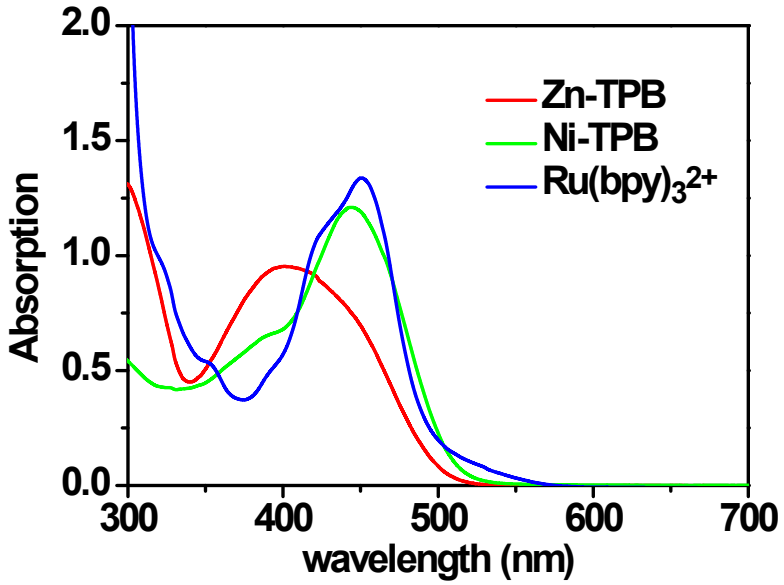

Figure S12. (Left) UV-Vis absorption difference spectra of Zn−**TPB** (40 μM) in CH_3CN/H_2O (1:1, pH 5.0) upon the addition of nitrobenzene (**1**). (Right) Nonlinear fitting of titration curve showing the calculation of the associate constant (K_{a1} = 1.2 × 10^3 M^{-1}, K_{a2} = 4.8 × 10^4 M^{-1}). Absorption was recorded at 454 nm.

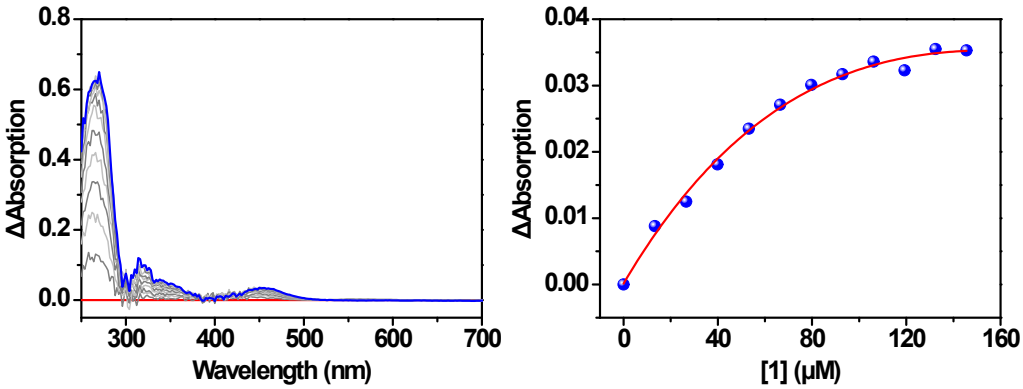

Figure S13. (Left) UV-Vis absorption difference spectra of Zn−**TPB** (20 μM) in CH_3CN/H_2O (1:1, pH 5.0) upon the addition of nitrosobenzene (**1a**). (Right) Nonlinear fitting of titration curve showing the calculation of the associate constant ($K_{a1} = 5.9 \times 10^3$ M^{-1}, $K_{a2} = 9.7 \times 10^5$ M^{-1}). Absorption was recorded at 454 nm.

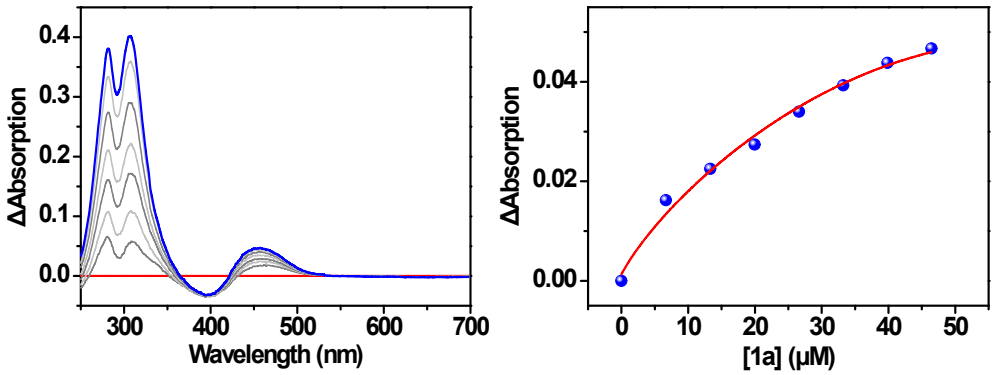

Figure S14. (Left) UV-Vis absorption difference spectra of Zn−**TPB** (20 μM) in CH_3CN/H_2O (1:1, pH 5.0) upon the addition of *N*-phenylhydroxylamine (**1b**). (Right) Nonlinear fitting of titration curve showing the calculation of the associate constant ($K_{a1} = 1.5 \times 10^{12}$ M^{-1}, $K_{a2} = 2.9 \times 10^{3}$ M^{-1}). Absorption was recorded at 402 nm.

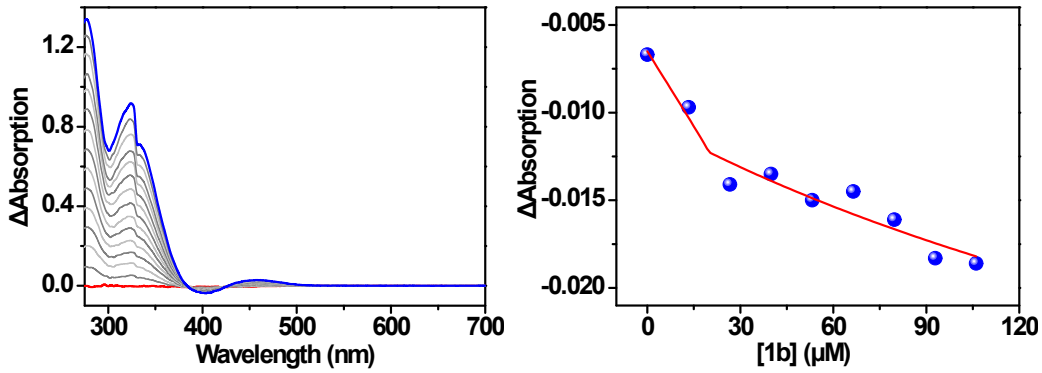

Figure S15. (Left) UV-Vis absorption difference spectra of Ni−**TPB** (40 μM) in CH_3CN/H_2O (1:1, pH 5.0) upon the addition of nitrosobenzene (**1**). (Right) Nonlinear fitting of titration curve showing the calculation of the associate constant (K_{a1} = 1.8 × 10^4 M^{-1}, K_{a2} = 8.4 × 10^4 M^{-1}). Absorption was recorded at 406 nm.

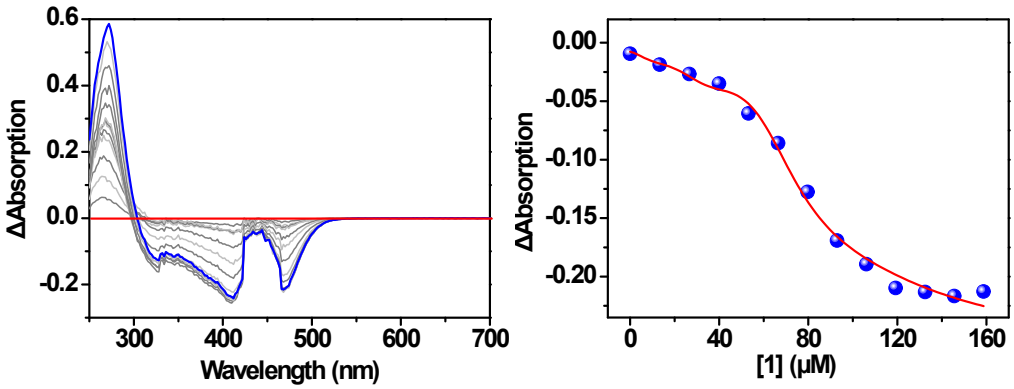

Figure S16. (Left) UV-Vis absorption difference spectra of Ni−**TPB** (20 μM) in CH_3CN/H_2O (1:1, pH 5.0) upon the addition of nitrosobenzene (**1a**). (Right) Nonlinear fitting of titration curve showing the calculation of the associate constant (K_{a1} = 5.2 × 10^3 M^{-1}, K_{a2} = 1.2 × 10^5 M^{-1}). Absorption was recorded at 450 nm.

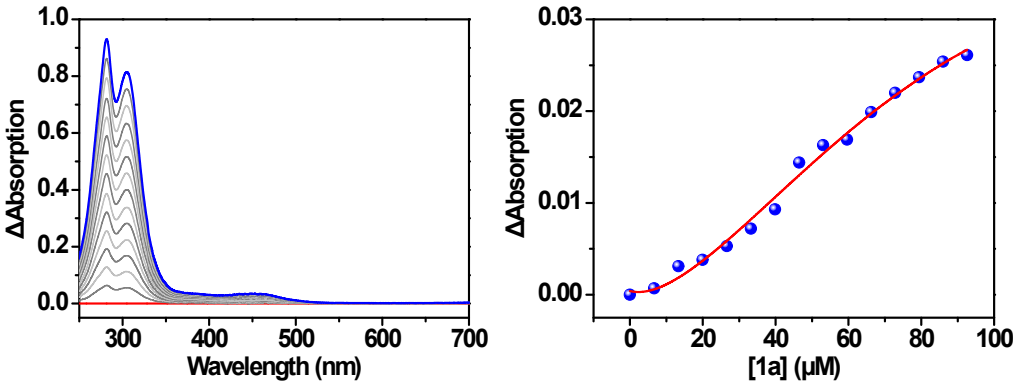

Figure S17. (Left) UV-Vis absorption difference spectra of Ni−**TPB** (20 μM) in CH_3CN/H_2O (1:1, pH 5.0) upon the addition of *N*-phenylhydroxylamine (**1b**). (Right) Nonlinear fitting of titration curve showing the calculation of the associate constant ($K_{a1} = 1.8 \times 10^4$ M^{-1}, $K_{a2} = 2.9 \times 10^5$ M^{-1}). Absorption was recorded at 446 nm.

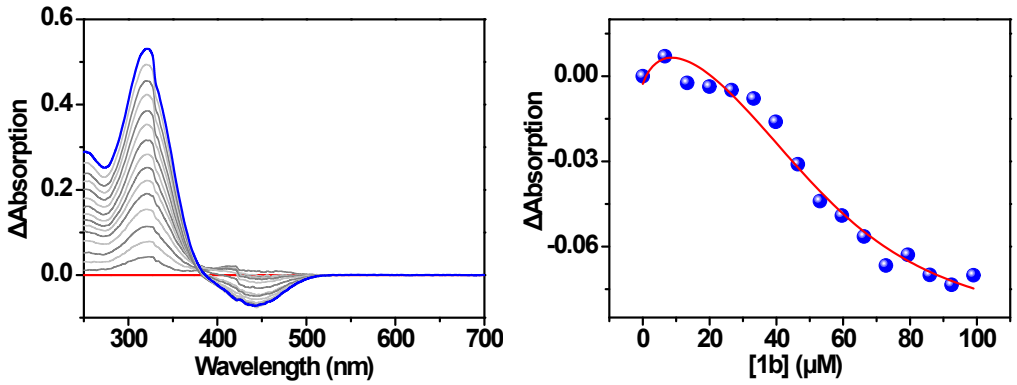

Figure S18. (Left) Family of UV-Vis of Zn−**TPB** (10 μM) in DMF/H_2O (1:1, pH 5.0) upon the addition of ATP. (Right) Nonlinear fitting of titration curve showing the calculation of the associate constant (K_a = 6.5 × 10^5 M^{-1}). Absorption was recorded at 450 nm.

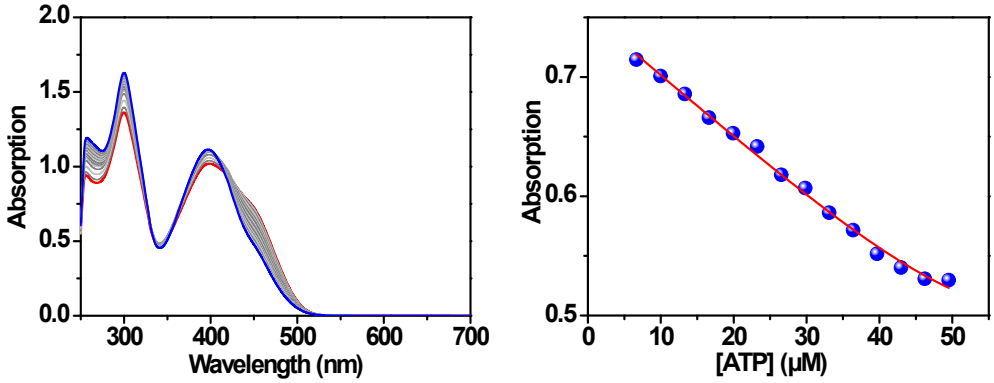

Figure S19. (Left) Family of UV-Vis of Ni−**TPB** (10 μM) in DMF/H_2O (1:1, pH 5.0) upon the addition of ATP. (Right) Nonlinear fitting of titration curve showing the calculation of the associate constant (K_a = 8.5 × 10^4 M^{-1}). Absorption was recorded at 390 nm.

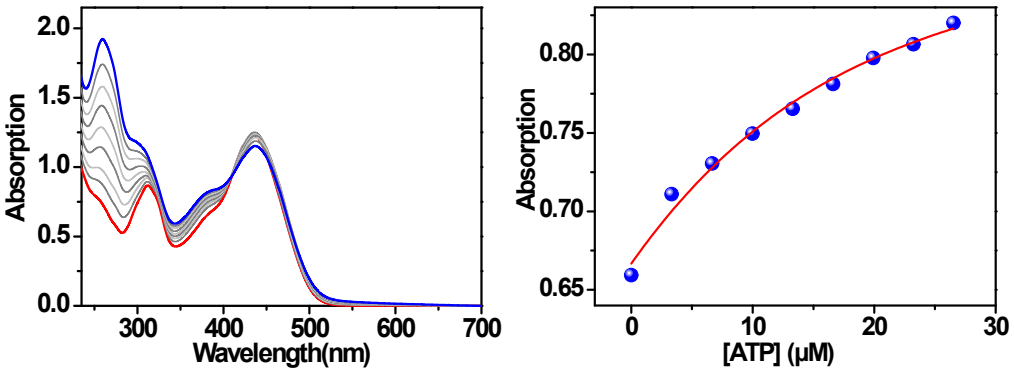

5.2 Luminescent Spectral Titrations

Figure S20. Luminescence spectra of Zn−**TPB** (10.0 μM) in CH_3CN/H_2O (1:1, pH 5.0) with exciting wavelength of 420 nm and 455 nm, respectively.

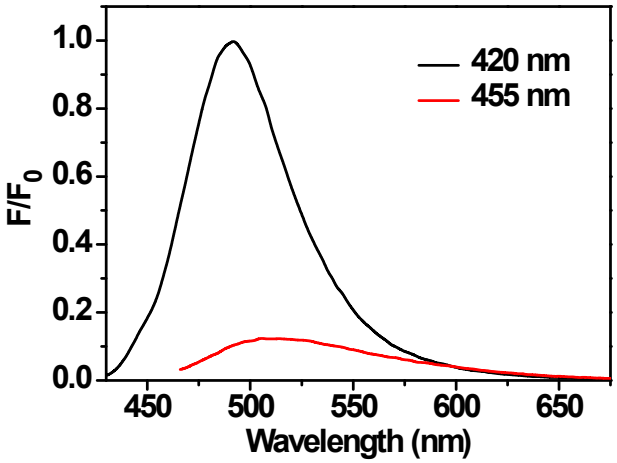

Figure S21. Luminescence spectra of $Ru(bpy)_3^{2+}$ (10.0 μM) in CH_3CN/H_2O (1:1, pH 5.0) with exciting wavelength at 420 nm and 455 nm, respectively.

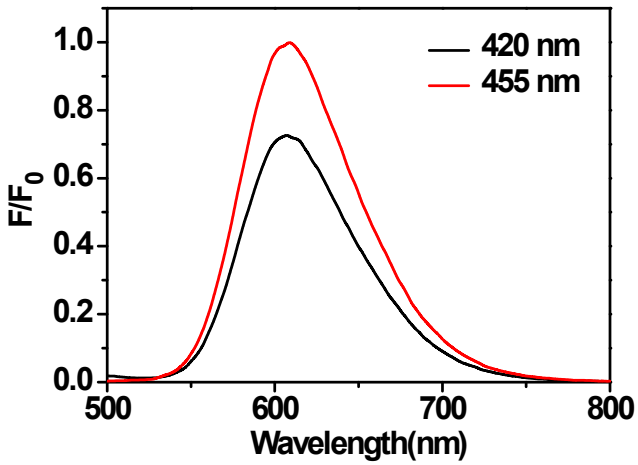

Figure S22. (Left) Family of luminescence spectra of Zn−**TPB** (10.0 μM) in CH_3CN/H_2O (1:1, pH 5.0) upon the addition of nitrobenzene (**1**) in CH_3CN solution; (Right) Nonlinear fitting of titration curve showing the calculation of the associate constant (K_{a1} = 8.6 × 10^3 M^{-1}, K_{a2} = 7.1 × 10^3 M^{-1}). Fluorescence intensity was recorded at 492 nm, and excited at 420 nm.

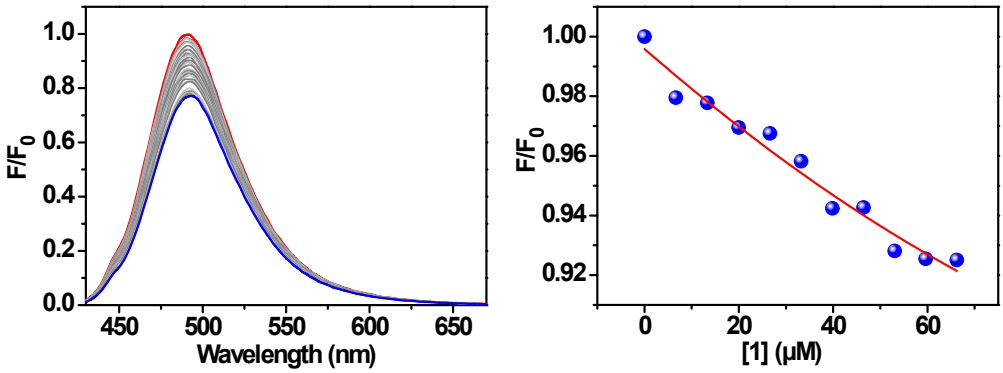

Figure S23. (Left) Family of luminescence spectra of Zn−**TPB** (10.0 μM) in CH_3CN/H_2O (1:1, pH 5.0) upon the addition of nitrosobenzene (**1a**) in CH_3CN solution; (Right) Nonlinear fitting of titration curve showing the calculation of the associate constant (K_{a1} = 1.1 × 10^4 M^{-1}, K_{a2} = 1.6 × 10^4 M^{-1}). Fluorescence intensity was recorded at 492 nm, and excited at 420 nm.

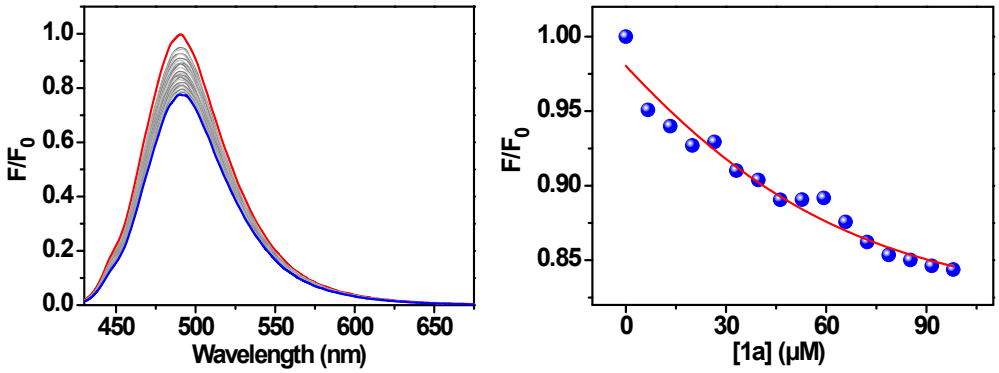

Figure S24. (Left) Family of luminescence spectra of Zn−**TPB** (10.0 μM) in CH_3CN/H_2O (1:1, pH 5.0) upon the addition of hydroxylamine (**1b**) in CH_3CN solution; (Right) Nonlinear fitting of titration curve showing the calculation of the associate constant (K_{a1} = 1.8 × 10^5 M^{-1}, K_{a2} = 3.3 × 10^3 M^{-1}). Fluorescence intensity was recorded at 492 nm, and excited at 420 nm.

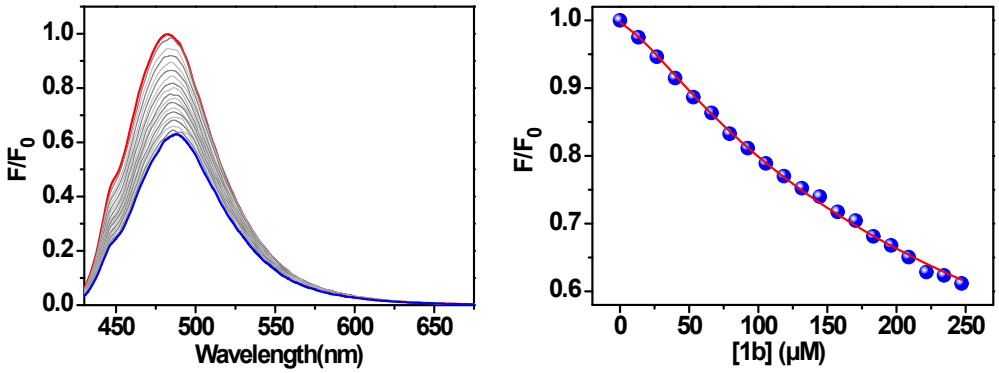

Figure S25. (Left) Family of luminescence spectra of Zn−**TPB** (10.0 μM) in CH_3CN/H_2O (1:1, pH 5.0) upon the addition of azoxybenzene (**1c**) in CH_3CN solution; (Right) Nonlinear fitting of titration curve showing the calculation of the associate constant (K_a = 3.7 × 10^2 M^{-1}). Fluorescence intensity was recorded at 492 nm, and excited at 420 nm.

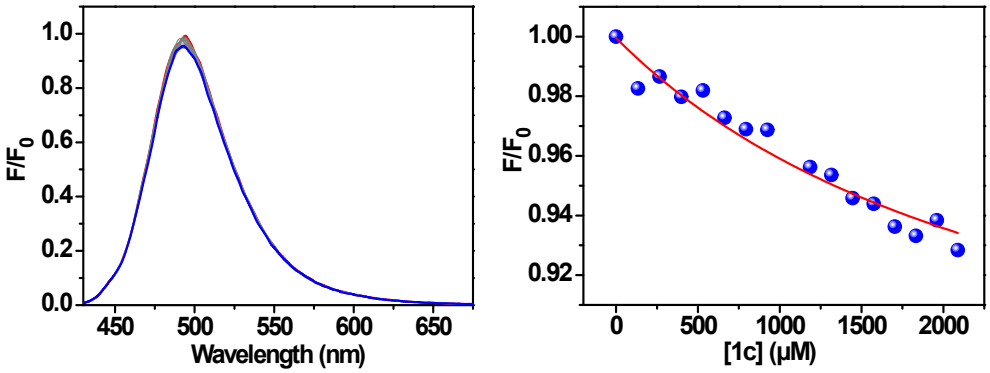

Figure S26. (Left) Family of luminescence spectra of Zn−**TPB** (10.0 μM) in CH_3CN/H_2O (1:1, pH 5.0) upon the addition of substrate **2** in CH_3CN solution; (Right) Stern-Volmer Fitting of titration curve showing the calculation of the associate constant (K = 5.3 × 10^2 M^{-1}). Fluorescence intensity was recorded at 492 nm, and excited at 420 nm.

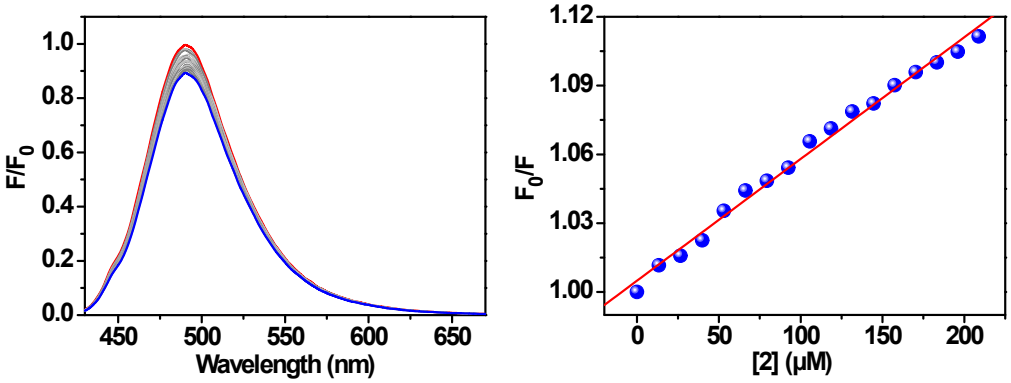

Figure S27. (Left) Family of luminescence spectra of Zn−**TPB** (10.0 μM) in CH_3CN/H_2O (1:1, pH 5.0) upon the addition of substrate **3** in CH_3CN solution; (Right) Nonlinear fitting of titration curve showing the calculation of the associate constant (K_a = 4.4 × 10^4 M^{-1}). Fluorescence intensity was recorded at 492 nm, and excited at 420 nm.

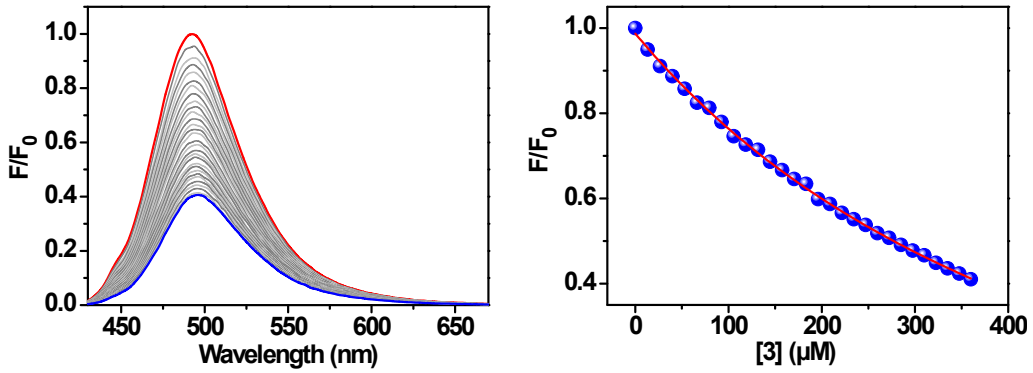

Figure S28. (Left) Family of luminescence spectra of Zn−**TPB** (10.0 μM) in DMF/H_2O (1:1, pH 5.0) upon the addition of **ATP** in water solution; (Right) Nonlinear fitting of titration curve showing the calculation of the associate constant (K_a = 7.8 × 10^5 M^{-1}). Fluorescence intensity was recorded at 506 nm, and excited at 420 nm.

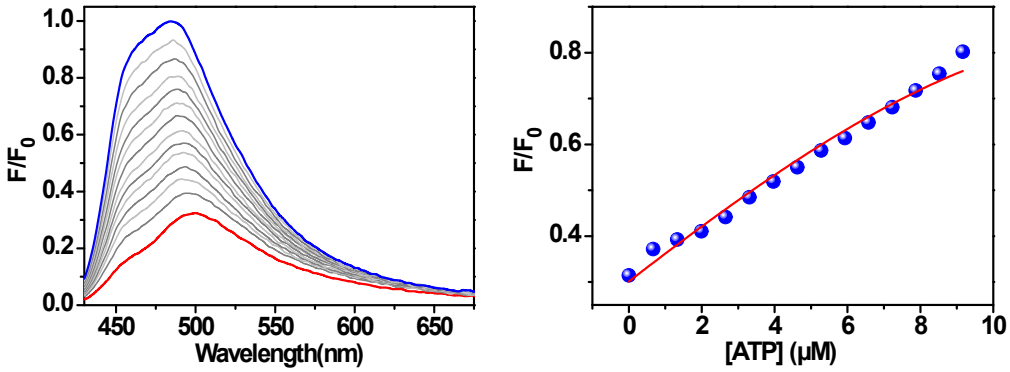

Figure S29. (Left) Family of luminescence spectra of $Ru(bpy)_3^{2+}$ (10.0 μM) in CH_3CN/H_2O (1:1, pH 5.0) solution upon the addition of Ni−**TPB** in CH_3CN solution; (Right) Stern-Volmer Fitting of titration curve showing the calculation of the associate constant (K = 3.3 × 10^5 M^{-1}). Fluorescence intensity was recorded at 610 nm, and excited at 455 nm.

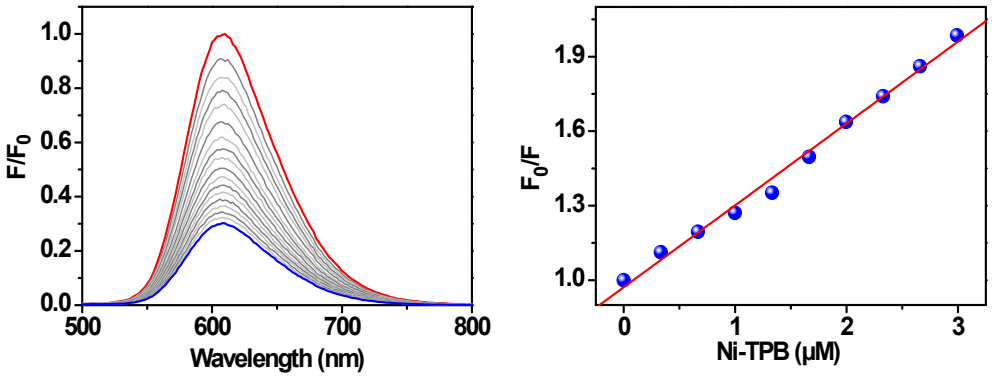

Figure S30. Family of luminescence spectra of Zn−**TPB** (10.0 μM) in CH_3CN/H_2O (1:1, pH 5.0) upon the addition of substrate **1** (0.1 mM), **1a** (0.1 mM) and **1b** (0.1 mM) in CH_3CN solution; Fluorescence intensity was excited at 420 nm.

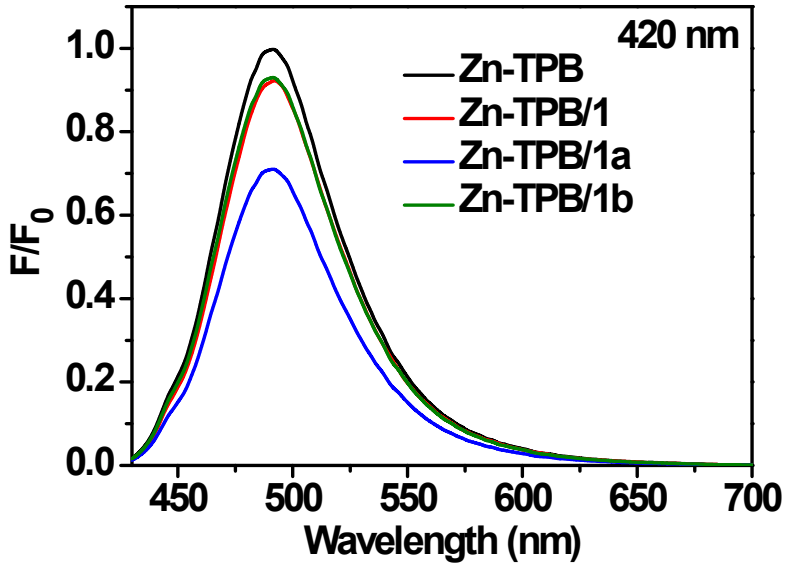

Figure S31. (Left) Family of luminescence spectra of $Ru(bpy)_3^{2+}$ (100 μM), Zn−**TPB**/$Ru(bpy)_3^{2+}$ (10.0/100 μM) and Ni−**TPB**/$Ru(bpy)_3^{2+}$ (10.0/100 μM) in CH_3CN/H_2O (1:1, pH 5.0); Fluorescence intensity was excited at 420 nm. (Right) Family of luminescence lifetime of $Ru(bpy)_3^{2+}$ (100 μM), Zn−**TPB**/$Ru(bpy)_3^{2+}$ (10.0/100 μM) and Ni−**TPB**/$Ru(bpy)_3^{2+}$ (10.0/100 μM) in CH_3CN/H_2O (1:1, pH 5.0); Fluorescence intensity was excited at 470 nm.

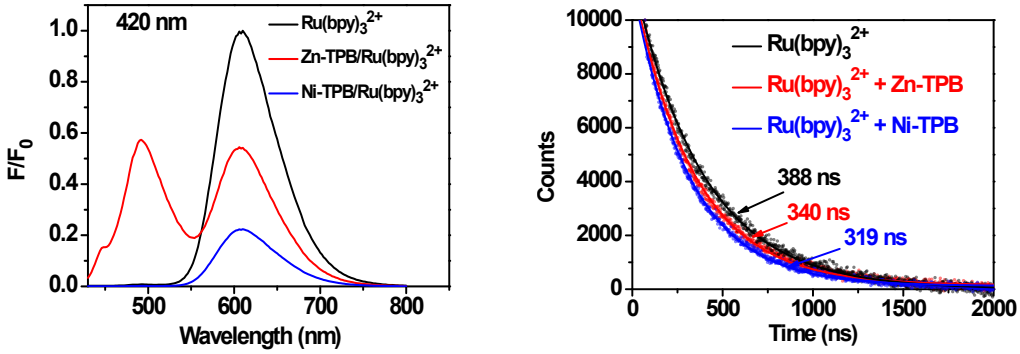

5.3 Isothermal Titration Calorimetry

The ITC experiments were performed by an isothermal titration microcalorimeter at atmospheric pressure and 25.00 °C, giving the association constants (*K*) and the thermodynamic parameters. A solution of guest in a 0.250 mL syringe was sequentially injected with stirring at 250 rpm into a solution of the host in the sample cell (1.30 mL volume). All the thermodynamic parameters reported in this work were obtained by using the 'independent' model.

Figure S32. Microcalorimetric titration of Zn−**TPB** with nitrobenzene (**1**) in CH_3CN/H_2O (1:1, pH 5.0) solution at 298.15K. (a) Raw data for sequential 25 injections (8 μL per injection) of **1** solution (10.0 mM) injecting into Zn−**TPB** solution (0.5 mM). (b) Apparent reaction heat obtained from the integration of calorimetric traces.

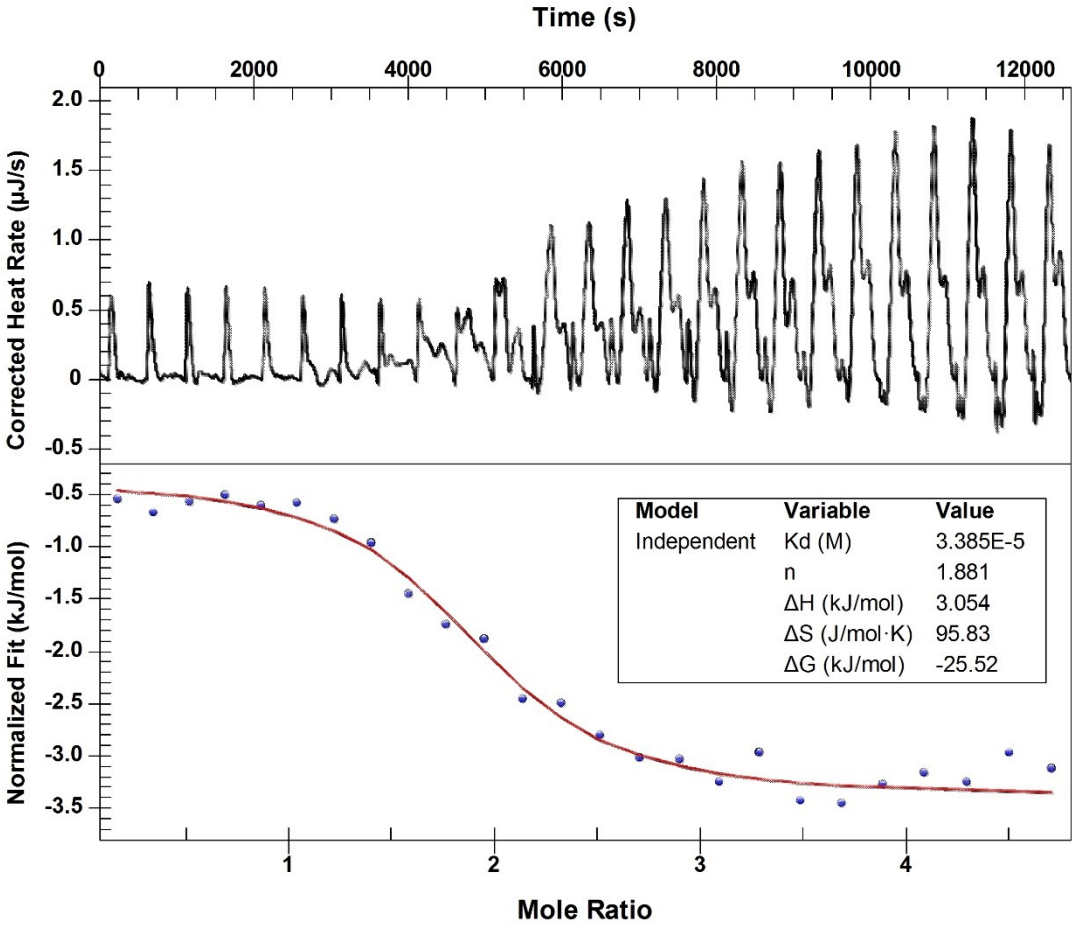

Figure S33. Microcalorimetric titration of Zn−**TPB** with intermediate nitrosobenzene (**1a**) in CH_3CN/H_2O (1:1, pH 5.0) solution at 298.15K. (a) Raw data for sequential 25 injections (10 μL per injection) of **1a** solution (10.0 mM) injecting into Zn−**TPB** solution (0.5 mM). (b) Apparent reaction heat obtained from the integration of calorimetric traces.

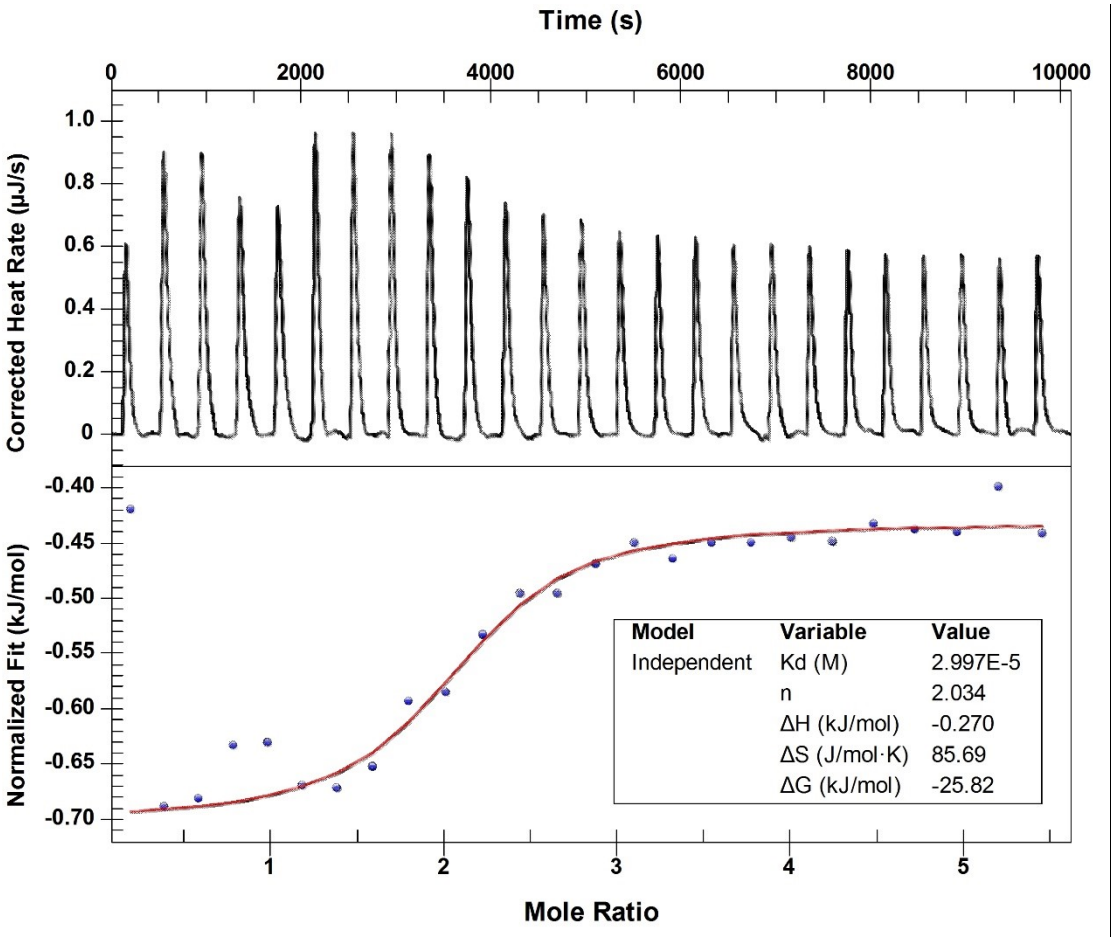

Figure S34. Microcalorimetric titration of Zn−**TPB** with intermediate phenylhydroxylamine (**1b**) in CH_3CN/H_2O (1:1, pH 5.0) solution at 298.15K. (a) Raw data for sequential 21 injections (10 μL per injection) of **1b** solution (2.0 mM) injecting into Zn−**TPB** solution (0.1 mM). (b) Apparent reaction heat obtained from the integration of calorimetric traces.

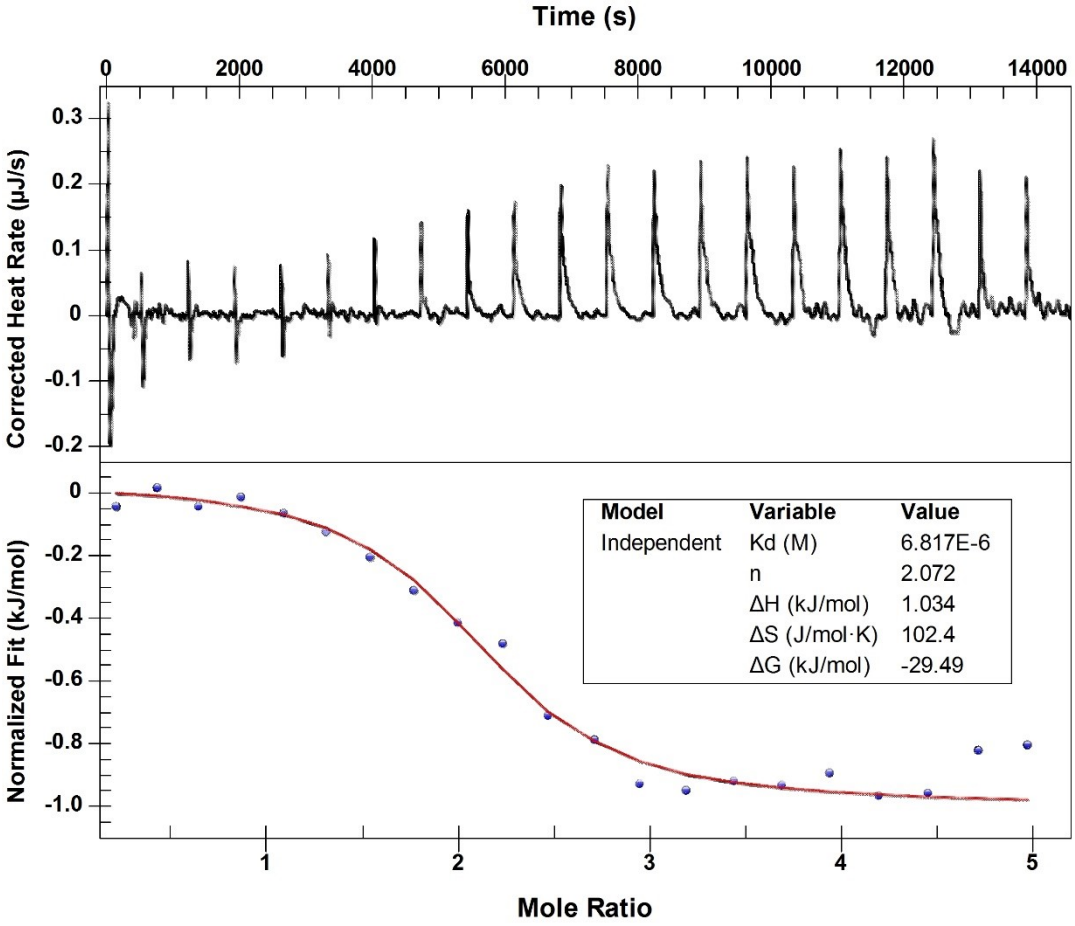

Figure S35. Microcalorimetric titration of Zn−**TPB** with substrate **2** in CH_3CN/H_2O (1:1, pH 5.0) solution at 298.15K. (a) Raw data for sequential 30 injections (8 μL per injection) of **2** solution (10.0 mM) injecting into Zn−**TPB** solution (1.0 mM). (b) Apparent reaction heat obtained from the integration of calorimetric traces.

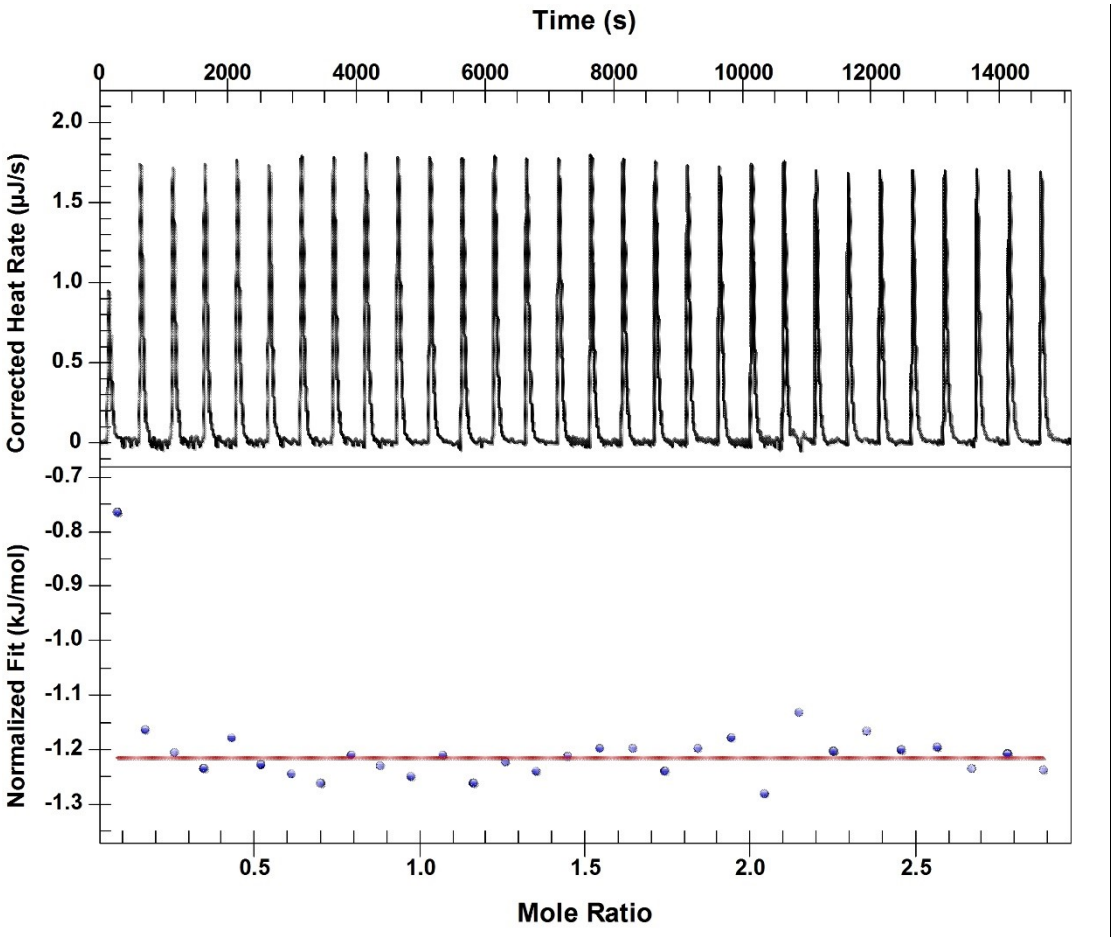

Figure S36. Microcalorimetric titration of Zn−**TPB** with substrate 1-nitrpyrene (**3**) in CH_3CN solution at 298.15K. (a) Raw data for sequential 30 injections (8 μL per injection) of **3** solution (7.0 mM) injecting into Zn−**TPB** solution (1.0 mM). (b) Apparent reaction heat obtained from the integration of calorimetric traces.

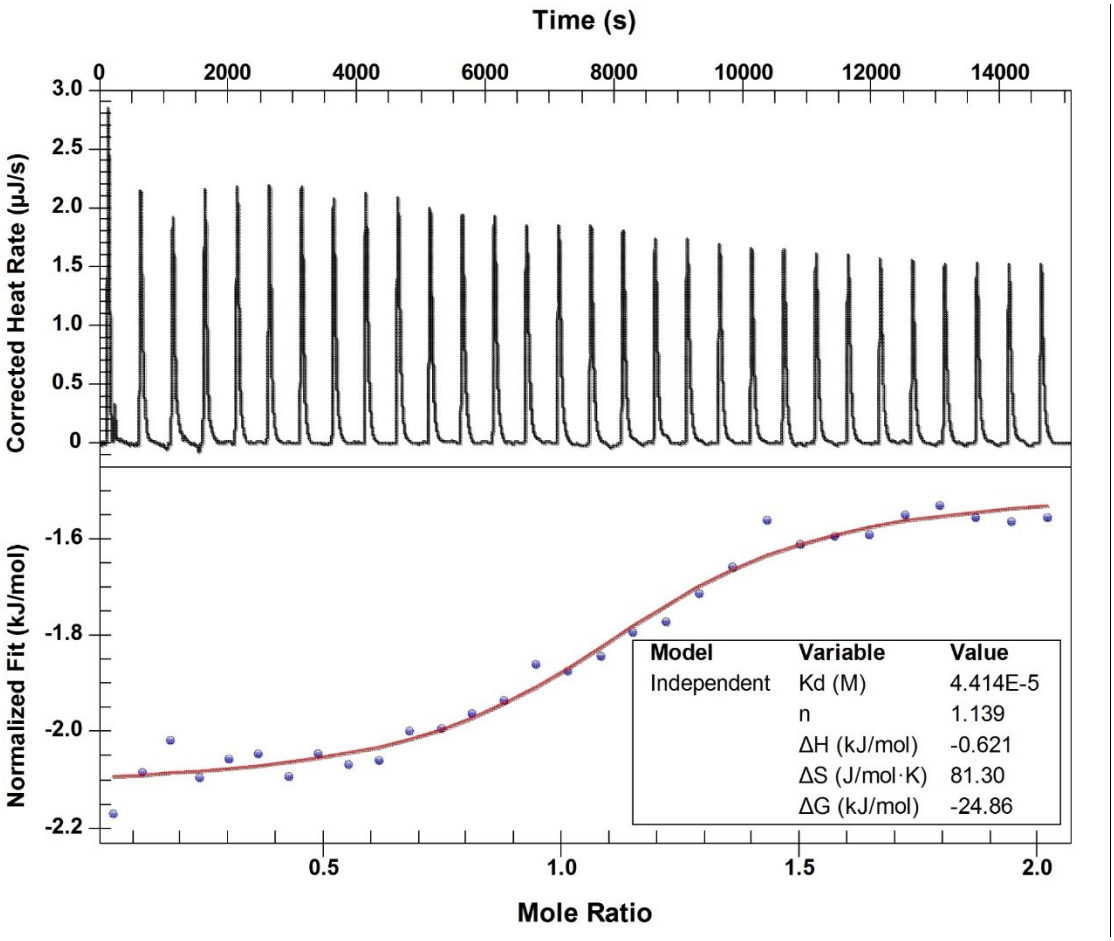

Figure S37. Microcalorimetric titration of Zn−**TPB** with guest **ATP** in DMF/H_2O solution at 298.15K. (Top) Raw data for sequential 30 injections (8 μL per injection) of **ATP** solution (0.5 mM) injecting into Zn−**TPB** solution (0.05 mM). (Bottom) Apparent reaction heat obtained from the integration of calorimetric traces.

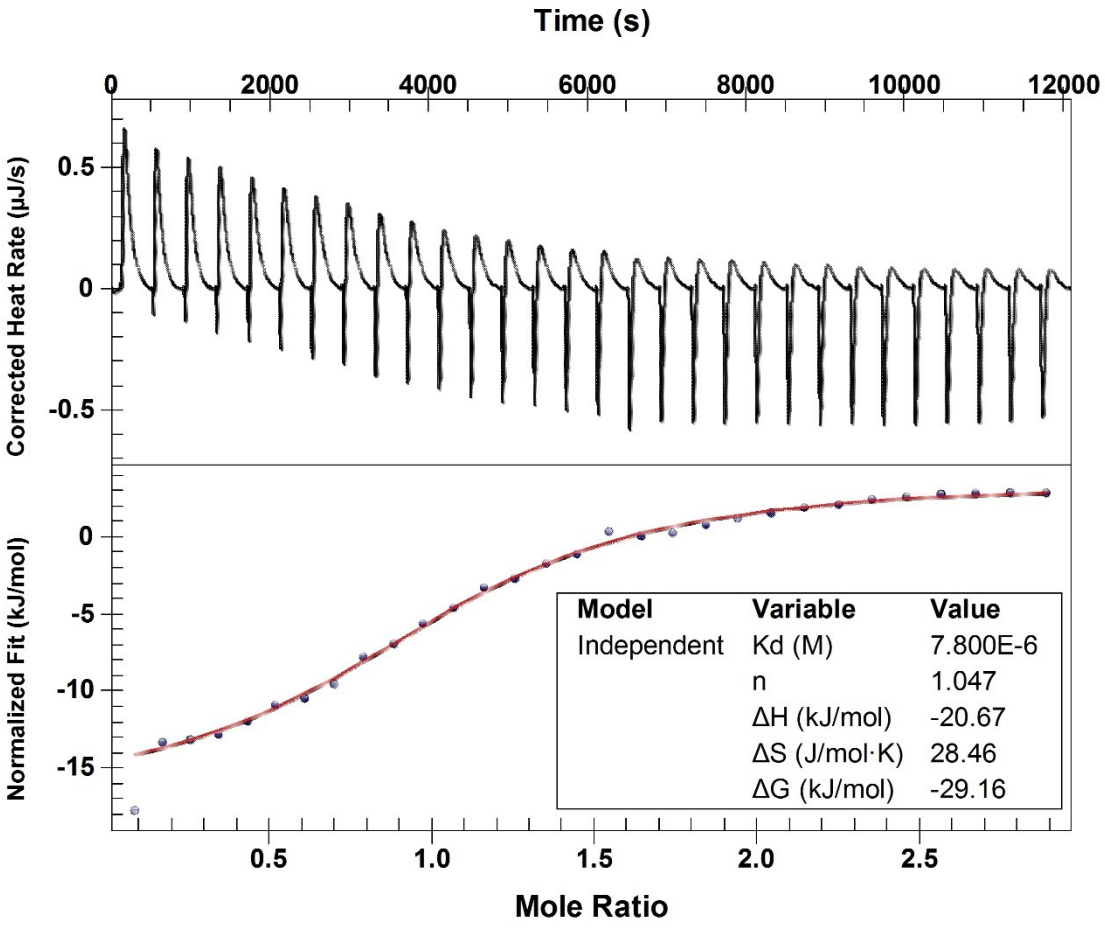

Figure S38. Microcalorimetric titration of Ni−**TPB** with nitrobenzene (**1**) in CH_3CN/H_2O (1:1, pH 5.0) solution at 298.15K. (a) Raw data for sequential 30 injections (8 μL per injection) of **1** solution (5.0 mM) injecting into Ni−**TPB** solution (0.25 mM). (b) Apparent reaction heat obtained from the integration of calorimetric traces.

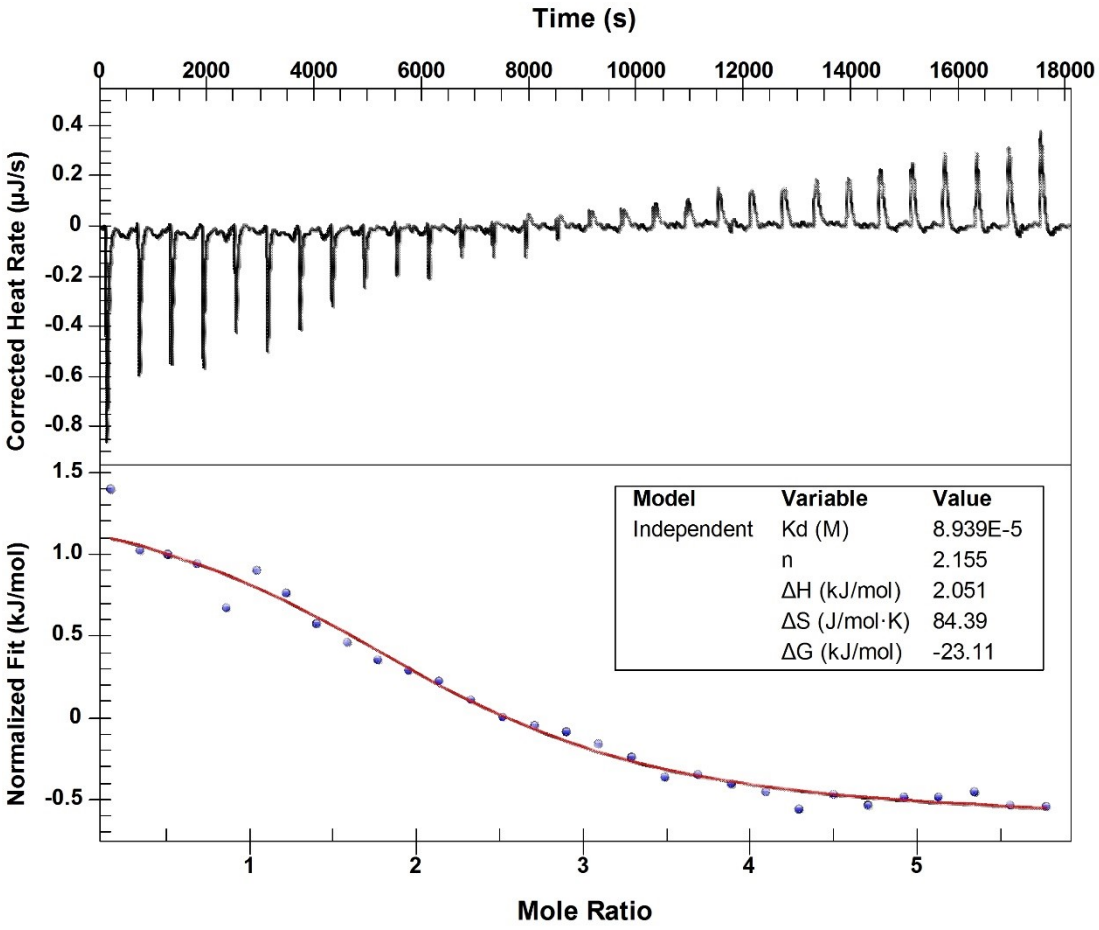

Figure S39. Microcalorimetric titration of Ni−**TPB** with intermediate nitrosobenzene (**1a**) in CH_3CN/H_2O (1:1, pH 5.0) solution at 298.15K. (a) Raw data for sequential 25 injections (10 μL per injection) of **1a** solution (4.5 mM) injecting into Ni−**TPB** solution (0.25 mM). (b) Apparent reaction heat obtained from the integration of calorimetric traces.

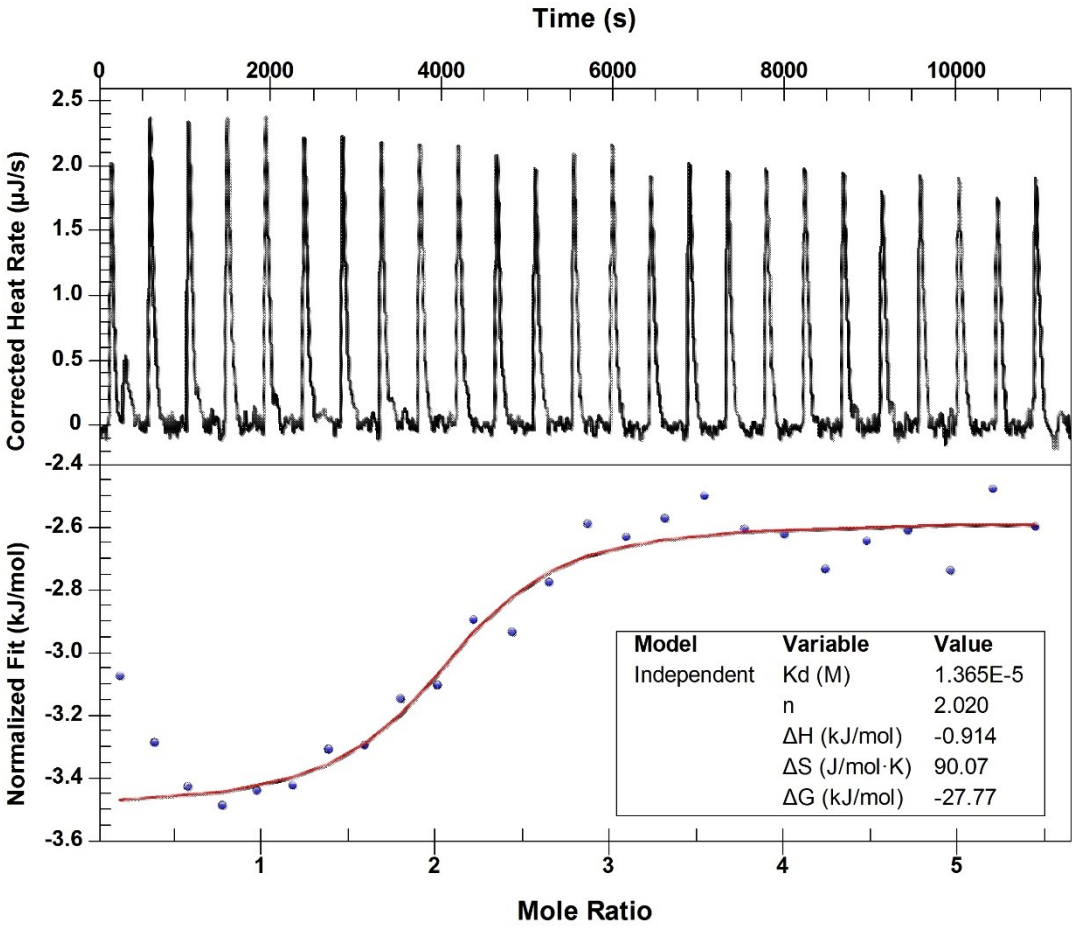

Figure S40. Microcalorimetric titration of Ni−**TPB** with intermediate phenylhydroxylamine (**1b**) in CH_3CN/H_2O (1:1, pH 5.0) solution at 298.15K. (a) Raw data for sequential 25 injections (10 μL per injection) of **1b** solution (2.0 mM) injecting into Ni−**TPB** solution (0.15 mM). (b) Apparent reaction heat obtained from the integration of calorimetric traces.

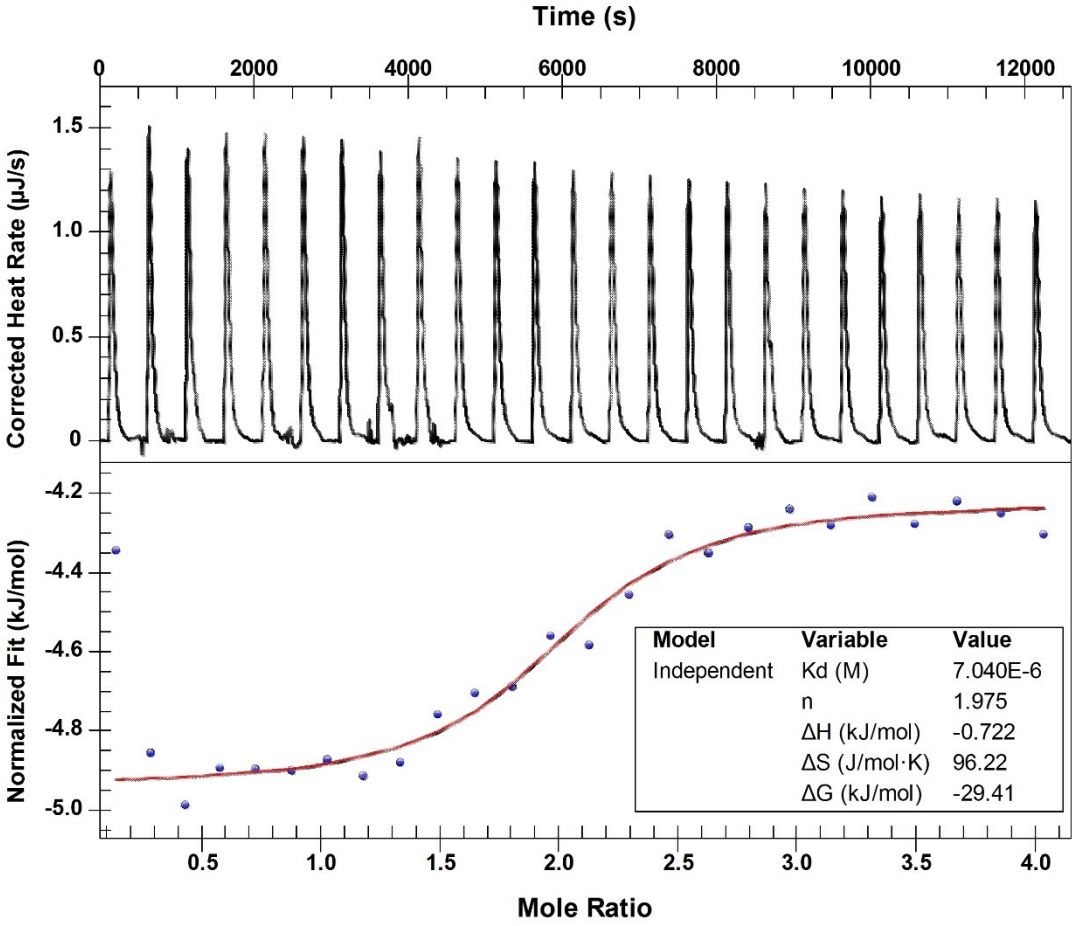

Figure S41. Microcalorimetric titration of Ni−**TPB** with product azoxybenzene (**1c**) in CH_3CN/H_2O (1:1, pH 5.0) solution at 298.15K. (a) Raw data for sequential 25 injections (10 μL per injection) of **1c** solution (5.0 mM) injecting into Ni−**TPB** solution (0.2 mM). (b) Apparent reaction heat obtained from the integration of calorimetric traces.

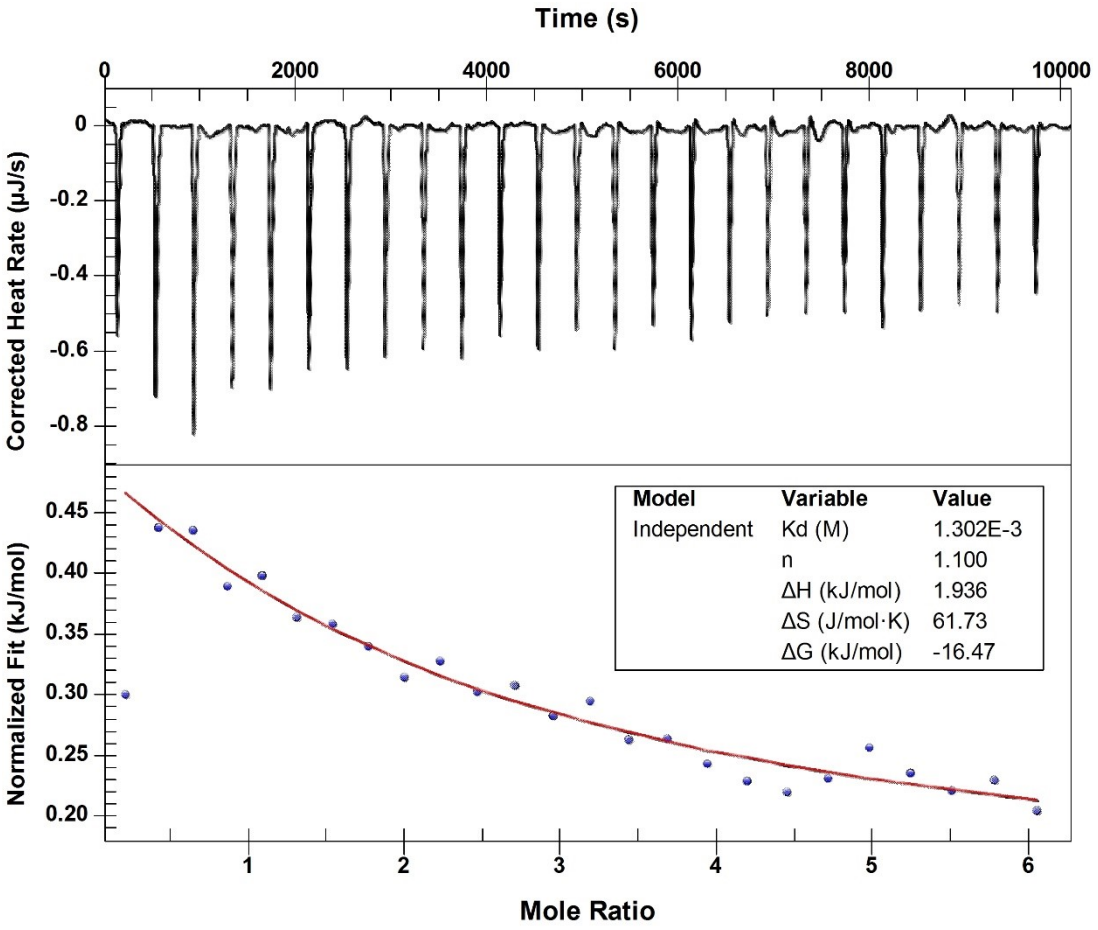

Figure S42. Microcalorimetric titration of Ni−**TPB** with substrate **2** in CH_3CN/H_2O (1:1, pH 5.0) solution at 298.15K. (a) Raw data for sequential 25 injections (10 μL per injection) of **2** solution (5.0 mM) injecting into Ni−**TPB** solution (0.5 mM). (b) Apparent reaction heat obtained from the integration of calorimetric traces.

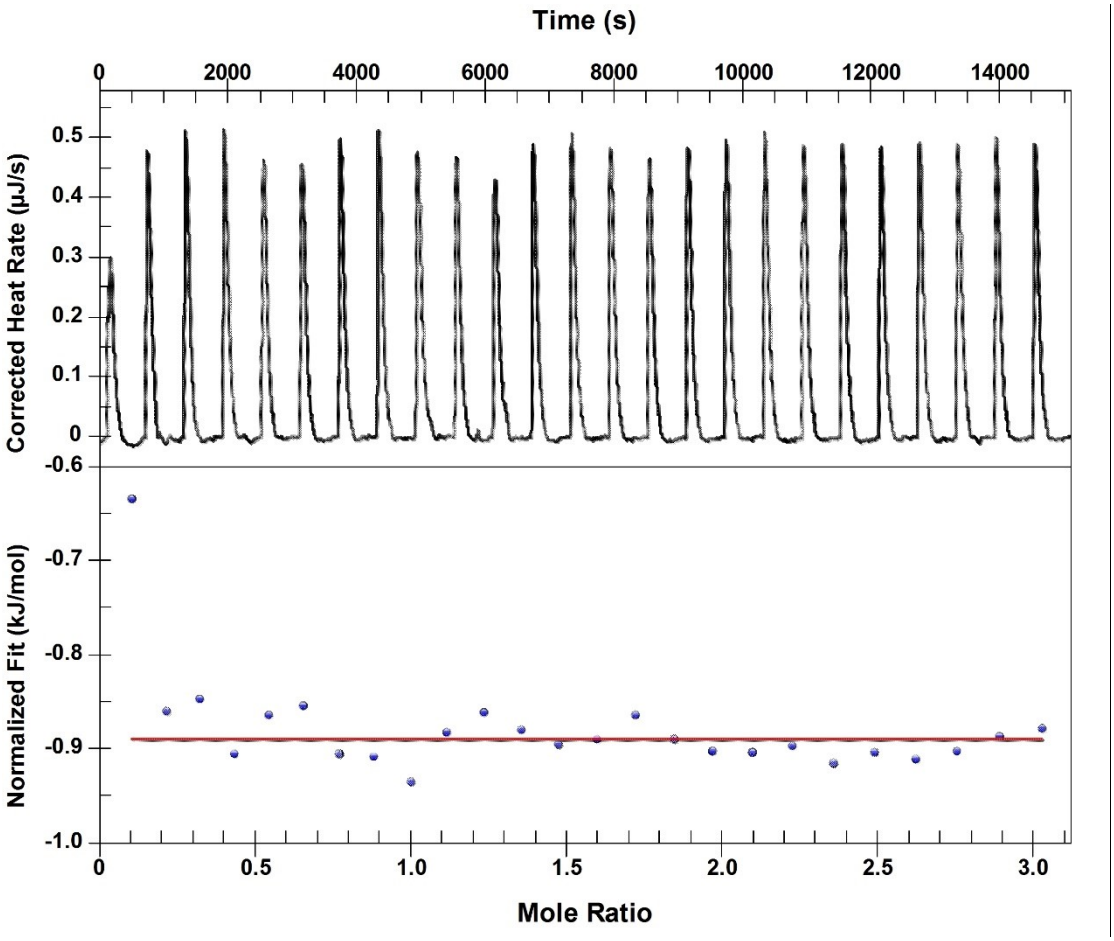

Figure S43. Microcalorimetric titration of Ni−**TPB** with substrate 1-nitropyrene (**3**) in CH_3CN/H_2O (1:1, pH 5.0) solution at 298.15K. (a) Raw data for sequential 20 injections (8 μL per injection) of **3** solution (7.0 mM) injecting into Ni−**TPB** solution (0.5 mM). (b) Apparent reaction heat obtained from the integration of calorimetric traces.

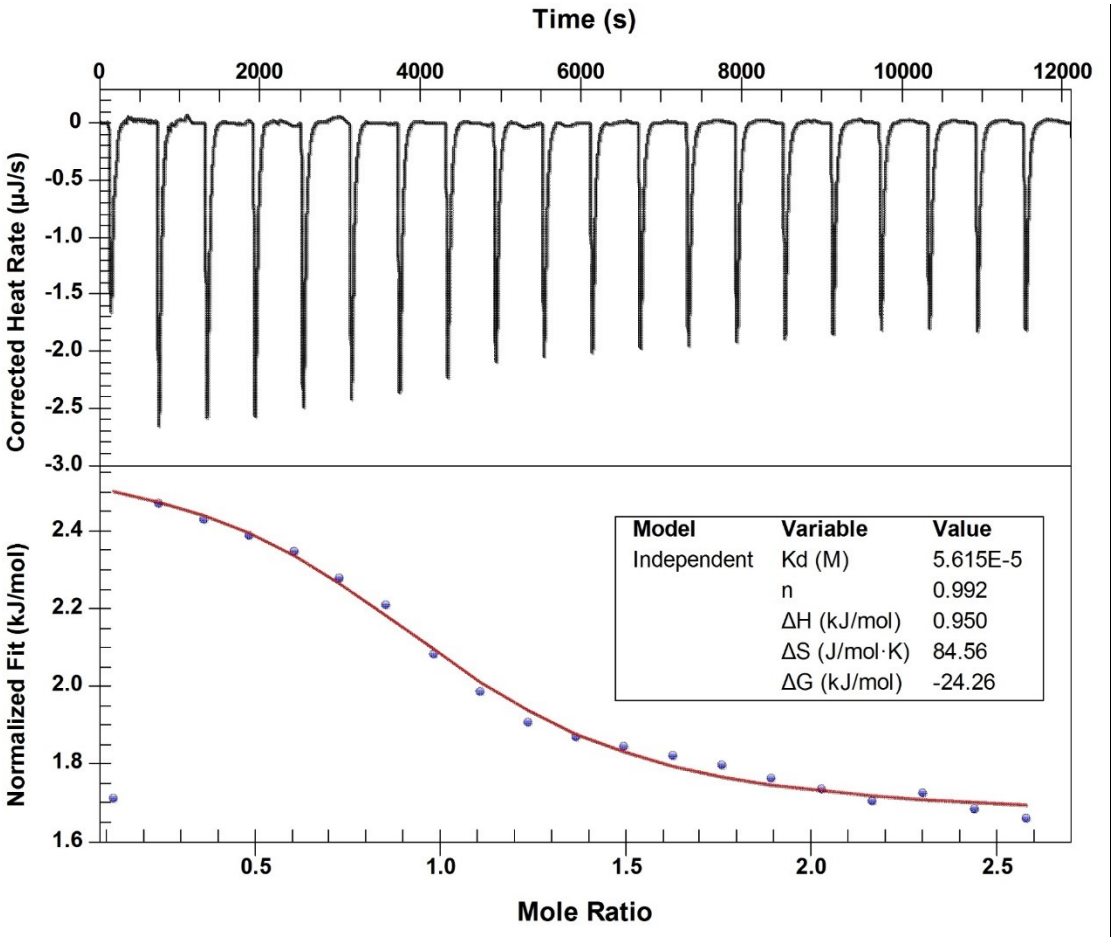

Figure S44. Microcalorimetric titration of Ni−**TPB** with guest **ATP** in DMF/H_2O solution at 298.15K. (Top) Raw data for sequential 25 injections (10 μL per injection) of **ATP** solution (1.0 mM) injecting into Ni−**TPB** solution (0.1 mM). (Bottom) Apparent reaction heat obtained from the integration of calorimetric traces.

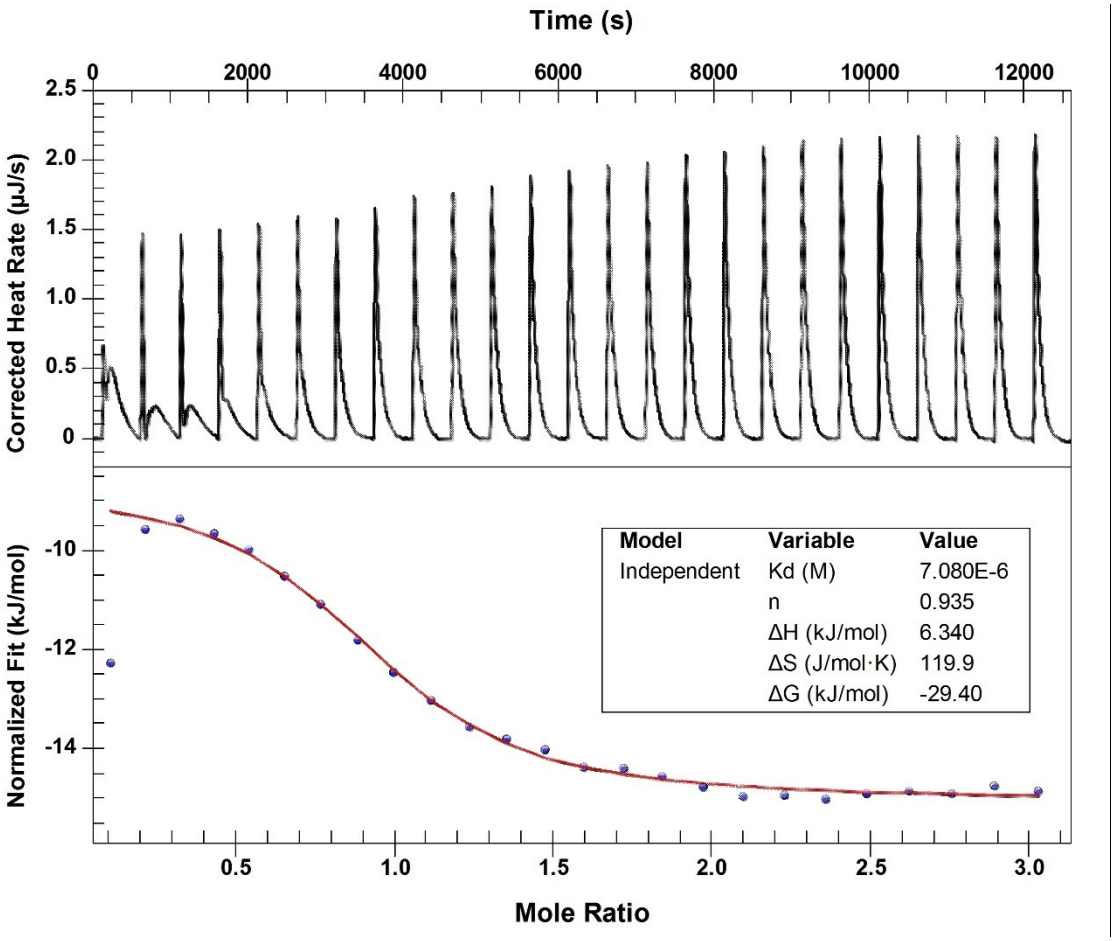

Figure S45. Microcalorimetric titration of Ni−**TPB** with substrate 2,6-dimethylpyridine in CH_3CN/H_2O (1:1, pH 5.0) solution at 298.15K. (a) Raw data for sequential 30 injections (8 μL per injection) of 2,6- dimethylpyridine solution (12.0 mM) injecting into Ni−**TPB** solution (0.5 mM). (b) Apparent reaction heat obtained from the integration of calorimetric traces.

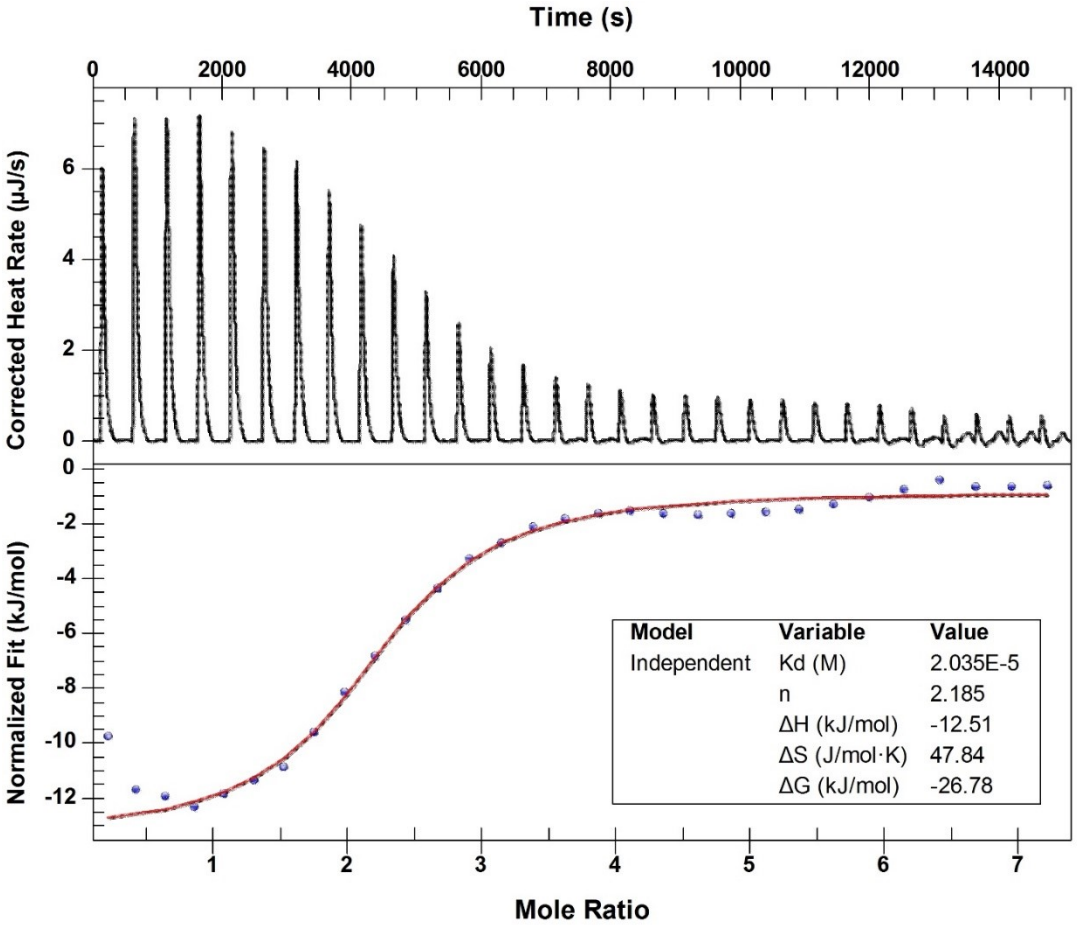

NMR Spectra of the host-guest complexes

Figure S46. ^{1}H-NMR spectrum (400 MHz) of **1** (10 mM, line 1), Zn−**TPB** (2.0 mM, line 2) with addition of **1** (0.6 mM for each line) in DMSO-d_6.

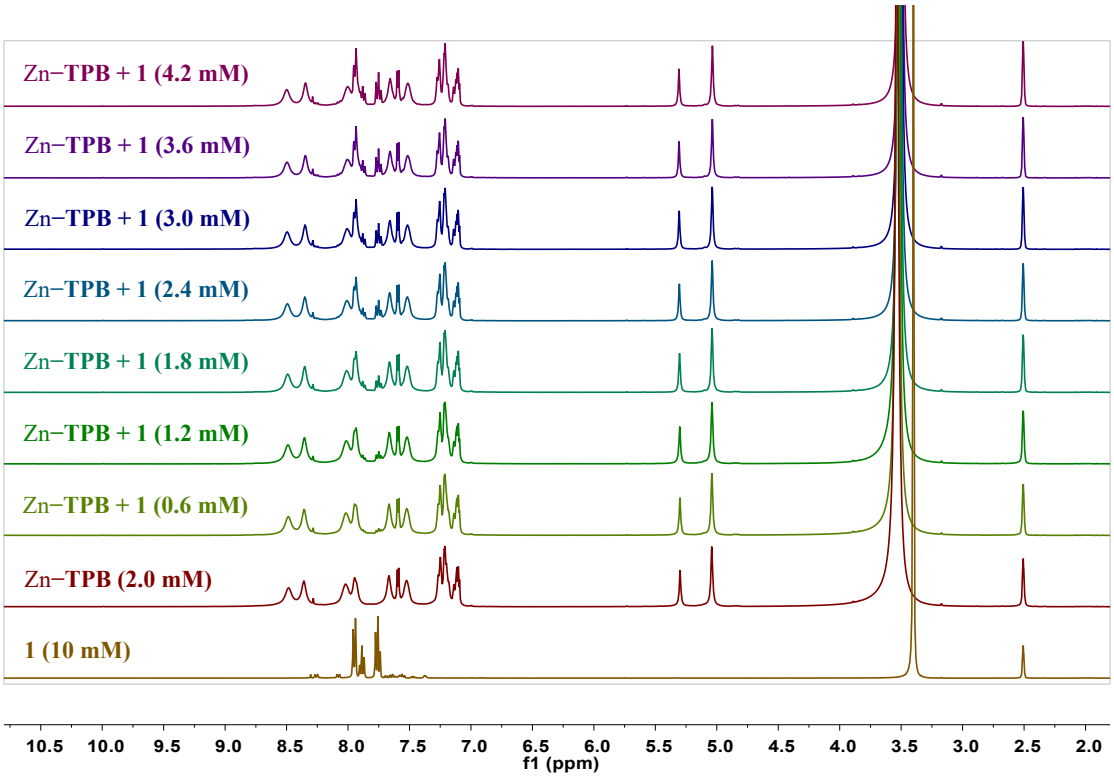

Figure S47. ^{1}H-NMR spectrum (400 MHz) of **1b** (10 mM, line 1), Zn−**TPB** (2.0 mM, line 2) with addition of **1b** (0.5 mM for each line) in DMSO-d_6. (bottom) Details of uphill and downhill of the protons of the molecular square.

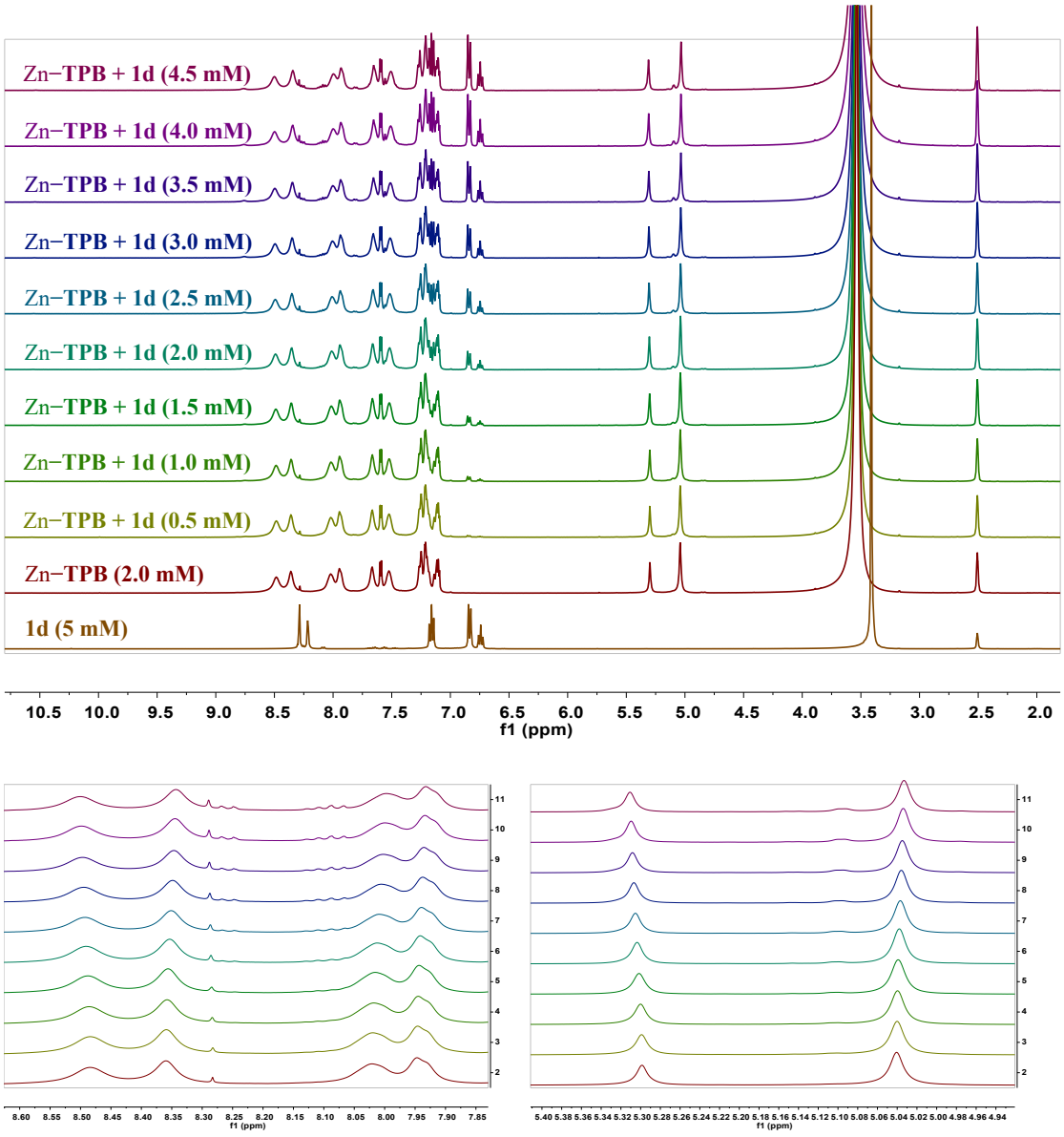

Figure S48. ^{1}H-NMR spectrum (400 MHz) of **1c** (5 mM, line 1), Zn−**TPB** (2.0 mM, line 2) with addition of **1c** (0.4 mM for each line) in DMSO-d_6.

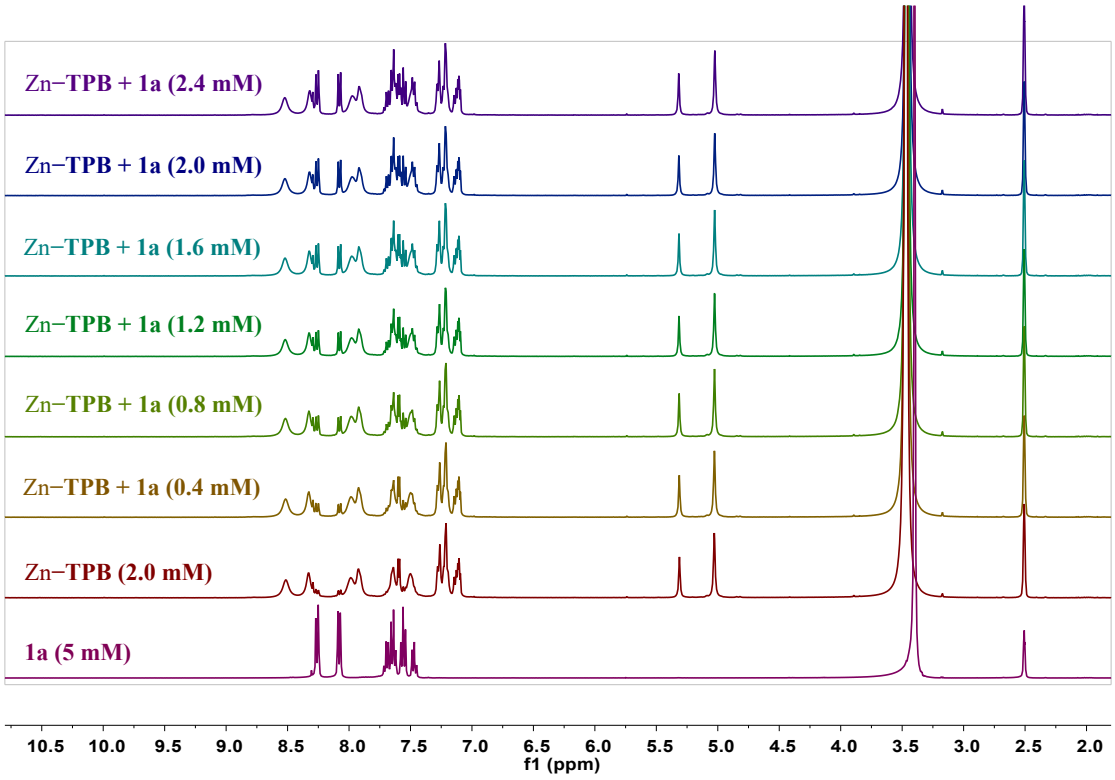

Figure S49. ^{1}H-NMR spectrum (400 MHz) of **ATP** (10 mM, line 1) in D_2O and Zn−**TPB** (2.0 mM, line 2) with addition of **ATP** (0.4 mM for each line) in DMSO-d_6/ D_2O. (bottom) Details of uphill and downhill of the protons of the molecular square.

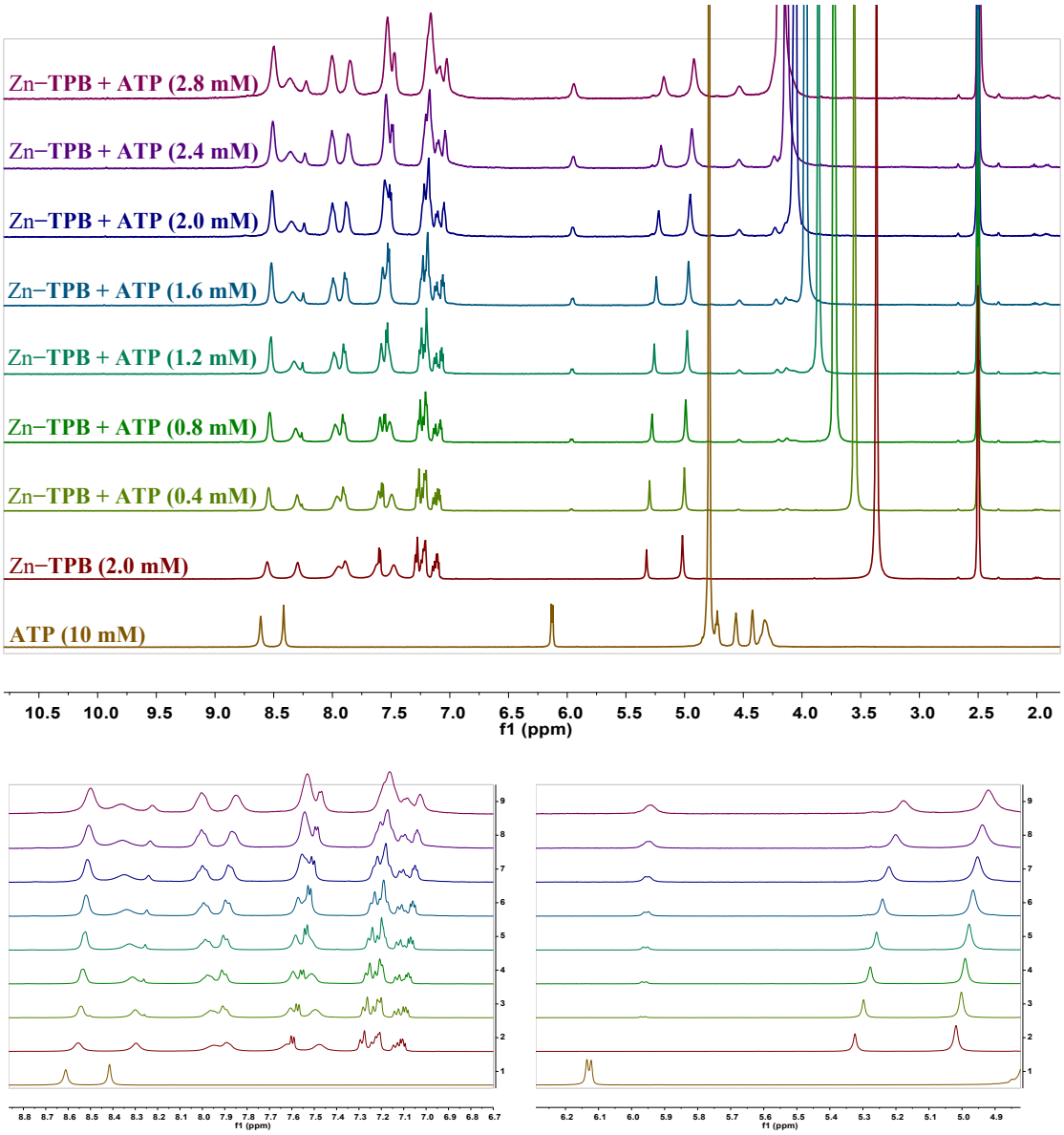

Figure S50. DOSY spectrum of Zn−**TPB** (2.0 mM) in DMSO-d_6.

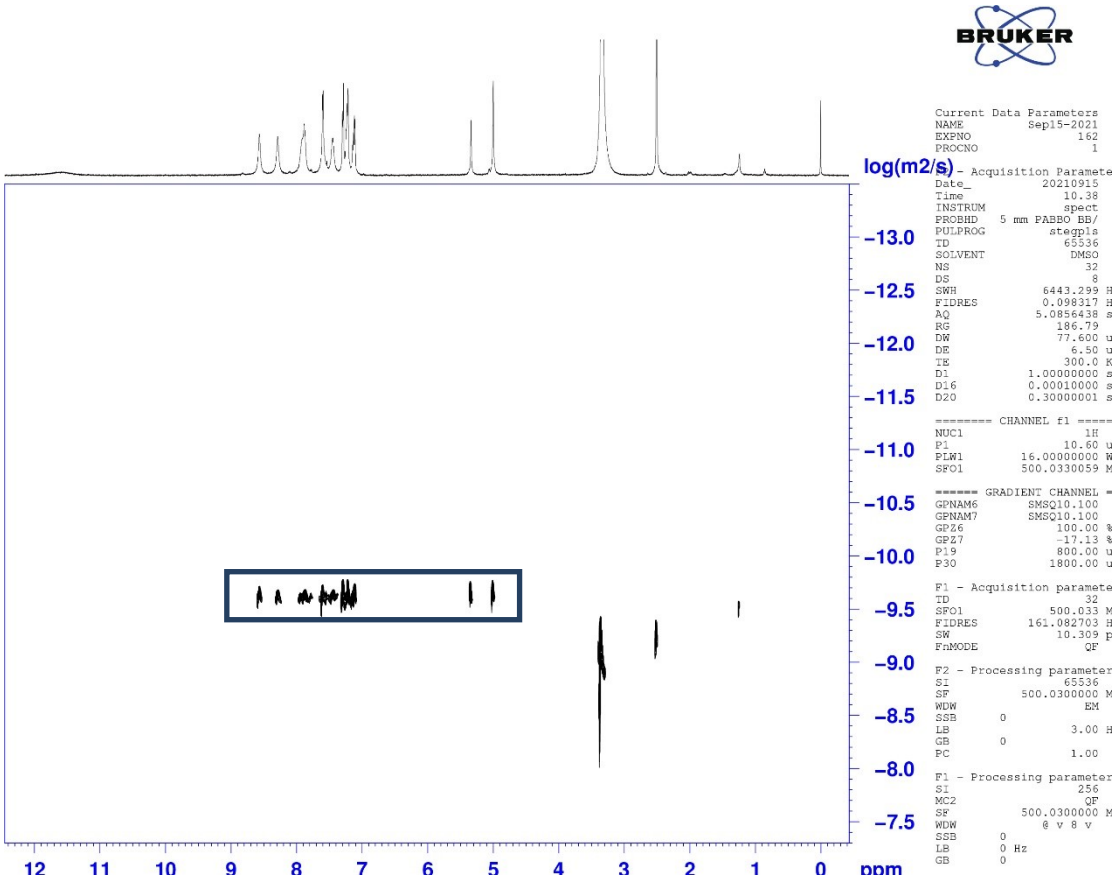

Figure S51. DOSY spectrum of Zn−**TPB** (2.0 mM) with **1** (4.0 mM) in DMSO-d_6.

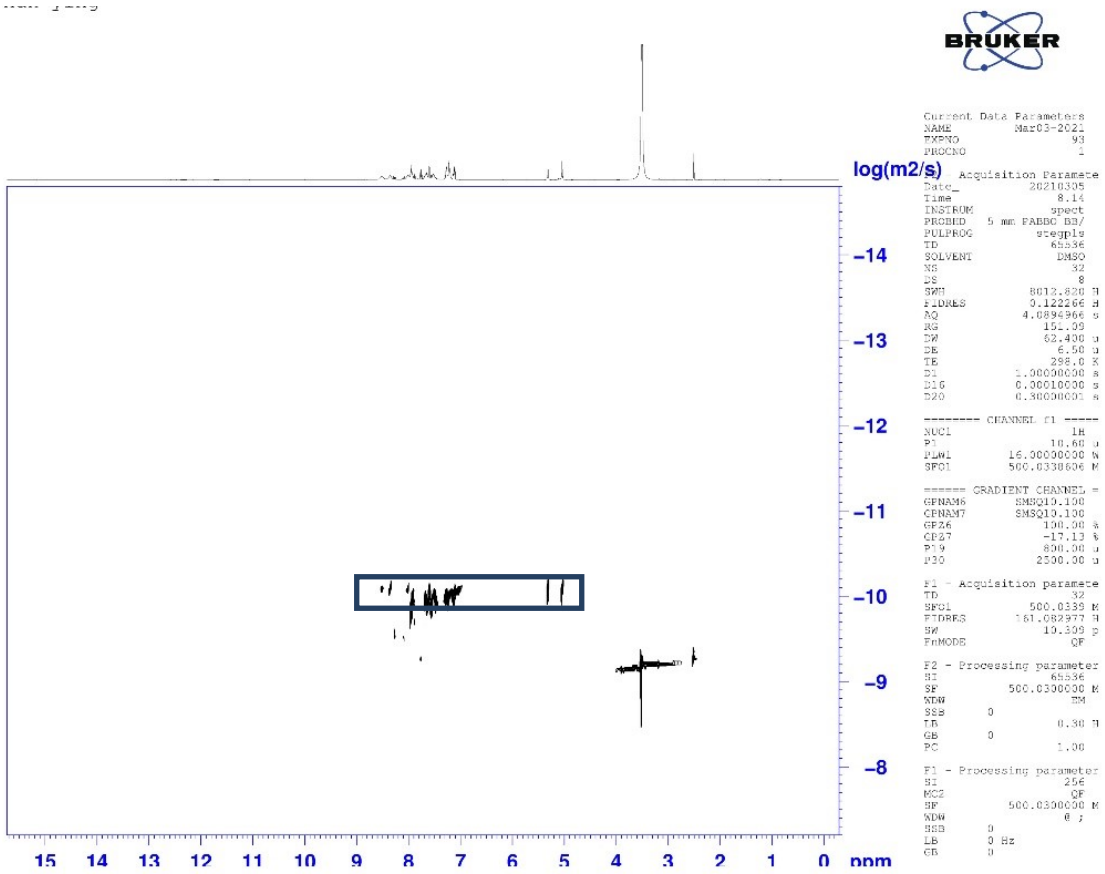

Figure S52. DOSY spectrum of Zn−**TPB** (2.0 mM) with **1c** (2.0 mM) in DMSO-d_6.

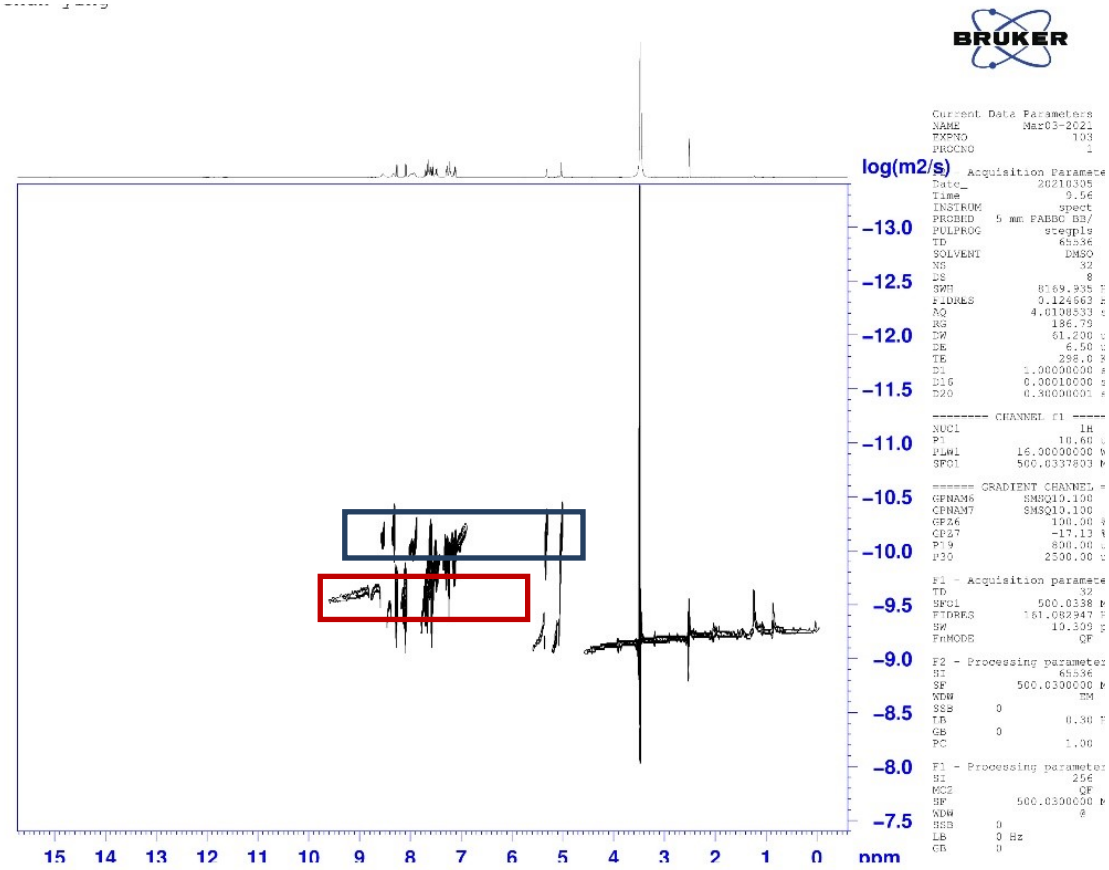

Figure S53. DOSY spectrum of Zn−**TPB** (2.0 mM) with **ATP** (2.0 mM) in DMSO-d_6/D_2O.

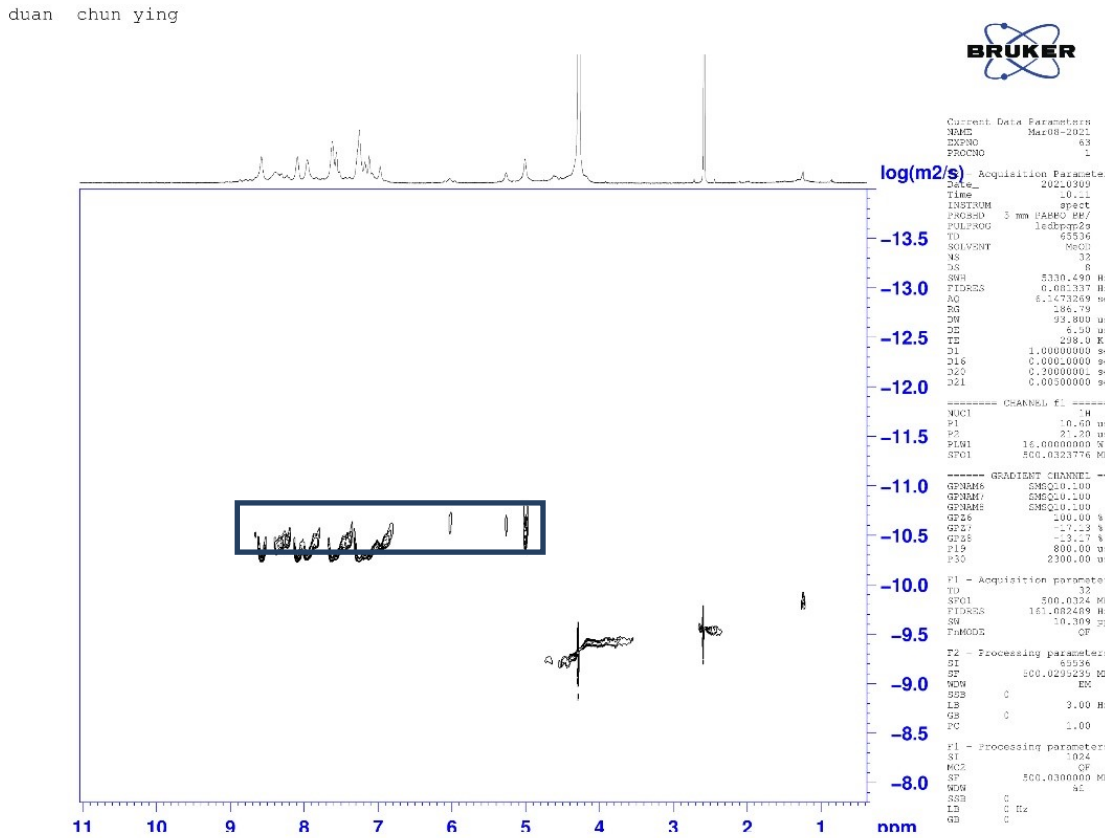

6. Data Relative to Reduction Reaction.

Figure S54. Initial formation rates of azoxy and amine compounds in the system containing Zn–**TPB** (50 μM), $Ru(bpy)_3^{2+}$ (0.5 mM) and $HCOOH/H_2A$ (0.05/0.1 M) in a CH_3CN/H_2O solution (1:1, pH 5.0) with different substrates (10.0 mM) under 420 nm LED light irradiation.

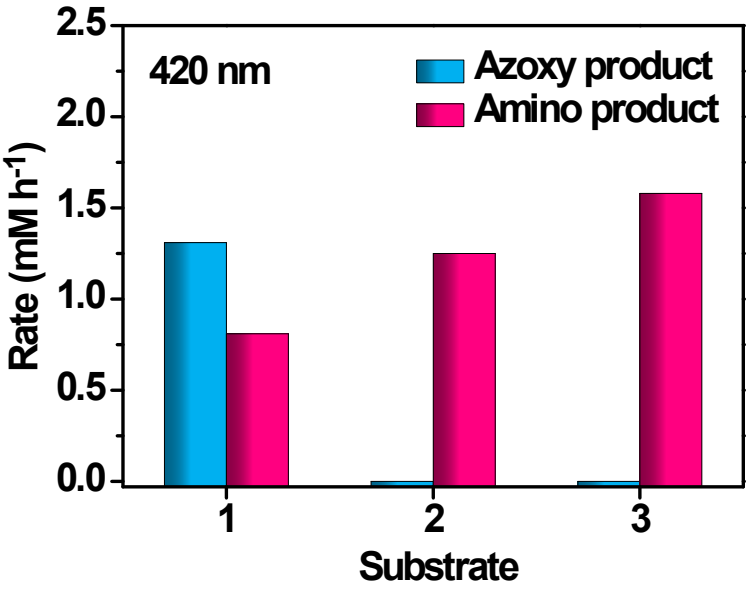

Figure S55. Initial formation rates of amine product in the system containing different substrates (10.0 mM) with $Ru(bpy)_3^{2+}$ (0.5 mM) and $HCOOH/H_2A$ (0.05/0.1 M) in a CH_3CN/H_2O solution (1:1, pH 5.0) under different wavelength irradiation.

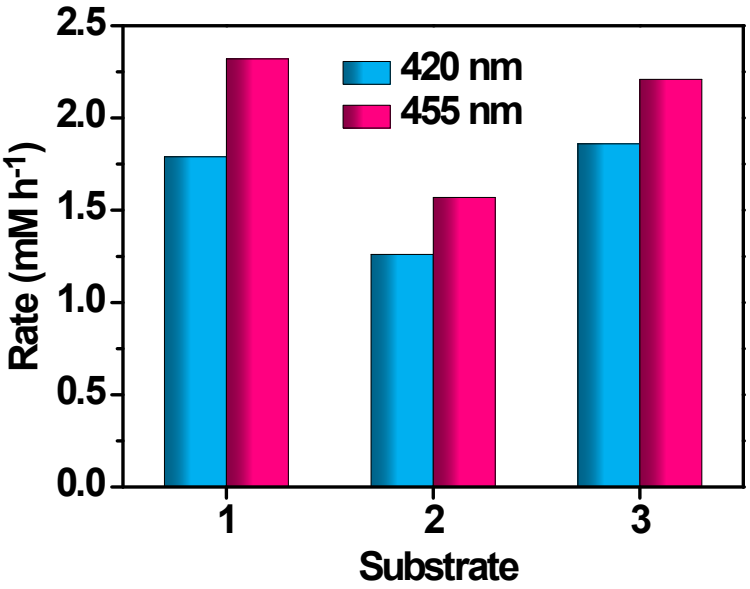

Figure S56. The formation rate ratio of amine product of substrate **1**, **2** or **3** in the system between 420 nm and 455 nm LED light irradiation. It showed that the ratio of fluorescence (F_{420}/F_{455}) and absorption (A_{420}/A_{455}) of $Ru(bpy)_3^{2+}$ under different excited wavelengths are proportional to the initial formation rate ratio of amine product (R_{420}/R_{455}).

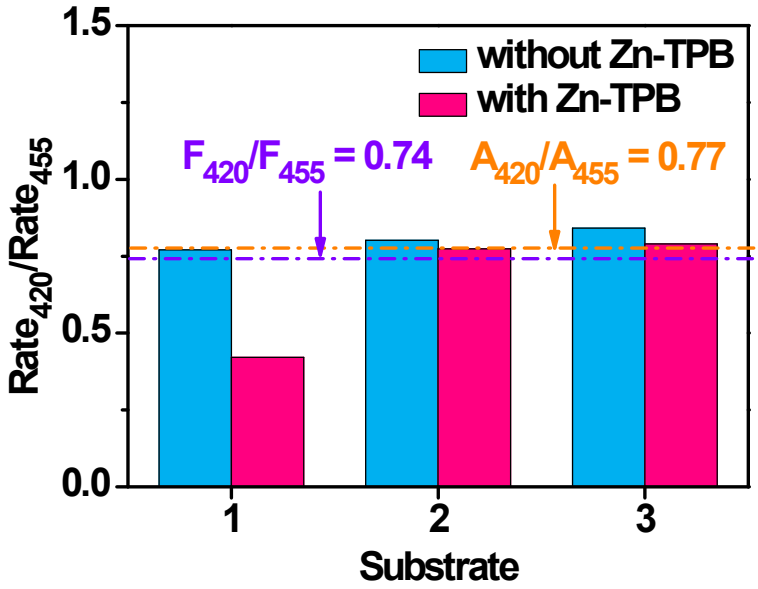

Figure S57. The relationship between fluorescence intensity and reaction selectivity. The fluorescence ratio $F_{Zn–TPB}/F_{Ru}$, The absorption ratio $A_{Zn–TPB}/A_{Ru}$, and the yield and rate ratio of **1c**/**1d** of the system under 420 nm or 455 nm LED light irradiation.

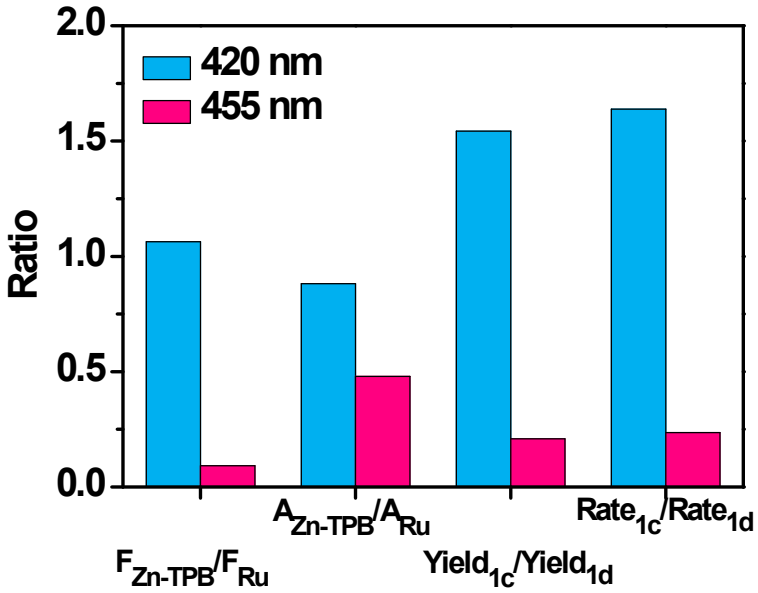

Irradiation Wavelength	F_{Zn-TPB}	F_{Ru}	Yield (1a) %	Yield (1b) %	F_{Zn-TPB}/F_{Ru}	1a/1b	$\frac{F_{Zn-TPB}}{F_{Ru}}/\frac{1a}{1b}$
420 nm	0.351	0.330	54	35	1.064	1.543	0.690
455 nm	0.041	0.454	17	81	0.090	0.209	0.434

Figure S58. Initial rates of the system containing substrate **1** (10.0 mM), $Ru(bpy)_3^{2+}$ (0.5 mM) and HCOOH/H_2A (0.05/0.1 M) in a CH_3CN/H_2O solution (1:1, pH 5.0) catalyzed by Zn–**TPB** (50 μM) or Ni–**TPB** (50 μM) under 420 nm or 455 nm LED light irradiation.

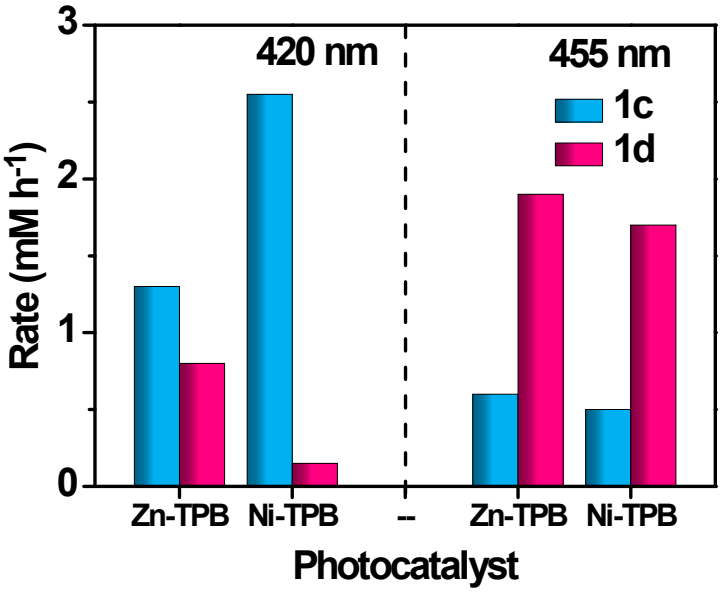

Figure S59. Initial rates of the system containing substrate (**1a** or **1b**, 10.0 mM), $Ru(bpy)_3^{2+}$ (0.5 mM) and HCOOH/H_2A (0.05/0.1 M) in a CH_3CN/H_2O solution (1:1, pH 5.0) catalyzed by Ni–**TPB** (50 μM) under 420 nm or 455 nm LED light irradiation.

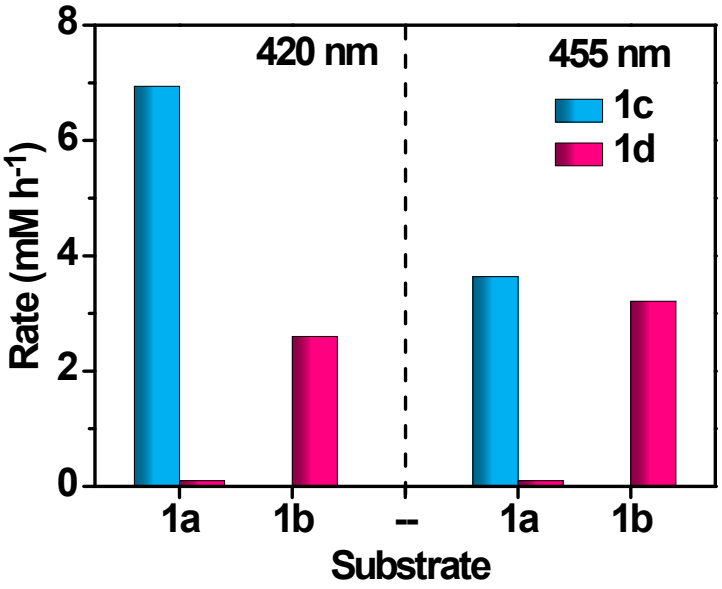

Figure S60. the hydrogenation reaction forming azoxy product and amino product by the system containing Ni–**TPB** (50 μM), $Ru(bpy)_3^{2+}$ (0.5 mM) and HCOOH/H_2A (0.05/0.1 M) with substrate **1** (10.0 mM), **2** (10.0 mM), substrate **1** (10.0 mM) with addition of ATP (20.0 mM) or substrate **1** (10.0 mM) with addition of 2,6-dimethylpyridine (50.0 mM) in a CH_3CN/H_2O solution (1:1, pH 5.0) under 420 nm illumination for 6h.

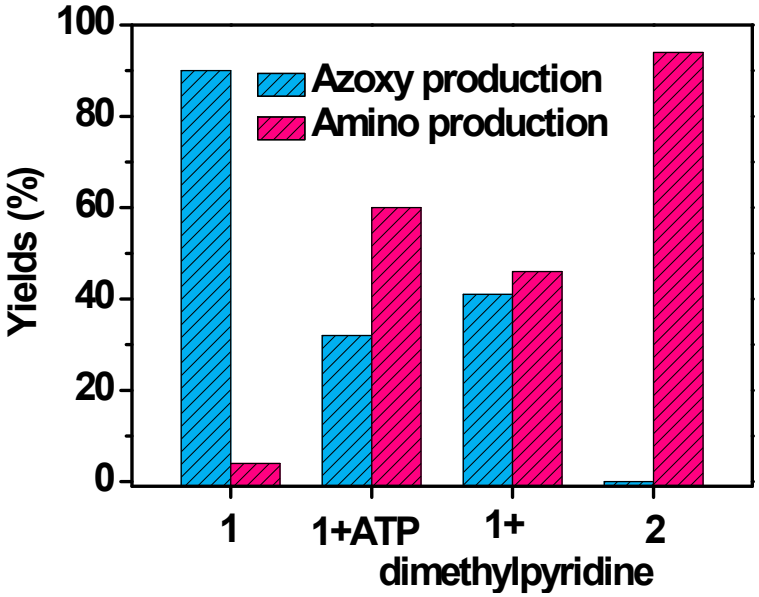

Figure S61. Gas chromatography spectroscopy of crude products of the system containing **1** (10.0 mM), $Ru(bpy)_3^{2+}$ (0.5 mM), $HCOOH/H_2A$ (0.05/0.1 M) with Zn–**TPB** (50 μM) or Ni–**TPB** (50 μM) in a CH_3CN/H_2O solution (1:1, pH 5.0) under 420 nm or 455 nm LED light irradiation within 6 h with 1,3,5-trimethoxybenzene added as internal standard.

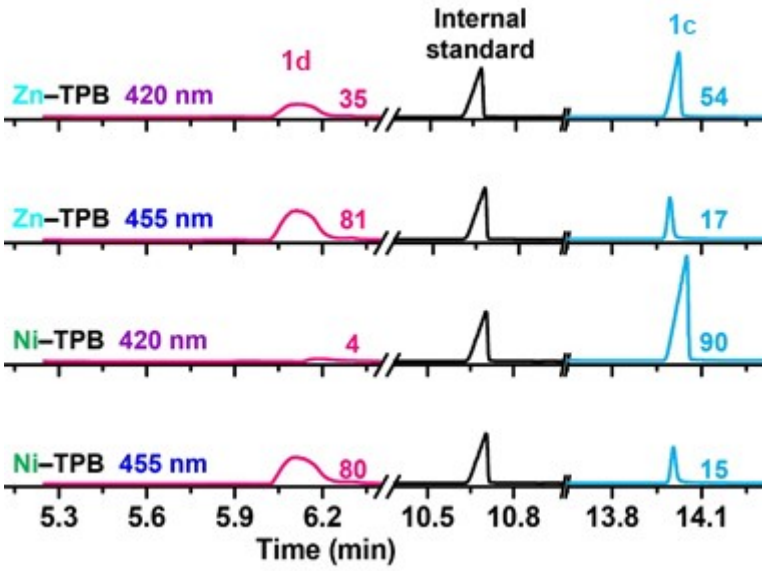

Figure S62 (Left) Differential pulse voltammetry (DPV) of nitrobenzene **1** (10 mM) and azoxybenzene **1c** (10 mM) in CH_3CN/H_2O (1:1, pH 5.0) containing 0.1 M $TBAPF_6$. (Right) Differential pulse voltammetry (DPV) of Zn–**TPB** (0.1 mM) and Ni–**TPB** (0.1 mM) in CH_3CN/H_2O (1:1, pH 5.0) containing 0.1 M $TBAPF_6$.

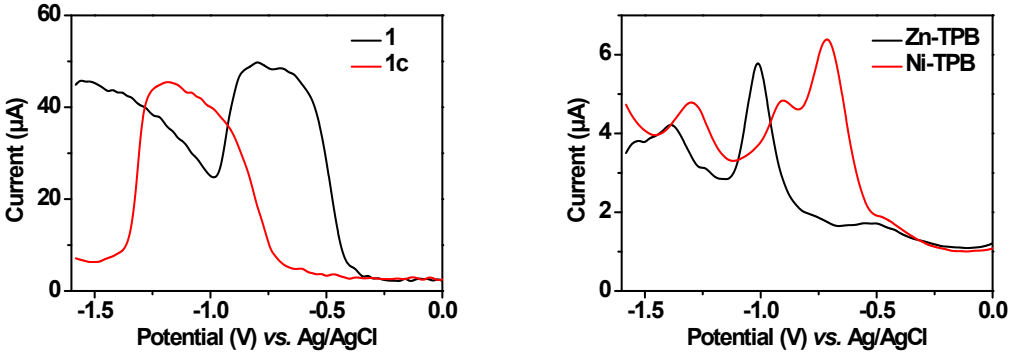

NMR spectra

Compounds **1c**[S8], **4c**[S8], **5c**[S9], **6c**[S8], **7c**[S8], **8c**[S8], **9c**[S8], **10c**[S10], **1d**[S11], **3d**[S12], **4d**[S11], **5d**[S11], **6d**[S11], **7d**[S11], **8d**[S11], **9d**[S11], **10d**[S13] were confirmed by comparisons with literature NMR data. All other new compounds were characterized by ^{1}H and ^{13}C NMR and HRMS.

(*Z*)-1,2-bis(4-((*E*)-3-ethoxy-3-oxoprop-1-en-1-yl)phenyl)diazene 1-oxide **(11c)**: HRMS calcd for $C_{22}H_{22}N_2O_5$, 394.1529; Found 395.1599 $[M+H]^+$.

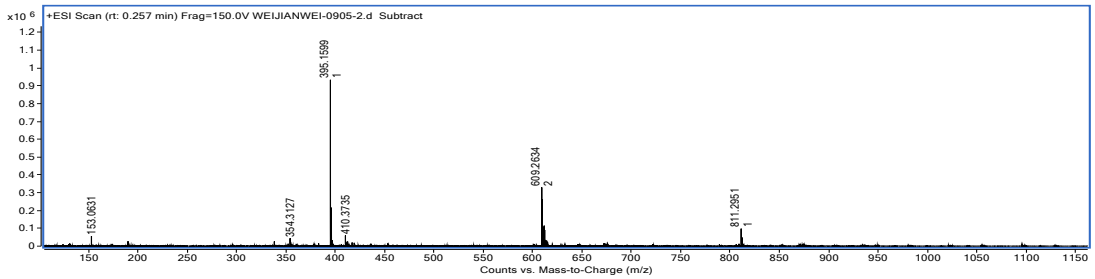

^{1}H NMR (400 MHz, $CDCl_3$) δ 8.33 (d, *J* = 8.4 Hz, 2H), 8.22 (d, *J* = 8.4 Hz, 2H), 7.80−7.58 (m, 6H), 6.52 (dd, *J* = 16.0, 11.2 Hz, 2H), 4.29 (dq, *J* = 7.2, 3.2 Hz, 4H), 1.36 (td, *J* = 7.2, 2.1 Hz, 6H).

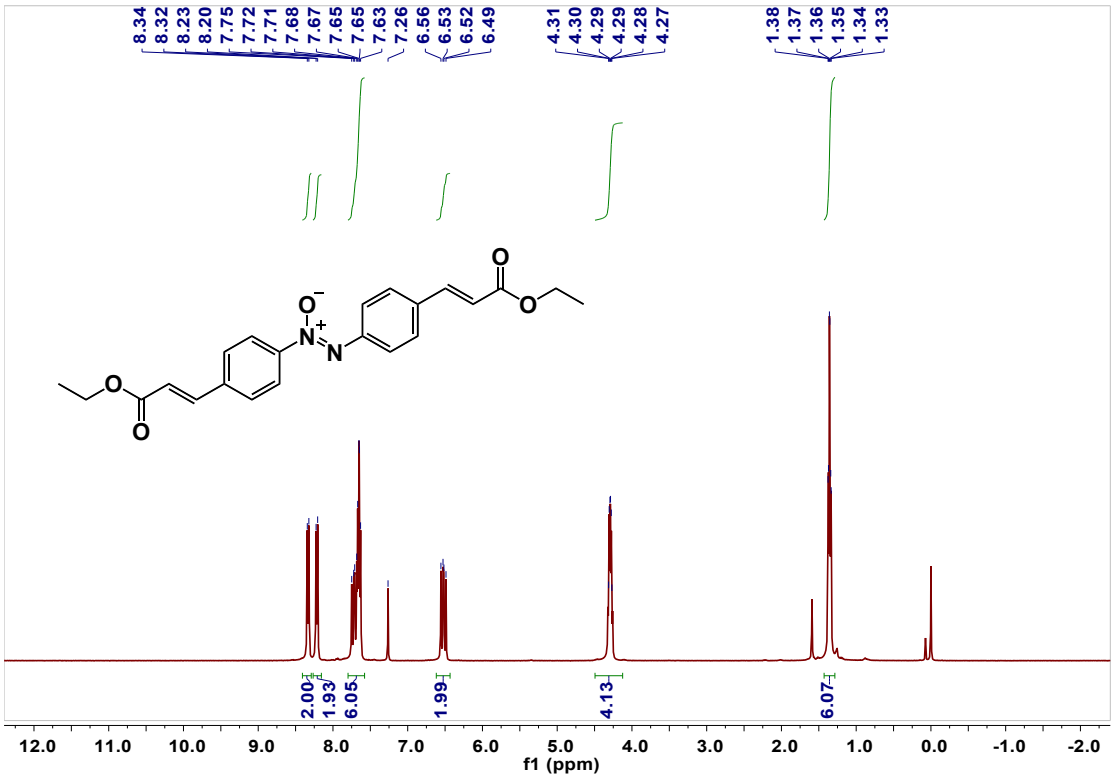

(*Z*)-1,2-bis(4-((*E*)-3-ethoxy-3-oxoprop-1-en-1-yl)phenyl)diazene 1-oxide **(11c)**: ^{13}C NMR (101 MHz, $CDCl_3$) δ 166.90, 166.54, 148.98, 143.41, 142.60, 138.04, 135.87, 128.60, 128.52, 126.34, 123.13, 121.11, 119.74, 60.96, 60.80, 14.46, 14.44.

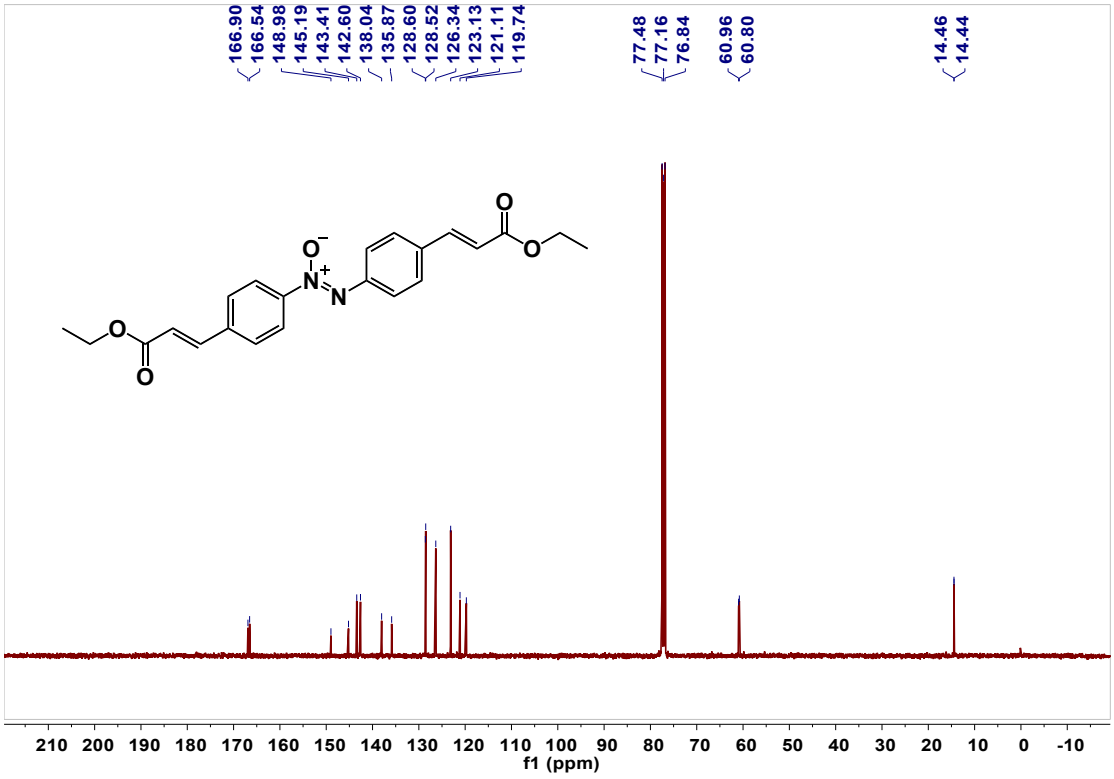

ethyl (*E*)-3-(4-aminophenyl)acrylate (**11d**): HRMS calcd for $C_{11}H_{13}NO_2$, 191.0946; Found 192.1015 $[M+H]^+$.

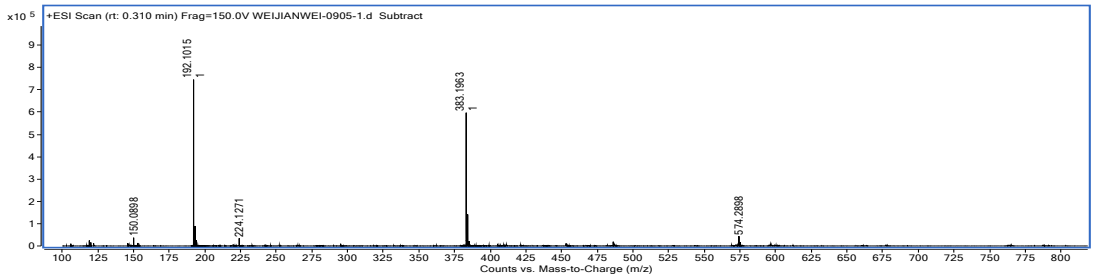

^{1}H NMR (400 MHz, $CDCl_3$) δ 7.59 (d, *J* = 15.9 Hz, 1H), 7.40−7.30 (m, 2H), 6.69−6.60 (m, 2H), 6.23 (d, *J* = 15.9 Hz, 1H), 4.24 (q, *J* = 7.1 Hz, 2H), 3.93 (s, 2H), 1.32 (t, *J* = 7.1 Hz, 3H).

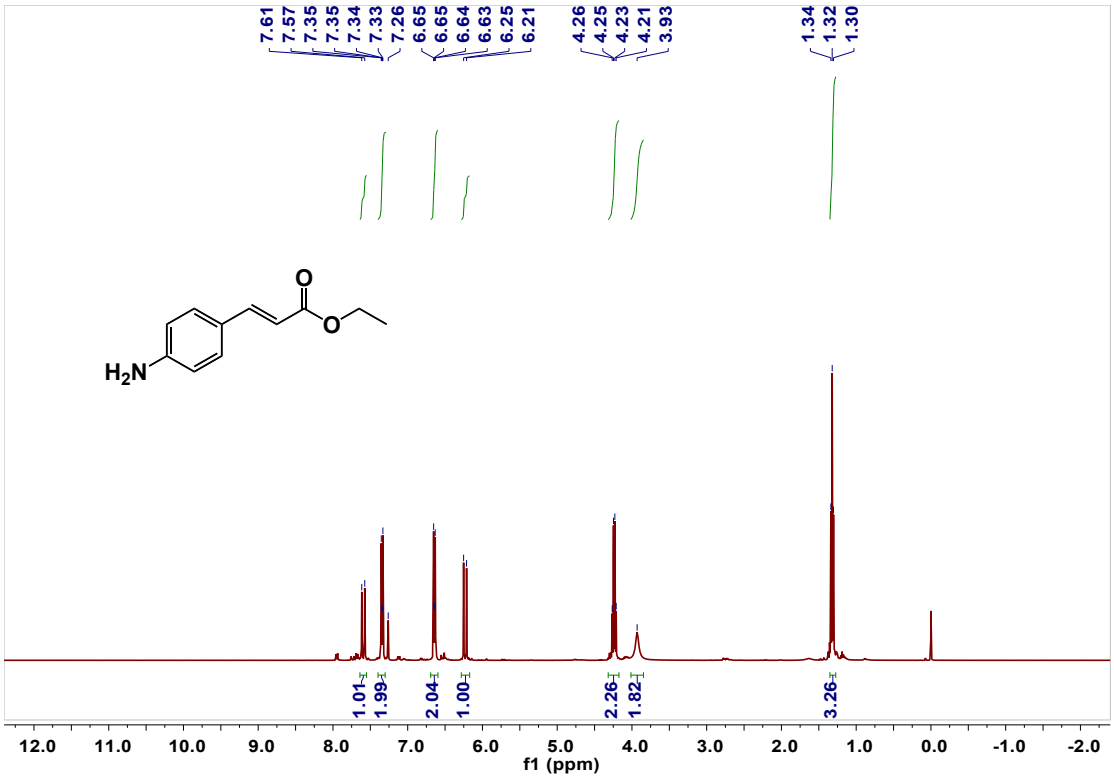

ethyl (*E*)-3-(4-aminophenyl)acrylate (**11d**): ^{13}C NMR (101 MHz, $CDCl_3$) δ 167.82, 148.77, 144.96, 129.98, 124.89, 114.95, 113.88, 60.29, 14.52.

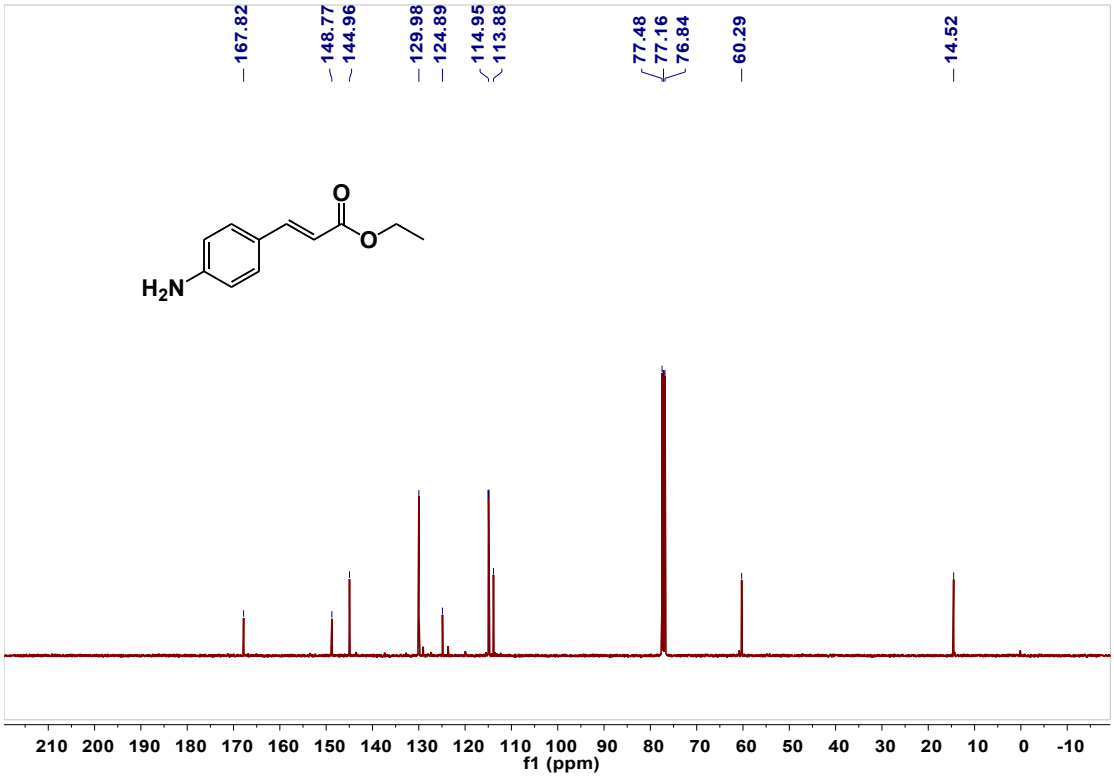

(*Z*)-1,2-bis(4-((1*E*,3*E*)-5-ethoxy-5-oxopenta-1,3-dien-1-yl)phenyl)diazene-1-oxide (**12c**): HRMS calcd for $C_{26}H_{26}N_2O_5$, 446.1842; Found 447.1909 $[M+H]^+$.

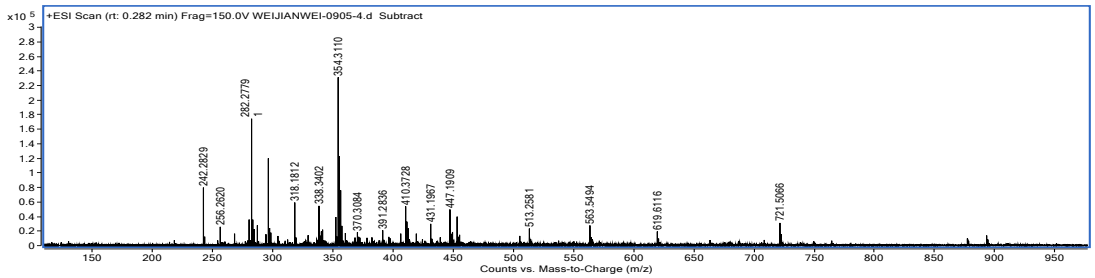

^{1}H NMR (400 MHz, $CDCl_3$) δ 8.31 (d, *J* = 8.7 Hz, 2H), 8.26−8.20 (m, 2H), 7.58 (dd, *J* = 8.7, 3.9 Hz, 4H), 7.46 (dd, *J* = 15.2, 8.7 Hz, 4H), 7.00−6.92 (m, 4H), 6.06 (dd, *J* = 15.3, 11.7 Hz, 2H), 4.25 (qd, *J* = 7.1, 2.2 Hz, 4H), 1.34 (td, *J* = 7.1, 1.2 Hz, 8H).

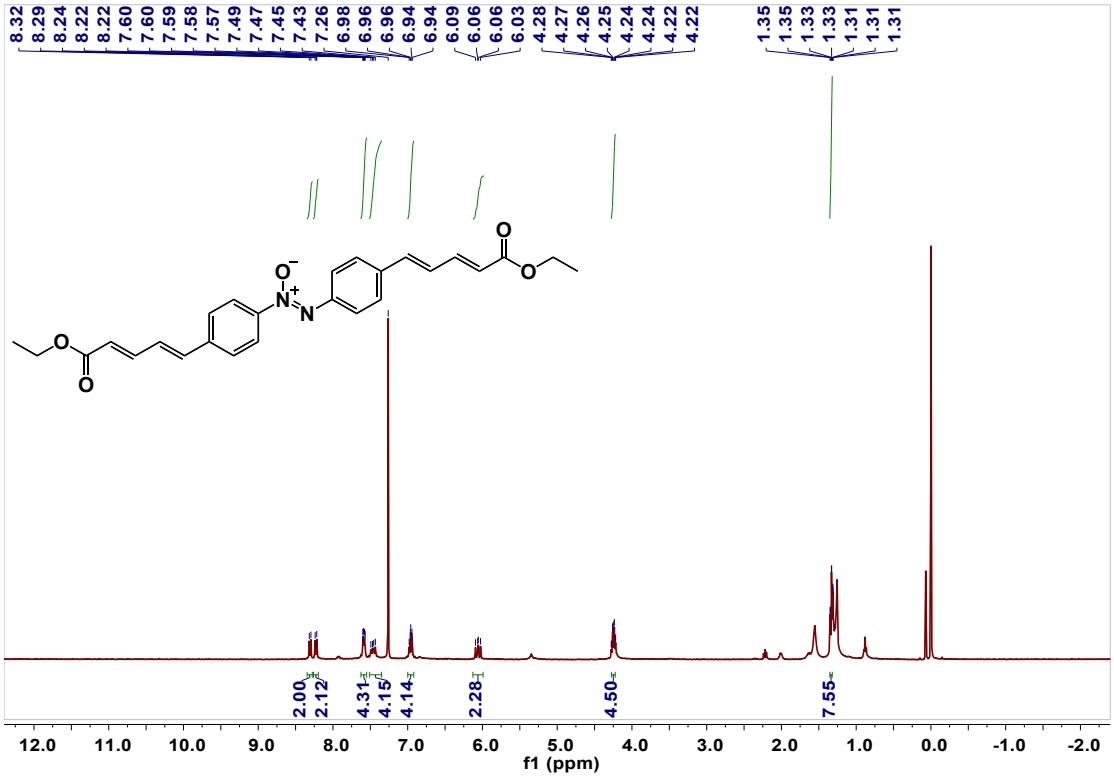

(*Z*)-1,2-bis(4-((1*E*,3*E*)-5-ethoxy-5-oxopenta-1,3-dien-1-yl)phenyl)diazene-1-oxide (**12c**): ^{13}C NMR (101 MHz, $CDCl_3$) δ 167.06, 166.90, 144.39, 144.28, 143.80, 139.31, 138.34, 137.56, 128.95, 128.11, 127.89, 127.65, 127.55, 126.46, 123.69, 123.23, 123.04, 122.44, 60.68, 60.59, 14.47, 14.26.

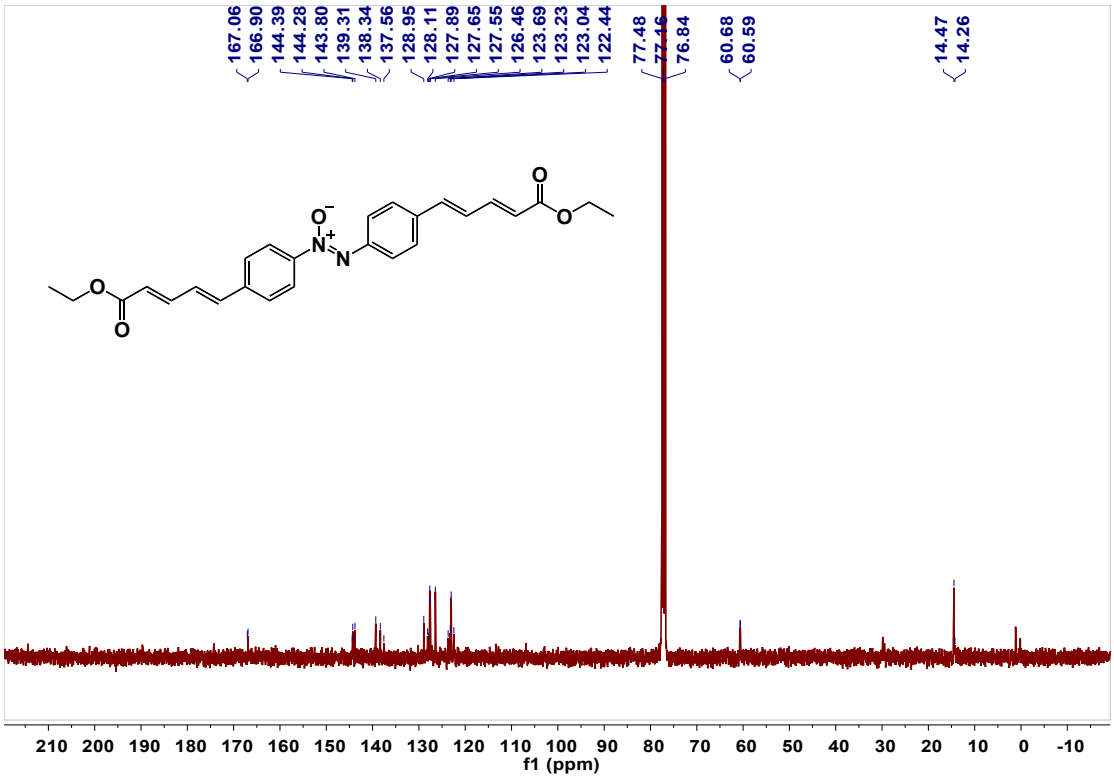

ethyl (2*E*,4*E*)-5-(4-aminophenyl)penta-2,4-dienoate (**12d**): HRMS calcd for $C_{13}H_{15}NO_2$, 217.1103; Found 218.1184 $[M+H]^+$.

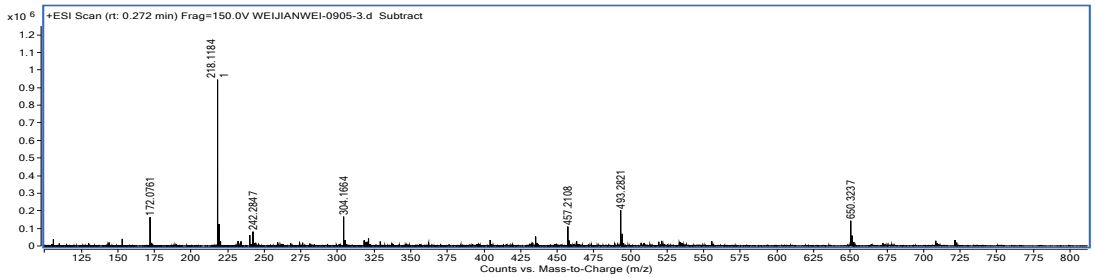

^{1}H NMR (400 MHz, $CDCl_3$) δ 7.43 (dd, *J* = 15.2, 10.9 Hz, 1H), 7.32−7.26 (m, 2H), 6.80 (d, *J* = 15.5 Hz, 1H), 6.74−6.67 (m, 1H), 6.64 (dd, *J* = 9.4, 2.9 Hz, 2H), 5.89 (d, *J* = 15.2 Hz, 1H), 4.21 (q, *J* = 7.2 Hz, 2H), 1.31 (t, *J* = 7.0 Hz, 3H).

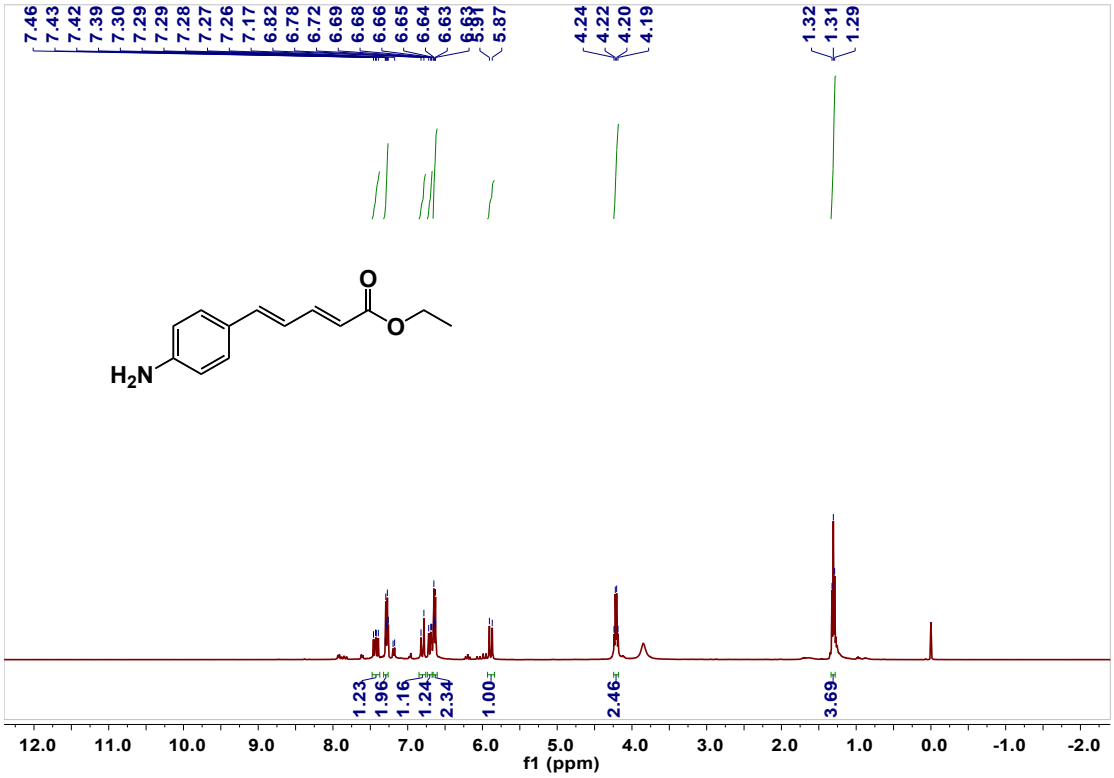

ethyl (2*E*,4*E*)-5-(4-aminophenyl)penta-2,4-dienoate (**12d**): ^{13}C NMR (101 MHz, $CDCl_3$) δ 167.58, 147.68, 145.62, 140.97, 128.92, 126.69, 122.71, 119.12, 115.12, 60.28, 14.49.

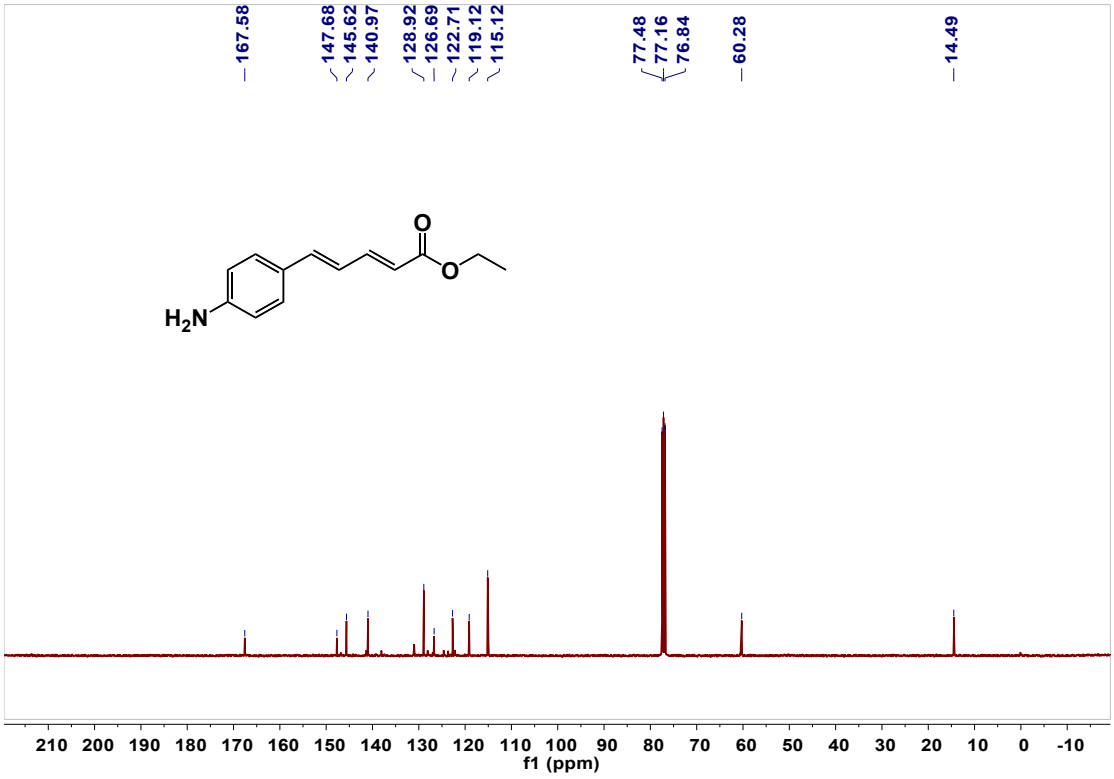

4,4"-di-tert-butyl-5'-nitro-1,1':3',1"-terphenyl (**2**): ^{1}H NMR (400 MHz, $CDCl_3$) δ 8.39 (d, *J* = 1.5 Hz, 2H), 8.10 (d, *J* = 1.6 Hz, 1H), 7.63−7.60 (m, 4H), 7.55−7.51 (m, 4H), 1.38 (s, 18H).

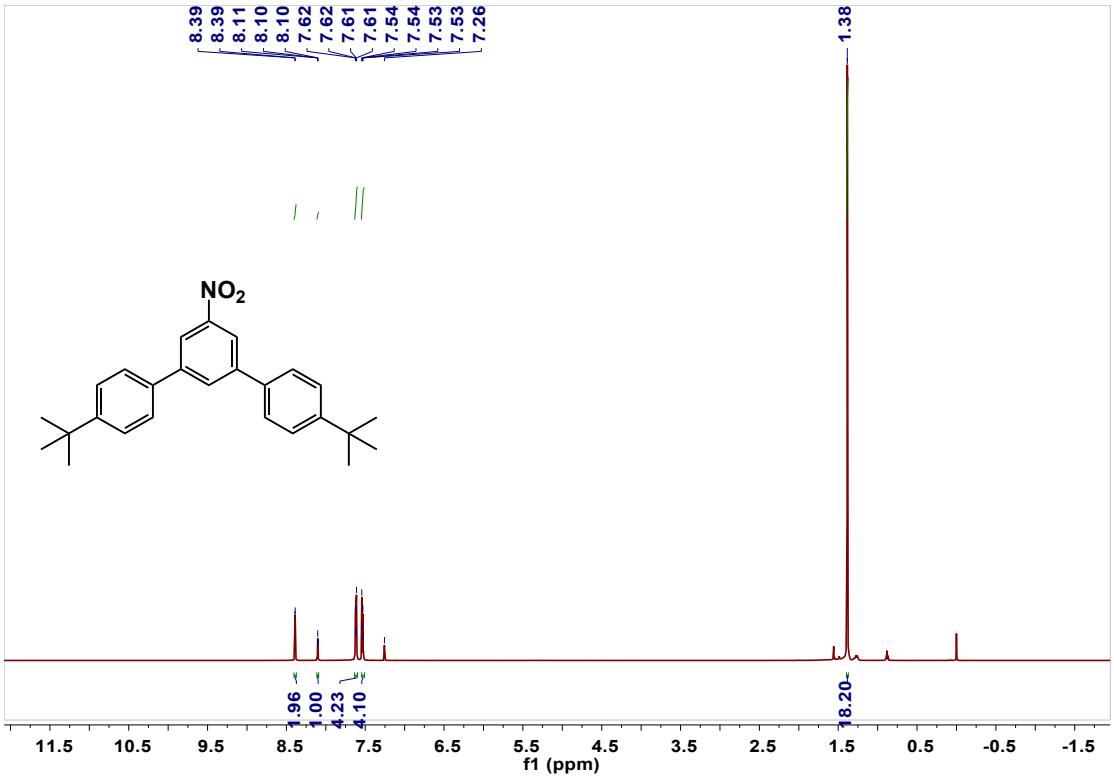

4,4"-di-tert-butyl-5'-nitro-1,1':3',1"-terphenyl (**2**): ^{13}C NMR (101 MHz, $CDCl_3$) δ 151.99, 149.39, 143.25, 136.13, 131.48, 127.06, 126.30, 120.31, 34.84, 31.46.

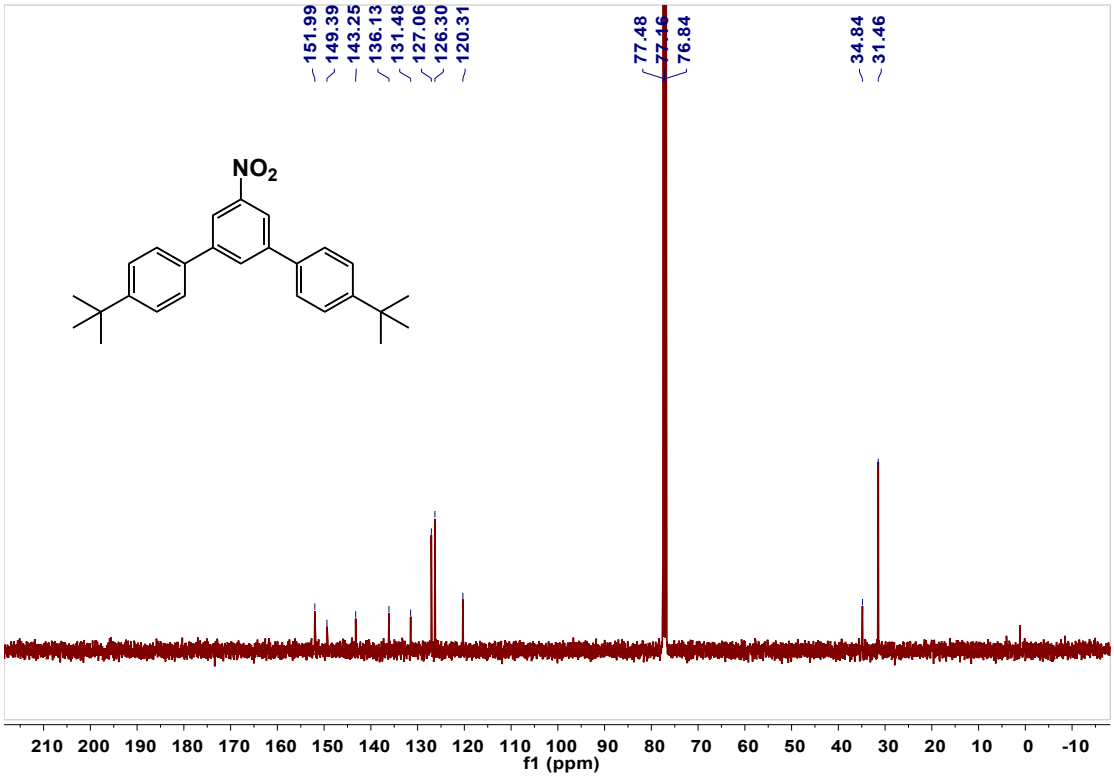

4,4"-di-tert-butyl-[1,1':3',1"-terphenyl]-5'-amine (**2d**): HRMS calcd for $C_{26}H_{31}N$, 357.2457; Found 358.2542 $[M+H]^+$.

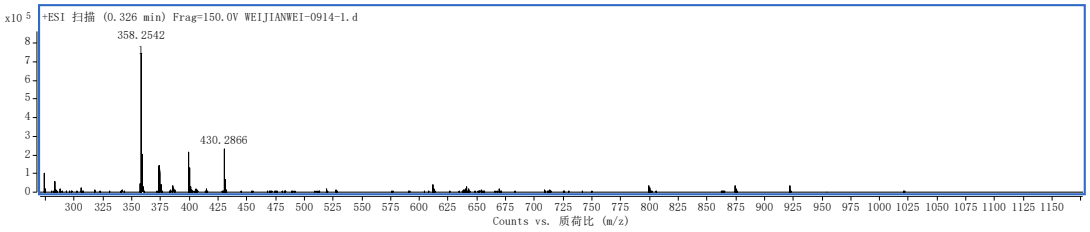

^{1}H NMR (400 MHz, $CDCl_3$) δ 7.55 (d, *J* = 8.4 Hz, 4H), 7.46 (d, *J* = 8.4 Hz, 4H), 7.29 (t, *J* = 1.5 Hz, 1H), 6.98 (d, *J* = 1.6 Hz, 2H), 1.37 (s, 18H).

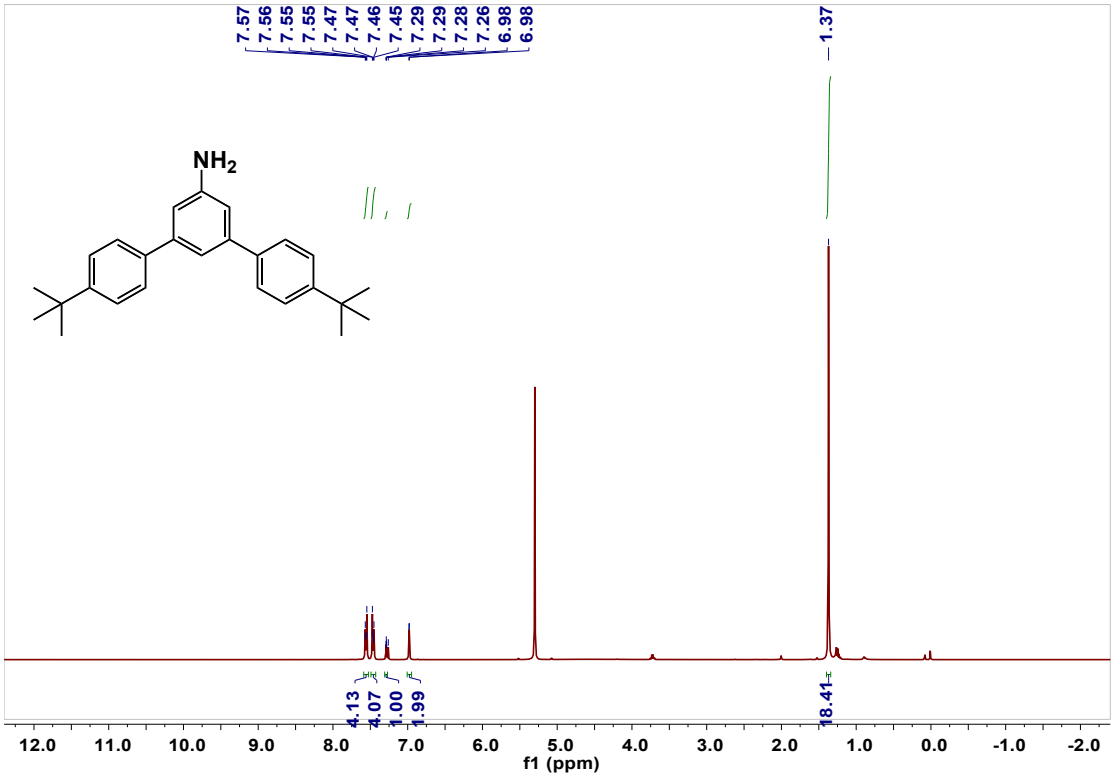

4,4"-di-tert-butyl-[1,1':3',1"-terphenyl]-5'-amine (**2d**): ^{13}C NMR (101 MHz, $CDCl_3$) δ 150.56, 145.15, 142.95, 138.42, 126.97, 125.79, 118.13, 113.69, 34.68, 31.51.

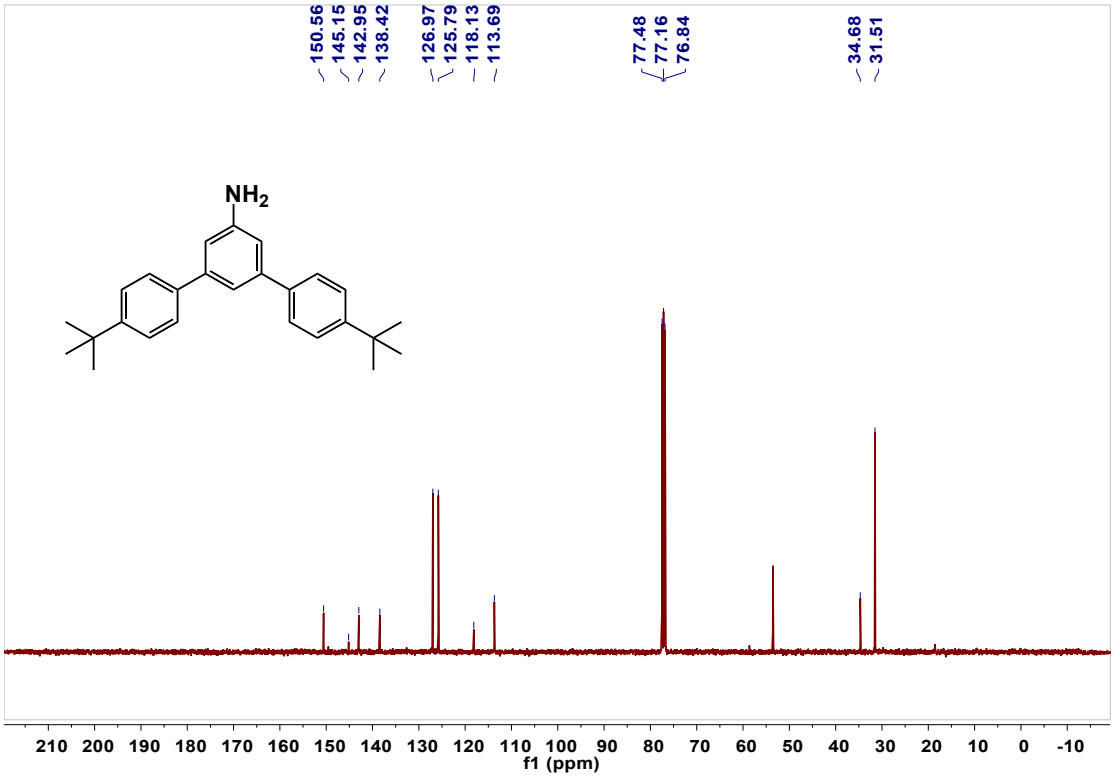

Compound α: ^{1}H NMR (400 MHz, $CDCl_3$): δ 7.34 (dd, *J* = 5.0, 1.4 Hz, 1H), 7.28 (d, *J* = 9.6 Hz, 4H), 7.22 (t, *J* = 7.5 Hz, 2H), 7.14 (t, *J* = 7.2 Hz, 1H), 7.07−6.99 (m, 2H), 4.89 (s, 1H), 4.73 (s, 2H), 3.61 (s, 6H).

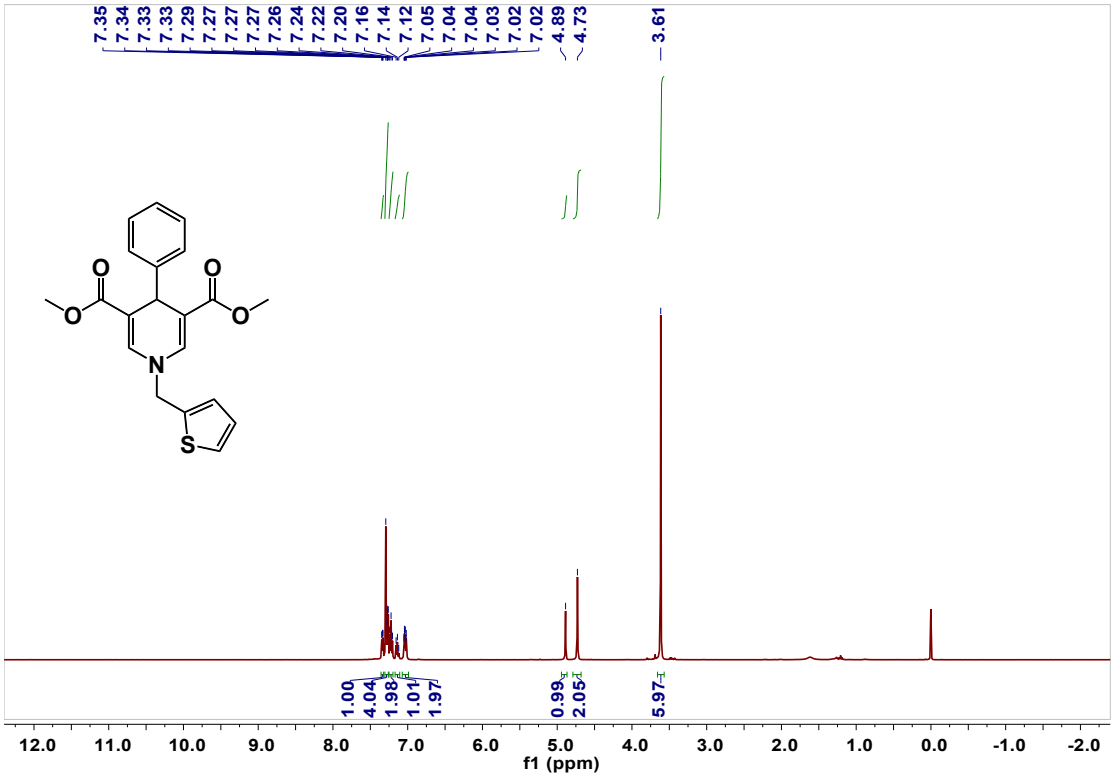

Compound α: ^{13}C NMR (101 MHz, $CDCl_3$) δ 167.22, 146.29, 138.75, 137.18, 128.27, 128.19, 127.46, 126.92, 126.62, 109.37, 53.35, 51.44, 37.45.

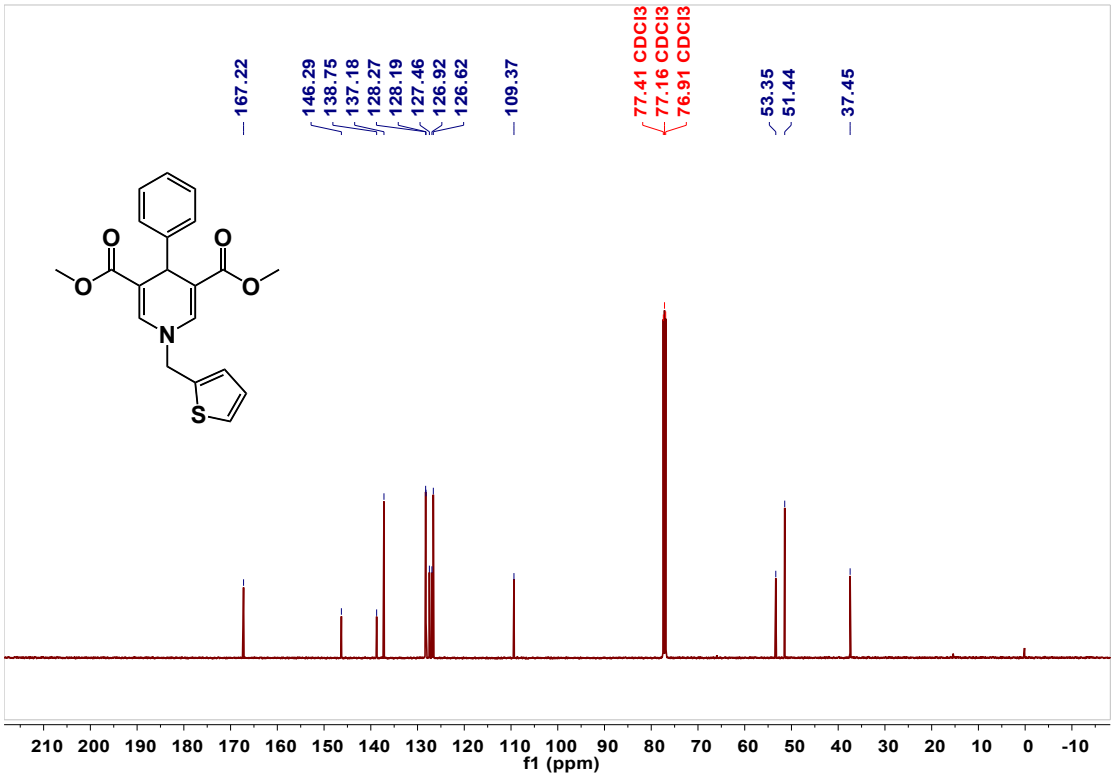

Compound β: ^{1}H NMR (400 MHz, DMSO-d_6) δ 8.66 (s, 2H), 7.53 (dd, J = 5.0, 1.3 Hz, 1H), 7.23−7.15 (m, 6H), 7.13 (dt, J = 4.7, 1.4 Hz, 1H), 7.11−7.03 (m, 2H), 5.00 (s, 1H), 4.80 (s, 2H), 4.15 (s, 4H).

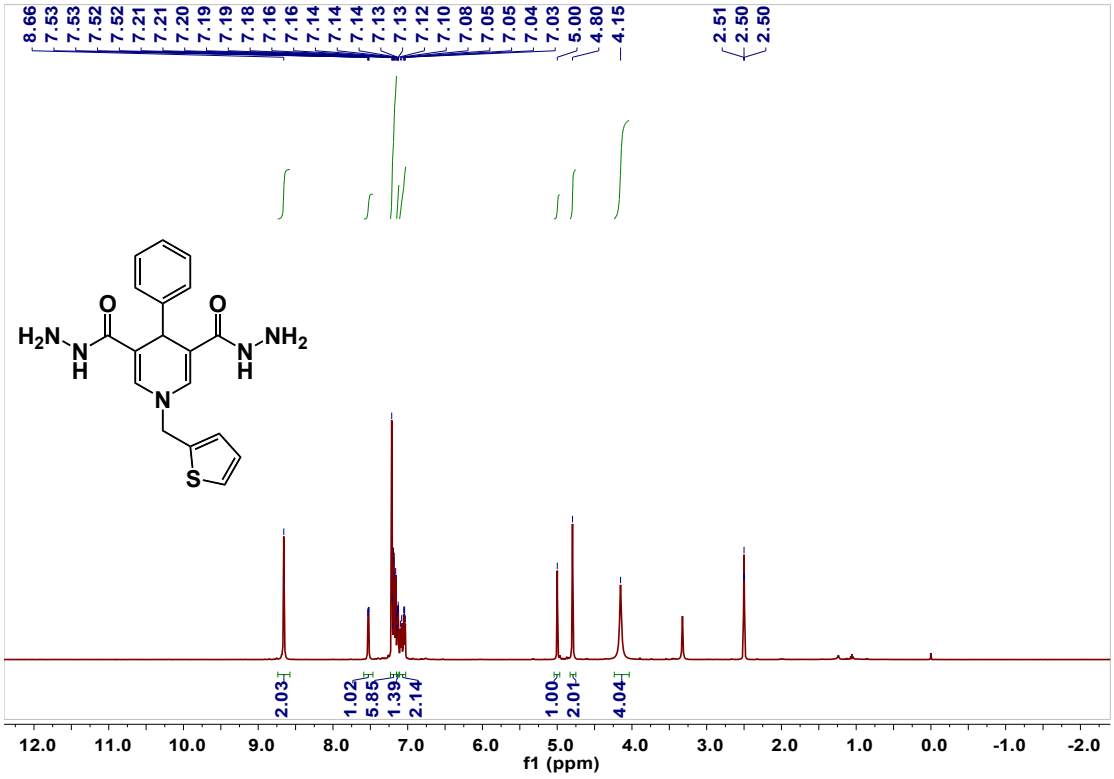

Compound β: ^{13}C NMR (101 MHz, DMSO-d_6) δ 166.44, 146.31, 140.27, 133.32, 127.87, 127.57, 127.12, 126.81, 126.36, 126.06, 109.01, 51.60, 35.40.

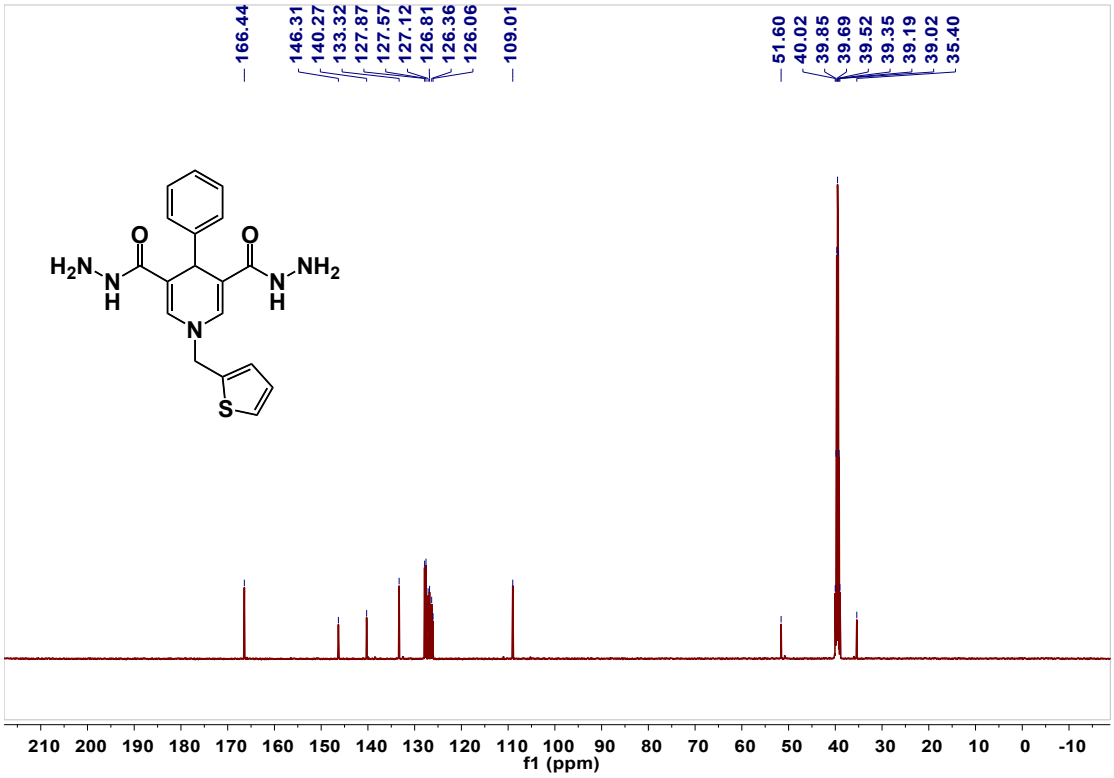

H_2**TPB**: ^{1}H NMR (400 MHz, DMSO-d_6) δ 11.37 (s, 2H), 8.58 (dt, J = 4.9, 1.4 Hz, 2H), 8.24 (s, 2H), 7.89−7.77 (m, 4H), 7.59 (dd, J = 5.0, 1.3 Hz, 1H), 7.51 (s, 2H), 7.37 (q, J = 4.5 Hz, 2H), 7.32−7.26 (m, 2H), 7.25−7.20 (m, 3H), 7.15−7.07 (m, 2H), 5.35 (s, 1H), 4.96 (s, 2H).

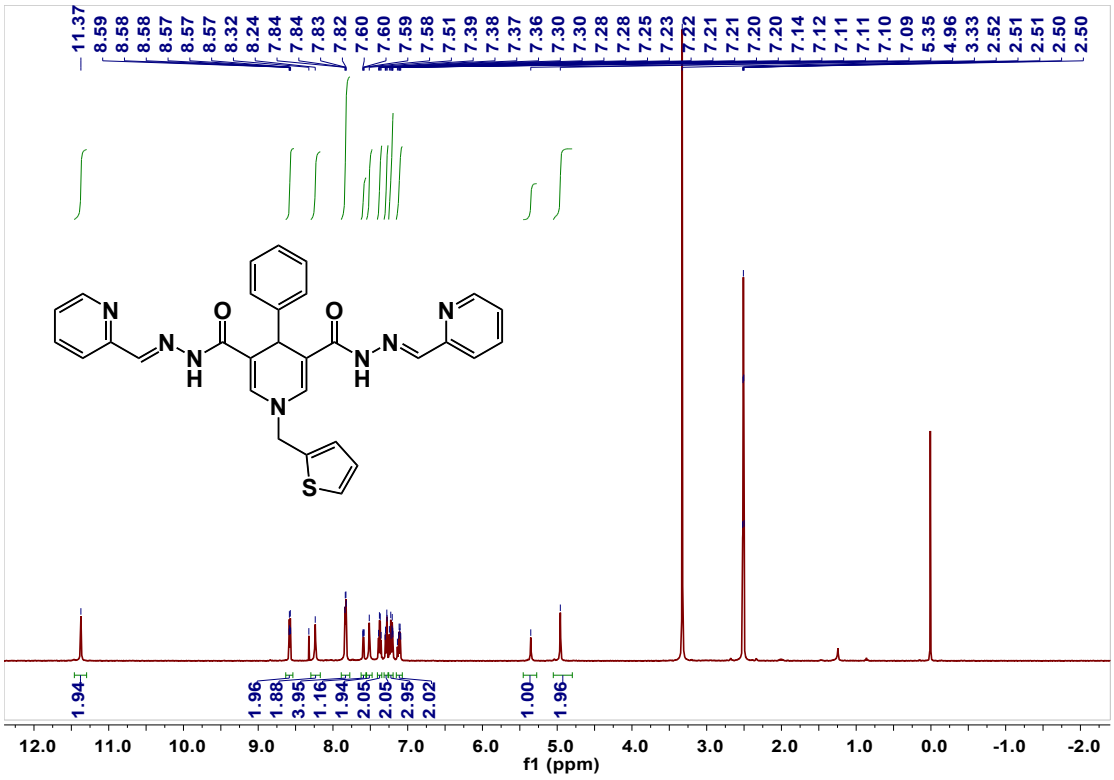

H_2**TPB**: ^{13}C NMR (101 MHz, DMSO-d_6) δ 163.81, 153.47, 149.42, 146.38, 145.27, 140.28, 136.72, 128.09, 127.70, 127.31, 126.68, 126.53, 126.28, 125.62, 124.01, 119.56, 109.39, 52.19, 36.12.

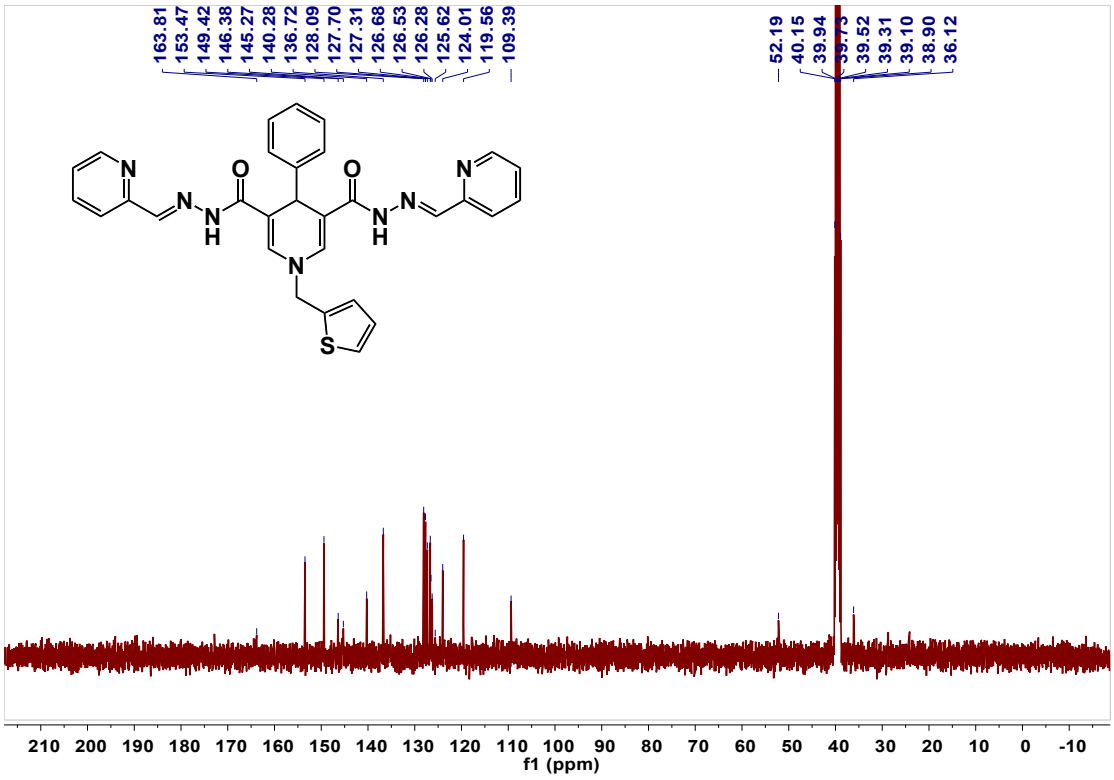

7. References.

S1. Thordarson P. Determining association constants from titration experiments in supramolecular chemistry. *Chem. Soc. Rev.*, **2011**, *40*, 1305–1323.

S2. Mai, A.; Valente, S.; Meade, S.; Carafa, V.; Tardugno, M.; Nebbioso, A.; Galmozzi, A.; Mitro, N.; Fabiani, E. D.; Altucci, L.; Kazantsev, A. Study of 1,4-Dihydropyridine Structural Scaffold: Discovery of Novel Sirtuin Activators and Inhibitors. *J. Med. Chem.* **2009**, *52*, 5496–5504.

S3. Ranford, J. D.; Vittal, J. J.; Wang, Y. M. Dicopper(II) Complexes of the Antitumor Analogues Acylbis(salicylaldehyde hydrazones) and Crystal Structures of Monomeric [Cu_2(1,3-propanedioyl bis(salicylaldehyde hydrazone))$(H_2O)_2$]·$(ClO_4)_2$·$3H_2O$ and Polymeric [{Cu_2(1,6-hexanedioyl bis(salicylaldehyde hydrazone))$(C_2H_5OH)_2$}$_m$]·$(ClO_4)_{2m}$·m(C_2H_5OH). *Inorg. Chem.* **1998**, *37*, 1226−1231.

S4. SMART Data Collection Software, version 5.629; Bruker AXS Inc.: Madison, WI, 2003.

S5. SAINT Data Reduction Software, version 6.54; Bruker AXS Inc.: Madison, WI, 2003.

S6. G. M. Sheldrick, SHELXTL97, Program for Crystal Structure Solution; University of Göttingen: Göttingen, Germany, 1997.

S7. A. L. Spek, Single-crystal structure validation with the program PLATON. *J. Appl. Crystallogr.* **2003**, *36*, 7−13.

S8. De Carvalho, G. S. G.; Chagas, L. H.; Fonseca, C. G.; De Castro, P. P.; Sant'Ana, A. C.; Leitão, A. A.; Amarante, G. W. Nb_2O_5 supported on mixed oxides catalyzed oxidative and photochemical conversion of anilines to azoxybenzenes. *New J. Chem.* **2019**, *43*, 5863−5871.

S9. Ferlin, F.; Cappelletti, M.; Vivani, R.; Pica, M.; Piermatti, M.; Vaccaro, L. Au@zirconium-phosphonate nanoparticles as an effective catalytic system for the chemoselective and switchable reduction of nitroarenes. *Green Chem.* **2019**, *21*, 614–626.

S10. Tanini, D.; Dalia, C.; Capperucci, A.; The polyhedral nature of selenium-catalysed reactions: Se(IV) species instead of Se(VI) species make the difference in the on water selenium-mediated oxidation of arylamines. *Green Chem.* **2021**, *23*, 5680–5686.

S11. Duan, Y.; Dong, X.; Song, T.; Wang, Z.; Xiao, J.; Yuan, Y.; Yang, Y. Hydrogenation of Functionalized Nitroarenes Catalyzed by Single-Phase Pyrite FeS_2 Nanoparticles on N,S-Codoped Porous Carbon. *ChemSusChem* **2019**, *12*, 4636–4644.

S12. Wang, C. Y.; Fu, C. F.; Liu, Y. H.; Peng, S. M.; Liu, S. T. Synthesis of Iridium Pyridinyl N-Heterocyclic Carbene Complexes and Their Catalytic Activities on Reduction of Nitroarenes. *Inorg. Chem.* **2007**, *46*, 5779–5786.

S13. Prathap, K. J.; Wu, Q.; Olsson, R. T.; Dinér, P. Catalytic Reductions and Tandem Reactions of Nitro Compounds Using in Situ Prepared Nickel Boride Catalyst in Nanocellulose Solution. *Org. Lett.* **2017**, *19*, 4746−4749.